AIP | Journal of Physical and Chemical Reference Data

A Fundamental Equation of State for Ethanol

J. A. Schroeder, S. G. Penoncello, and J. S. Schroeder

Citation: Journal of Physical and Chemical Reference Data **43**, 043102 (2014); doi: 10.1063/1.4895394
View online: http://dx.doi.org/10.1063/1.4895394
View Table of Contents: http://scitation.aip.org/content/aip/journal/jpcrd/43/4?ver=pdfcov
Published by the AIP Publishing

Articles you may be interested in

A New Functional Form and New Fitting Techniques for Equations of State with Application to Pentafluoroethane (HFC-125)
J. Phys. Chem. Ref. Data **34**, 69 (2005); 10.1063/1.1797813

A Fundamental Equation for Trifluoromethane (R-23)
J. Phys. Chem. Ref. Data **32**, 1473 (2003); 10.1063/1.1559671

A Reference Equation of State for the Thermodynamic Properties of Nitrogen for Temperatures from 63.151 to 1000 K and Pressures to 2200 MPa
J. Phys. Chem. Ref. Data **29**, 1361 (2000); 10.1063/1.1349047

New Equation of State for Ethylene Covering the Fluid Region for Temperatures From the Melting Line to 450 K at Pressures up to 300 MPa
J. Phys. Chem. Ref. Data **29**, 1053 (2000); 10.1063/1.1329318

An International Standard Equation of State for the Thermodynamic Properties of HFC-125 (Pentafluoroethane)
J. Phys. Chem. Ref. Data **27**, 775 (1998); 10.1063/1.556021

This article is copyrighted as indicated in the article. Reuse of AIP content is subject to the terms at: http://scitation.aip.org/termsconditions. Downloaded to IP: 131.111.164.128 On: Tue, 21 Oct 2014 07:26:40

A Fundamental Equation of State for Ethanol

J. A. Schroeder, S. G. Penoncello,[a] and J. S. Schroeder

Center for Applied Thermodynamic Studies, University of Idaho, Moscow, Idaho 83844, USA

(Received 29 May 2014; accepted 25 August 2014; published online 13 October 2014)

The existing fundamental equation for ethanol demonstrates undesirable behavior in several areas and especially in the critical region. In addition, new experimental data have become available in the open literature since the publication of the current correlation. The development of a new fundamental equation for ethanol, in the form of Helmholtz energy as a function of temperature and density, is presented. New, nonlinear fitting techniques, along with the new experimental data, are shown to improve the behavior of the fundamental equation. Ancillary equations are developed, including equations for vapor pressure, saturated liquid density, saturated vapor density, and ideal gas heat capacity. Both the fundamental and ancillary equations are compared to experimental data. The fundamental equation can compute densities to within ±0.2%, heat capacities to within ±1%–2%, and speed of sound to within ±1%. Values of the vapor pressure and saturated vapor densities are represented to within ±1% at temperatures of 300 K and above, while saturated liquid densities are represented to within ±0.3% at temperatures of 200 K and above. The uncertainty of all properties is higher in the critical region and near the triple point. The equation is valid for pressures up to 280 MPa and temperatures from 160 to 650 K. © *2014 AIP Publishing LLC.* [http://dx.doi.org/10.1063/1.4895394]

Key words: caloric properties; density; equation of state; ethanol; ethyl alcohol; fundamental equation; thermodynamic properties.

CONTENTS

1. Introduction 4
   1.1. Prior correlations of thermodynamic properties of ethanol 4
   1.2. The functional form of the fundamental equation 4
   1.3. Physical constants and characteristic properties 5
2. Experimental Data 5
   2.1. Critical point data 5
   2.2. Pressure–density–temperature data 5
   2.3. Isobaric heat capacity data 7
   2.4. Isochoric heat capacity data 8
   2.5. Sound speed data 8
   2.6. Second virial coefficient data 10
   2.7. Vapor pressure data 10
   2.8. Saturated liquid density data 11
   2.9. Saturated vapor density data 12
   2.10. Ideal gas heat capacity data 12
3. The Ancillary Equations 12
   3.1. Comparison of data to equations 13
   3.2. Ancillary equation fitting method 13
   3.3. The vapor pressure equation 13
   3.4. The saturated liquid density equation 14
   3.5. The saturated vapor density equation 15
4. Properties of the Ideal Gas 15
   4.1. The ideal gas heat capacity equation 15
   4.2. The ideal gas Helmholtz energy equation . 16
5. Properties of the Real Fluid 16
   5.1. The functional form of the residual portion of the fundamental equation 16
   5.2. Fitting procedure and results 17
   5.3. Data selection 17
      5.3.1. Pressure–density–temperature data selection 18
      5.3.2. Isobaric heat capacity data selection. 18
      5.3.3. Sound speed data selection 19
      5.3.4. Vapor pressure data selection 19
      5.3.5. Saturated liquid density data selection 19
      5.3.6. Saturated vapor density data selection 19
      5.3.7. Unused data forms 19
6. Comparison of the Fundamental Equation to the Data 20
   6.1. Comparison to $p\rho T$ data 20
   6.2. Comparison to near-critical and supercritical pressure data 22
   6.3. Comparison to isobaric heat capacity data . 22
   6.4. Comparison to isochoric heat capacity data 22
   6.5. Comparison to sound speed data 22
   6.6. Comparison to second virial coefficient data 24
   6.7. Comparison to vapor pressure data 24
   6.8. Comparison to saturated liquid density data 24

[a]Author to whom correspondence should be addressed; electronic mail: stevep@uidaho.edu.
© 2014 AIP Publishing LLC.

This article is copyrighted as indicated in the article. Reuse of AIP content is subject to the terms at: http://scitation.aip.org/termsconditions. Downloaded to IP: 131.111.164.128 On: Tue, 21 Oct 2014 07:26:40

6.9. Comparison to saturated vapor density data 24
6.10. Comparison to the ancillary equations ... 25
7. Behavior of the Fundamental Equation 25
7.1. Behavior of the $p\rho T$ surface 27
7.2. Behavior of the vapor densities 27
7.3. Behavior in the critical region 30
7.4. Behavior of the isobaric and isochoric heat capacities 32
7.5. Behavior of the sound speed 32
7.6. Behavior of the characteristic equations ... 33
7.7. Behavior of the saturated densities 36
8. Conclusions and Recommendations 37
8.1. Conclusions 37
8.2. Recommendations 37
9. Appendix A: Thermodynamic Equations 37
10. Appendix B: Thermodynamic Property Tables of Ethanol at Saturation 39
11. References 41

List of Tables

1. Existing equations of state for ethanol 4
2. Physical constants and characteristic properties of ethanol 5
3. Summary of $p\rho T$ data 6
4. Summary of isobaric heat capacity data 7
5. Summary of isochoric heat capacity data 8
6. Summary of sound speed data 9
7. Summary of second virial coefficient data 10
8. Summary of vapor pressure data 10
9. Summary of saturated liquid density data 11
10. Summary of saturated vapor density data 12
11. Constants for the vapor pressure equation, Eq. (9) 13
12. Statistical calculations for the vapor pressure equation, Eq. (9) 14
13. Constants for the saturated liquid density equation, Eq. (10) 14
14. Statistical calculations for the saturated liquid density equation, Eq. (10) 15
15. Constants for the saturated vapor density equation, Eq. (11) 15
16. Statistical calculations for the saturated vapor density equation, Eq. (11) 16
17. Constants of the ideal gas heat capacity equation, Eq. (18) 16
18. Constants of the ideal gas Helmholtz energy equation, Eq. (19) 17
19. Constants of the residual portion of the fundamental equation of state, Eq. (21) 17
20. Statistical comparisons of $p\rho T$ data to the fundamental equations 20
21. Comparisons of near-critical and supercritical pressure data to the fundamental equations 24
22. Comparisons of isobaric heat capacity data to the fundamental equations 26
23. Comparisons of isochoric heat capacity data to the fundamental equations 27
24. Comparisons of sound speed data to the fundamental equations 28
25. Comparisons of second virial coefficient data to the fundamental equations 30
26. Comparisons of vapor pressure data to the fundamental equations 31
27. Comparisons of saturated liquid density data to the fundamental equations 33
28. Comparisons of saturated vapor density data to the fundamental equations 34
29. Comparison of the selected critical point to the fundamental equation 34
30. Calculated values of properties for algorithm verification 38

List of Figures

1. Distribution of pressure-temperature critical data. 5
2. Distribution of density-temperature critical data. 5
3. Representative distribution of experimental $p\rho T$ data 6
4. Representative distribution of experimental isobaric heat capacity data 8
5. Distribution of experimental isochoric heat capacity data 8
6. Representative distribution of experimental sound speed data 9
7. The (a) *trans* and (b) *gauche* conformers of ethanol 12
8. Experimental deviations for the vapor pressure data 13
9. Experimental deviations for the saturated liquid density data 14
10. Experimental deviations for the saturated vapor density data 15
11. Experimental deviations for the ideal gas heat capacity data 16
12. Pressure-temperature plot of data used to fit the fundamental equation 18
13. Temperature-density plot of data used to fit the fundamental equation 18
14. Comparisons of $p\rho T$ data to the fundamental equations 23
15. Comparisons of near-critical and supercritical pressure data to the fundamental equations 25
16. Comparisons of isobaric heat capacity data to the fundamental equations 27
17. Comparison of isochoric heat capacity data to the fundamental equations 27
18. Comparisons of sound speed data to the fundamental equations 29
19. Comparison of second virial coefficient data to the fundamental equations 29

This article is copyrighted as indicated in the article. Reuse of AIP content is subject to the terms at: http://scitation.aip.org/termsconditions. Downloaded to IP: 131.111.164.128 On: Tue, 21 Oct 2014 07:26:40

20. Comparison of vapor pressure data to the fundamental equations 29
21. Comparison of saturated liquid density data to the fundamental equations..... 30
22. Comparison of saturated vapor density data to the fundamental equations..... 32
23. Deviations of the ancillary equations from the fundamental equation..... 33
24. Isothermal behavior of the fundamental equation developed in this work 33
25. Isothermal behavior of the fundamental equation of Dillon and Penoncello..... 33
26. Virial coefficient behavior of the fundamental equation developed in this work..... 34
27. Virial coefficient behavior of the fundamental equation of Dillon and Penoncello 34
28. Isothermal behavior of the vapor density of ethanol..... 34
29. Isothermal behavior near the critical point of the fundamental equation developed in this work... 35
30. Isothermal behavior near the critical point of the fundamental equation of Dillon and Penoncello. 35
31. Isobaric heat capacity behavior of the fundamental equation developed in this work..... 35
32. Comparison of vapor-phase heat capacity data from Counsell *et al.* to the fundamental equation presented in this work. 35
33. Isobaric heat capacity behavior of the fundamental equation of Dillon and Penoncello..... 35
34. Isochoric heat capacity behavior of the fundamental equation developed in this work..... 35
35. Isochoric heat capacity behavior of the fundamental equation of Dillon and Penoncello. 36
36. Sound speed behavior of the fundamental equation developed in this work..... 36
37. Sound speed behavior of the fundamental equation of Dillon and Penoncello. 36
38. Characteristic curves for ethanol and R-125..... 36
39. Characteristic curves of the fundamental equation of Dillon and Penoncello. 36
40. Behavior of the rectilinear diameter for the fundamental equation developed in this work. 36

List of Symbols

Symbol	Physical quantity	Unit
a	Specific Helmholtz free energy	J mol^{-1}
B	Second virial coefficient	dm^3 mol^{-1}
C	Third virial coefficient	(dm^3 mol^{-1})^2
c	Speed of light in a vacuum	m s^{-1}
$c_p, \hat{c}_p$	Isobaric heat capacity	J mol^{-1} K^{-1}, kJ kg^{-1} K^{-1}
$c_v, \hat{c}_v$	Isochoric heat capacity	J mol^{-1} K^{-1}, kJ kg^{-1} K^{-1}
c_σ	Saturation heat capacity	J mol^{-1} K^{-1}
d	Exponent on density	
g	Specific Gibbs energy	J mol^{-1}
$h, \hat{h}$	Specific enthalpy	J mol^{-1}, kJ kg^{-1}
h	Planck constant	J s
k_B	Boltzmann constant	J K^{-1}
k	Exponent fit variable	
l	Exponent on density	
M	Molar mass	g mol^{-1}
N	Coefficient	
p	Pressure	MPa
R	Molar gas constant	J mol^{-1} K^{-1}
$s, \hat{s}$	Specific entropy	J mol^{-1} K^{-1}, kJ kg^{-1} K^{-1}
t	Exponent on temperature	
T	Temperature	K
u	Specific internal energy	J mol^{-1}
v	Molar volume	dm^3 mol^{-1}
w	Speed of sound	m s^{-1}
x	Coefficient for Eq. (19)	
y	Coefficient for Eq. (19)	
Z	Compressibility factor	
α	Reduced Helmholtz energy [$\alpha = a/RT$]	
β	Gaussian term coefficient	
γ	Gaussian term constant	
δ	Reduced density [$\delta = \rho/\rho_c$]	
ε	Gaussian term constant	
η	Gaussian term coefficient	
θ	Characteristic temperature	K
$\rho, \hat{\rho}$	Density	mol dm^{-3}, kg m^{-3}
σ	Standard deviation	
τ	Inverse reduced temperature [$\tau = T_c/T$]	
Φ	Rectilinear diameter of density	mol dm^{-3}
φ	Fugacity coefficient	
ν	Vibrational wave number	cm^{-1}
ω	Acentric factor	

Symbol	Physical quantity
	Superscripts
0	Ideal gas property
r	Residual property
$'$	Saturated liquid property
$''$	Saturated vapor property
	Subscripts
0	Reference state property
c	Critical point property
calc	Calculated using an equation
exp	Experimental value
i	Property of the ith constituent
l	Liquid-state property
nbp	Normal boiling point property
r	Reduced property (divided by critical property)
tp	Triple-point property
v	Vapor-state property
σ	Saturation property
	Accents
^	Mass-based property

This article is copyrighted as indicated in the article. Reuse of AIP content is subject to the terms at: http://scitation.aip.org/termsconditions. Downloaded to IP: 131.111.164.128 On: Tue, 21 Oct 2014 07:26:40

1. Introduction

Ethanol (C_2H_5OH) is an important chemical with many applications. It is a feedstock in many industrial processes, as well as an intermediate in the chemical synthesis of esters, organic and cyclic compound chains, detergents, paints, cosmetics, aerosols, perfumes, medicine, food, and others.[1] It is used extensively as a solvent and as a polar cosolvent in supercritical fluid technologies to enhance the solubility of solutes and improve the selectivity of supercritical solvents.[2] Aqueous mixtures of ethanol are also used as natural refrigerants and latent heat storage material.[3] Furthermore, ethanol is widely used as a fuel additive and alternative biofuel. The pervasiveness of ethanol in industrial applications demands an accurate, wide-range fundamental equation for ethanol.

1.1. Prior correlations of thermodynamic properties of ethanol

Table 1 summarizes existing equations of state for ethanol. The accuracy of these equations is determined by several factors, particularly the data selected for the correlation and the type of equation used. The fundamental equation of state published by Dillon and Penoncello[13] is the only existing equation of state for ethanol that is in the form of dimensionless Helmholtz energy. It covers a range of 250–570 K at pressures up to 280 MPa and was developed using linear fitting techniques. However, the equation exhibits unphysical behavior in the critical region. In particular, the critical isotherm has a negative slope at the critical point, where it should increase monotonically. The equation also exhibits poor extrapolation behavior.

Since the work of Dillon and Penoncello,[13] nonlinear equation fitting algorithms and equation forms have become available. Nonlinear fitting has many benefits over the linear algorithm and equation form. Primarily, it is better able to accurately model the critical region. The new algorithm also allows many more data types to be fit simultaneously, including heat capacities, saturation data, and others that could not be used directly in earlier work. Finally, nonlinear fitting results in a more flexible equation, thereby reducing the number of terms necessary for a good equation.

In addition to improved fitting techniques, new experimental data have become available in the open literature since Dillon and Penoncello[13] published their equation. Therefore, the purpose of this work was to develop a fundamental equation that fits the best available experimental data and improves upon the accuracy and extrapolation behavior of the equation by Dillon and Penoncello.[13]

1.2. The functional form of the fundamental equation

The fundamental equation presented in this work covers a range of temperatures from 160 to 650 K and pressures up to 280 MPa. The equation form chosen uses Helmholtz energy as the dependent variable, with independent variables of density, ρ, and temperature, T. Thus, the fundamental equation in its most general form is

$$a(\rho, T) = a^0(\rho, T) + a^r(\rho, T), \tag{1}$$

where $a^0(\rho, T)$ is the ideal-gas contribution to the Helmholtz energy, and $a^r(\rho, T)$ is the residual Helmholtz energy. The residual portion is included to account for intermolecular forces. This functional form is made more practical when it is in the form of dimensionless Helmholtz energy, α. Then Eq. (1) becomes

$$\frac{a(\rho, T)}{RT} = \alpha(\delta, \tau) = \alpha^0(\delta, \tau) + \alpha^r(\delta, \tau), \tag{2}$$

where R is the molar gas constant, and density and temperature have been reduced by the critical parameters to a dimensionless form, such that $\delta = \rho/\rho_c$ and $\tau = T_c/T$. Since the equation is in the form of Helmholtz energy, it is fundamental in nature and describes the entire thermodynamic surface. The Helmholtz energy fundamental equation is particularly useful because all other thermodynamic properties can be determined solely from derivatives of the dimensionless Helmholtz energy surface; no integration is necessary. This is important because derivatives of the fundamental equation are significantly easier to calculate than integrals. Subsequent sections in this work will describe the development of the functional forms of the ideal-gas contribution to the equation (Sec. 4) and the residual contribution to the equation (Sec. 5).

TABLE 1. Existing equations of state for ethanol

Author	Temperature range (K)	Pressure range (MPa)	Equation form	Year
Bhattacharyya and Thodos[4]	155–929	255	Density correlation	1965
Gomez-Nieto and Thodos[5]	349–623	0.008–45	Benedict-Webb-Rubin	1976
Cibulka and Nagata[6]	273–323	NR[a]	Association model	1987
Cho *et al.*[7]	NR	1200	Perturbed hard chain	1988
Lee and Chao[8]	364–511	NR	Augmented BACK	1988
Sun *et al.*[9]	273–333	280	Tait equation	1989
Massucci and Wormald[10]	348–631	0.04–6.1	Cubic equation	1992
Sauermann *et al.*[11]	263–457	0.01–0.032	Strobridge equation	1995
Fotouh and Shukla[12]	242–514	6.15	Peng-Robinson	1997
Dillon and Penoncello[13]	250–570	0–280	Dimensionless Helmholtz	2002
Kiselev *et al.*[14]	NR	NR	GC SAFT	2005

[a]NR = not reported.

This article is copyrighted as indicated in the article. Reuse of AIP content is subject to the terms at: http://scitation.aip.org/termsconditions. Downloaded to IP: 131.111.164.128 On: Tue, 21 Oct 2014 07:26:40

TABLE 2. Physical constants and characteristic properties of ethanol

Symbol	Physical quantity	Value	Units
R	Molar gas constant	8.314 4621	J mol^{-1} K^{-1}
M	Molar mass	46.068 44	g mol^{-1}
ω	Acentric factor	0.646	
T_c	Critical temperature	514.71	K
p_c	Critical pressure	6.268	MPa
ρ_c	Critical density	5.93	mol dm^{-3}
T_{tp}	Triple-point temperature	159	K
p_{tp}	Triple-point pressure	7.185×10^{-10}	MPa
ρ_{tpv}	Vapor density at the triple point	5.43×10^{-10}	mol dm^{-3}
ρ_{tpl}	Liquid density at the triple point	19.731	mol dm^{-3}
T_{nbp}	Normal boiling point temperature	351.57	K
ρ_{nbpv}	Vapor density at the normal boiling point	0.0358	mol dm^{-3}
ρ_{nbpl}	Liquid density at the normal boiling point	15.985	mol dm^{-3}
T_0	Reference temperature for ideal gas properties	273.15	K
p_0	Reference pressure for ideal gas properties	0.001	MPa
h_0^0	Reference ideal gas enthalpy at T_0	52 811.79	J mol^{-1}
s_0^0	Reference ideal gas entropy at T_0	209.5830	J mol^{-1} K^{-1}

This work also contains an ideal gas heat capacity equation and ancillary equations for the vapor pressure and saturation density curves. The ideal gas heat capacity equation is an integral part of the fundamental equation. However, the ancillary equations are generally only used as an initial estimate in the iterative process of fitting the residual portion of the fundamental equation or as an initial estimate of the saturation states.

The equation developed in this work is based on experimental data collected from an extensive literature review. Data forms used to fit the equation include pressure–density–temperature, isobaric heat capacity, sound speed, ideal gas heat capacity, vapor pressure, and saturated liquid density. Data were selected based on sample purity, experimental accuracy, and comparison to data in similar regions.

1.3. Physical constants and characteristic properties

Table 2 provides a list of physical constants and reference properties used in this work. It also includes several characteristic properties of ethanol as calculated by the equation of state developed in this work.

2. Experimental Data

The units chosen for this work were MPa for pressure, mol dm^{-3} for density, K for temperature, J for energy, and m s^{-1} for sound speed. All experimental data were converted from their original units to these units, as necessary. All temperatures were converted to the ITS–90 scale.

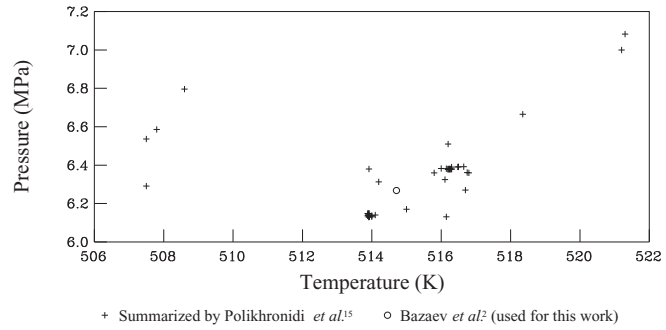

FIG. 1. Distribution of pressure-temperature critical data.

2.1. Critical point data

A vast amount of data exists for the critical point of ethanol. These data are summarized by Polikrhonidi *et al.*[15] The data exhibit a significant amount of scatter, as shown in Figs. 1 and 2. The data are clearly bimodal for the critical temperature and pressure. The critical temperature data lie mostly near 513.9 and 516.2 K, and the critical pressure data lie near 6.15 and 6.38 MPa. The critical density has a single mode near 6.0 mol dm^{-3}. The scatter results from two difficulties. First, critical properties are difficult to measure and have a high level of uncertainty. Second, ethanol has a strong affinity for water; impurities of water in samples of ethanol have a strong effect on the experimental results. Higher water content in a sample produces higher critical temperatures and pressures.[16] In general, reported sample purity was higher for the data at pressures near 6.15 MPa than for the data near 6.38 MPa. The critical point recommended by Bazaev *et al.*[2] ($T_c = 514.71$ K, $p_c = 6.268$ MPa, $\rho_c = 5.93$ mol dm^{-3}) falls between the two groups, but appears to be of excellent quality. Their critical point was selected for this work.

2.2. Pressure–density–temperature data

Many data sources exist for the pressure–density–temperature ($p\rho T$) relationship of ethanol. These are all listed in Table 3. Of these, a selection of data has been mapped out on pressure-temperature coordinates in Fig. 3. Many sources listed in Table 3 only provide data at atmospheric pressure or near room temperature. For the sake of clarity, these data have

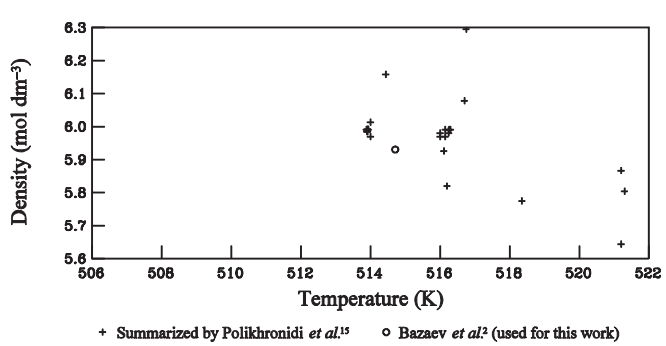

FIG. 2. Distribution of density-temperature critical data.

This article is copyrighted as indicated in the article. Reuse of AIP content is subject to the terms at: http://scitation.aip.org/termsconditions. Downloaded to IP: 131.111.164.128 On: Tue, 21 Oct 2014 07:26:40

TABLE 3. Summary of $p\rho T$ data

Author	Points	p (MPa)	ρ (mol dm^{-3})	T (K)
Álvarez *et al.*[17]	6	0.101	16.8–17.2	288–313
Aminabhavi and Patil[18]	3	0.101	16.9–17.1	298–308
Aralaguppi *et al.*[19]	3	0.101	16.9–17.0	298–308
Aralaguppi and Baragi[20]	3	0.101	16.9–17.1	298–308
Arbusow[21]	5	0.1–0.101	16.0–16.1	351
Bazaev *et al.*[2]	158	0.224–40.3	1.99–10.8	373–673
Benson and D'Arcy[22]	2	0.101	16.9–17.2	288–308
Bhagwat and Subnis[23]	7	0.101	16.8–17.3	303–323
Bich *et al.*[24]	34	0.039–0.171	0.014–0.033	348–631
Bridgman[25]	126	0.039–463	16.0–23.3	293–353
Dzida and Marczak[26]	6	0.101	16.7–17.1	293–318
Easteal and Woolf[27]	6	50–250	0.023–0.025	298
García-Miaja *et al.*[28]	6	0.101	16.7–17.1	293–318
Golik[29]	8	0.101	15.7–17.1	293–363
Golubev *et al.*[30]	106	1–50	2.37–19.5	200–570
Gómez *et al.*[31]	3	0.101	16.5–17.0	298–328
Gonçalves *et al.*[1]	175	0.1–35	16.0–17.9	278–353
González *et al.*[32]	3	0.1	17.0–17.1	293–303
Gupta and Hanks[33]	24	2.76–22.1	15.8–17.9	273–363
Hilczer and Goc[34]	7	8.11–44.6	17.1–17.7	298
Hu *et al.*[35]	5	0.101	16.9–17.0	298–303
Hugo *et al.*[36]	195	0.1–300	17.8–21.0	180–253
Kadam *et al.*[37]	2	0.101	16.8–17.0	298–308
Kalafati *et al.*[38]	216	0.875–21.5	0.259–14.2	423–573
Khasanshin and Aleksandrov[39]	22	0.101	16.0–19.7	159–351
Kitajima *et al.*[40]	116	5.74–28.9	15.3–17.6	283–418
Kubota *et al.*[41]	46	0.1–310	16.5–19.7	298–323
Langa *et al.*[42]	3	0.101	16.8–17.3	283–313
Lasarte *et al.*[43]	15	0.1–20	16.8–17.7	283–313
Ling and Van Winkle[44]	3	0.101	16.1–16.9	303–348
Lo and Stiel[45]	162	8.27–68.9	4.66–15.2	473–623
Matkowska *et al.*[46]	117	0.1–35	16.2–17.9	283–343
Mutalik *et al.*[47]	3	0.101	16.9–17.1	298–308
Nikam *et al.*[48]	7	0.101	16.8–17.0	298–313
Ormanoudis *et al.*[49]	12	0.101–33.8	16.9–17.6	288–308
Ortega[50]	6	0.101	16.7–17.1	293–318
Ozawa *et al.*[51]	44	0.1–196	16.1–19.3	298–348
Papaioannou *et al.*[52]	12	0.101–33.8	16.9–17.6	288–308
Papaioannou *et al.*[53]	10	0.1–33.9	17.0–17.6	298
Pečar and Določek[54]	15	0.1–40	16.1–17.7	298–348
Peleteiro *et al.*[55]	5	0.101	16.9–17.2	288–308
Peleteiro *et al.*[56]	7	0.101	16.9–17.4	278–308
Rattan *et al.*[57]	2	0.101	16.9–17.1	298–308
Rodríguez *et al.*[58]	4	0.101	16.8–17.1	293–313
Sauermann *et al.*[11]	97	0.1–56.7	13.6–17.9	263–483
Schroeder *et al.*[59]	25	0.101	17.1–18.4	223–293
Sommer *et al.*[60]	222	0–30.0	12.1–18.6	233–473
Takiguchi and Uematsu[61]	116	0.015–200	15.8–19.1	310–363
Takiguchi and Uematsu[3]	259	0.1–200	11.7–19.1	310–480
Tammann and Ruhenbeck[62]	113	0.098–245	10.3–19.8	293–673
Tanaka *et al.*[63]	44	7.01–310	16.8–19.7	298–323
Tu *et al.*[64]	3	0.101	16.7–17.0	298–318
Vercher *et al.*[65]	6	0.101	16.5–17.4	278–328
Walsh and Rice[66]	2	4730–11000	27.2–30.6	294–299
Wankhede *et al.*[67]	4	0.101	16.9–17.1	293–308
Watson *et al.*[68]	70	0.1–65	16.4–18.1	293–333
Watts and Louie[69]	37	0.014–14.9	15.2–17.1	308–384
Wilson *et al.*[70]	65	0.055–0.387	0.015–0.124	373–473
Yusa *et al.*[71]	24	37–208	17.2–19.3	298–328
Zafarani-Moattar and Tohidifar[72]	5	0.101	16.5–17.2	288–328
Zéberg-Mikkelsen *et al.*[73]	79	0.1–45	16.1–18.0	283–353

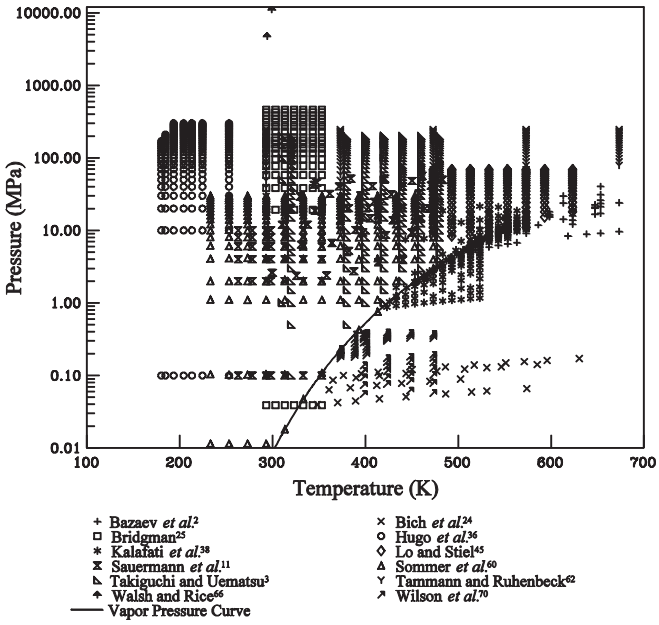

FIG. 3. Representative distribution of experimental $p\rho T$ data.

been excluded from Fig. 3 and are not discussed further in this review. However, all data are compared to the fundamental equation in Sec. 6.

Bazaev *et al.*[2] used a constant-volume method to determine both one- and two-phase density data of ethanol (99.8 mol. % purity). The uncertainties of the density, temperature, and pressure measurements were 0.15%, 15 mK, and 0.05%, respectively. Bich *et al.*[24] reported density data on ethanol (0.02 wt. % moisture content and 0.001 wt. % impurities). These data were also used to determine second virial coefficients. The data of Bridgman[25] were obtained with a piston and cylinder apparatus. No purity was reported; however, the presence of some water and inorganic impurities in the sample is acknowledged.

Golik *et al.*[29] listed density data. However, reported values appear to be smoothed from the experimental data. Golubev *et al.*[30] reported density data for ethanol (99.84% purity) with an uncertainty of 0.1% for densities higher than 6.51 mol dm^{-3} and up to 0.3% for smaller densities. The measurements were performed with a hydrostatic weighing method. However, the experimental data have been smoothed. Gonçalves *et al.*[1] used a vibrating-tube densimeter to obtain density data with an estimated uncertainty of 0.5 kg m^{-3}. The sample (99.8 wt. % original purity) was purified by using molecular sieves. Gupta and Hanks[33] measured specific volumes of ethanol (99.9% purity) in a pressurized cylinder. The precision of the volume measurements was reported as ± 0.01 cm^3 mol^{-1}. Dillon and Penoncello[13] noted that these data should be considered for future work.

Hugo *et al.*[36] reported specific volumes of ethanol (99.85% purity, less than 0.13% water content) for both the liquid and solid states. Measurements were taken by inductively recording the displacement of a moving piston. The experimental

This article is copyrighted as indicated in the article. Reuse of AIP content is subject to the terms at: http://scitation.aip.org/termsconditions. Downloaded to IP: 131.111.164.128 On: Tue, 21 Oct 2014 07:26:40

uncertainty was estimated to be 0.5%. Kalafati *et al.*[38] used a constant-volume piezometer to determine specific volumes. However, the sample was a mixture of 96% ethanol and 4% water. Kitajima *et al.*[40] reported densities of ethanol (99.8 vol. % purity) with an uncertainty of 0.16%. The data were determined by weighing the sample and placing it in a calorimeter of known volume. Kubota *et al.*[41] used a modified Adams piezometer to measure the specific volume of ethanol (99.9 wt. % purity). The uncertainty of these measurements was stated to be 0.09%.

Lasarte *et al.*[43] measured the density of ethanol (99.8 mol. % purity) using an apparatus based on the vibrating-tube principle. The experimental uncertainty of the density is 0.5 kg m^{-3}. Lo and Stiel[45] report compressibility factors for ethanol (99.95% purity). The data were obtained by a constant-volume method and are estimated to have an uncertainty of 0.4%. However, the data reported have been smoothed. Matkowska *et al.*[46] used a vibrating-tube densimeter to determine densities of ethanol. The original purity was 99.9%, but was dried over molecular sieves over several days and found to have a final water content of 23 ppm. The measurement uncertainty was estimated to be 0.04 kg m^{-3}. Ozawa *et al.*[51] determined the specific volume of ethanol (99.9 mol. % purity) in a glass piezometer tube with a glass float. The estimated uncertainty of the measurements is 0.2%, based on a comparison with the data of Bridgman.[25] Pečar and Določek[54] provided extensive data on water-ethanol mixtures as well as data for pure ethanol (99.8 wt. % purity with less than 0.2 wt. % water content). Measurements were carried out with a vibrating-tube densimeter and had an estimated uncertainty of 0.1 kg m^{-3}.

Sauermann *et al.*[11] used two different apparatuses to measure the density of ethanol (99.90 vol. % purity before being dried over molecular sieves). For isothermal measurements at low temperatures, a vibrating-tube densimeter yielded data with an uncertainty of 0.023%. Isochoric measurements at higher temperatures were taken in a constant-volume vessel with an uncertainty of 0.06%. Sommer *et al.*[60] used a single-sinker densimeter, based on the Archimedes buoyancy principle, to determine densities for liquid ethanol (99.9 wt. % purity before degassing). The uncertainty of the data was estimated to be 0.015% within a 95% confidence interval.

Takiguchi and Uematsu[3] measured the density of ethanol (99.5 vol. % purity before fractional distillation and drying by molecular sieve) with a metal-bellows variable volumometer. The estimated uncertainty was 0.10%. Takiguchi and Uematsu[61] performed density measurements over a narrower range of temperatures with the same method, purity, and uncertainty. Tanaka *et al.*[63] utilized a modified Adams piezometer to obtain specific volume measurements of ethanol (99.5 vol. % purity before fractional distillation). The estimated uncertainty of the measurements was 0.05%. Walsh and Rice[66] used a shock-wave-reflection method to determine very-high-pressure densities of ethanol. No purity or uncertainty was reported. Watson *et al.*[68] calculated high-pressure density data for ethanol (99.8 vol. % purity) with a vibrating-tube densimeter. The estimated uncertainty was 0.5 kg m^{-3}.

Watts and Louie[69] measured densities of liquid ethanol (99.5% purity) with an equilibrium cell and a liquid densimeter. The manufacturer of the densimeter reported an overall uncertainty of 0.5 kg m^{-3}. Wilson *et al.*[70] used a Kay-type PVT tube to determine the specific volume of ethanol (200 proof, dried over activated silica gel). The maximum uncertainty of the measurements was reported to be 0.25%. Dillon and Penoncello[13] found these data to be inappropriate for their fundamental equation. Yusa *et al.*[71] collected compression data for ethanol (99.90% purity) with a piston and cylinder arrangement. The experimental uncertainty was 1.20%. Zéberg-Mikkelsen *et al.*[73] utilized a vibrating-tube densimeter to take density measurements for ethanol (99.9% purity). The estimated uncertainty was 0.1 kg m^{-3}.

2.3. Isobaric heat capacity data

Numerous authors report isobaric heat capacity data for ethanol. These are summarized in Table 4. Figure 4 represents the full range of isobaric heat capacity data for ethanol on pressure-temperature coordinates. Most of the works listed in Table 4 only report data at atmospheric pressure, for temperatures of 200–300 K. For the sake of clarity, these are not included in Fig. 4, and most are not discussed further. However, all data are compared to the fundamental equation in Sec. 6.

Counsell *et al.*[77] measured vapor-phase isobaric heat capacities of ethanol (99.95 mol. %) in a vapor-flow calorimeter. No experimental uncertainty was stated. Dong *et al.*[78] used a

TABLE 4. Summary of isobaric heat capacity data

		p (MPa)		T (K)	
Author	Points	Min	Max	Min	Max
Bennewitz and Rossner[74]	2	0.1	0.1	164	350
Benson and D'Arcy[22]	2	0.101	0.101	288	308
Blacet *et al.*[75]	9	0.101	0.101	303	343
Bose[76]	8	0.101	0.101	278	315
Counsell *et al.*[77]	25	0.025	0.101	330	475
Dong *et al.*[78]	24	0.034	0.101	331	424
Eucken and Franck[79]	7	0.101	0.101	203	351
Fiock *et al.*[80]	8	0.101	0.101	313	383
Fortier *et al.*[81]	2	0.101	0.101	298	298
Fulem *et al.*[82]	16	4.9	4.9	326	471
Garcia-Miaja *et al.*[28]	6	0.101	0.101	293	318
Gibson *et al.*[83]	11	0.101	0.101	196	271
Haida *et al.*[84]	46	0.101	0.101	182	301
Hwa and Ziegler[85]	41	0.101	0.101	165	304
Kelley[86]	20	0.101	0.101	164	294
Khasanshin and Aleksandrov[39]	22	0.101	0.101	159	351
Mazur[87]	34	0.101	0.101	192	298
Mitsukuri and Hara[88]	25	0.101	0.101	184	269
Parks[89]	7	0.101	0.101	160	298
Pedersen *et al.*[90]	16	0.101	0.101	301	344
Peleteiro *et al.*[55]	4	0.101	0.101	288	303
Peleteiro *et al.*[56]	5	0.101	0.101	283	303
Rivkin and Vinnikova[91]	6	0.101	0.101	298	323
Sinke and De Vries[92]	9	0.1	0.1	354	437
Stephens and Olson[93]	11	0.101	0.101	266	318
Strömsöe *et al.*[94]	12	0.101	0.101	357	591
Vercher *et al.*[65]	6	0.101	0.101	278	328
Veselý *et al.*[95]	3	0.101	0.101	298	318
Williams and Daniels[96]	7	0.101	0.101	301	330
Yu *et al.*[97]	4	0.101	0.101	405	515

This article is copyrighted as indicated in the article. Reuse of AIP content is subject to the terms at: http://scitation.aip.org/termsconditions. Downloaded to IP: 131.111.164.128 On: Tue, 21 Oct 2014 07:26:40

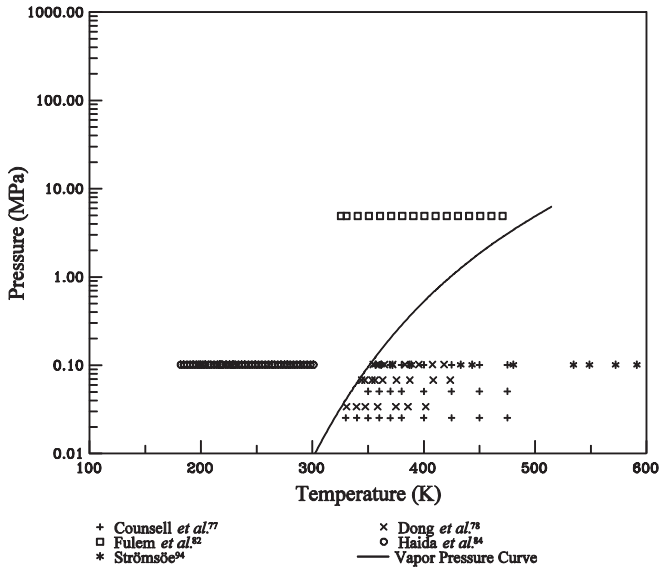

FIG. 4. Representative distribution of experimental isobaric heat capacity data.

Newsham vaporization calorimeter as well as a Pitzer gaseous heat capacity flow calorimeter to collect data. The sample purity was stated to be 99.95%. Experimental uncertainties were estimated to be 0.4%. Fulem *et al.*[82] measured liquid-phase heat capacities of ethanol (99.99 mol. %) using a commercial heat conduction calorimeter (SETARAM C–80). The estimated uncertainty was 1%. The authors noted that these data could legitimately be considered saturation heat capacity data, since they are so close to the saturated liquid curve; however, they were not used in this work.

Haida *et al.*[84] used an adiabatic calorimeter to measure liquid- and glassy-phase heat capacity data for ethanol (99.86 mol. %). No experimental uncertainty was listed. Hwa and Ziegler[85] measured heat capacities of ethanol (99.95 mol. %) using an adiabatic calorimeter. The estimated uncertainty of their measurements was 0.2%. Kelley[86] measured heat capacities of ethanol (99.96%) with a stated uncertainty of 1%. The data from Khasanshin and Aleksandrov[39] were smoothed from experimental data.

Sinke and De Vries[92] measured heat capacities of vapor-phase ethanol in a flow calorimeter. No sample purity was reported. The experimental uncertainty of the measurements was reported to be 0.2 cal mol^{-1} K^{-1} (or roughly 1%). Strömsöe *et al.*[94] measured heat capacities of vapor-phase ethanol (99.8 vol. %), using a flow calorimeter. The estimated uncertainty of the heat capacity measurements was 0.3%.

2.4. Isochoric heat capacity data

Only two sources report isochoric heat capacity data. These are both listed in Table 5 and mapped out on temperature-density coordinates in Fig. 5.

Kitajima *et al.*[40] used an adiabatic twin-cell calorimeter to measure liquid-phase, isochoric heat capacities of ethanol (99.8 mass%, including 0.08 mass% water). The estimated uncertainty of isochoric heat capacity measurements was 2.2%. Polikhronidi *et al.*[15] reported isochoric heat capacity for ethanol (99.97 mol. %) in both the single- and two-phase regions, but only comparisons to single-phase data have been included in this work. Measurements were taken in a high-temperature and pressure, adiabatic, nearly constant-volume calorimeter. The estimated uncertainty of the measurements was 2%–3% in the near-critical and supercritical regions, 1.0%–1.5% in the liquid phase, and 3%–4% in the vapor phase.

TABLE 5. Summary of isochoric heat capacity data

Author	Points	ρ (mol dm^{-3}) Min	ρ (mol dm^{-3}) Max	T (K) Min	T (K) Max
Polikhronidi *et al.*[15]	371	4.2	7.93	493	541
Kitajima *et al.*[40]	116	15.3	17.6	283	418

2.5. Sound speed data

Table 6 summarizes all sound speed data. Figure 6 shows a plot of a selection of the sound speed data on temperature-pressure coordinates. The data selected for Fig. 6 are representative of the entire region covered by sound speed data found in the literature. For the sake of clarity, sources that only reported sound speed data at atmospheric pressure were not included in Fig. 6. Most of these are not discussed further.

Alexandrov and Kochetkov[98] measured the speed of sound of ethanol (99.94% pure) for 5.6 MHz ultrasonic waves. They reported the raw data, as well as data corrected for water content of the sample. The correction factor reduced the speed of sound by approximately 0.3 m/s. Álvarez *et al.*[17] used an Anton Paar DSA 5000 vibrating-tube densimeter and sound analyzer to measure sound speeds of ethanol (>99% purity). No experimental uncertainty was given. Brown *et al.*[99] measured the speed of sound of ethanol (purity not specified) with an uncertainty of 1%. They used a diamond-anvil high-pressure cell and a laser-induced phonon spectroscopy technique to take measurements. Carnevale and Litovitz[100] utilized a high-pressure ultrasonic

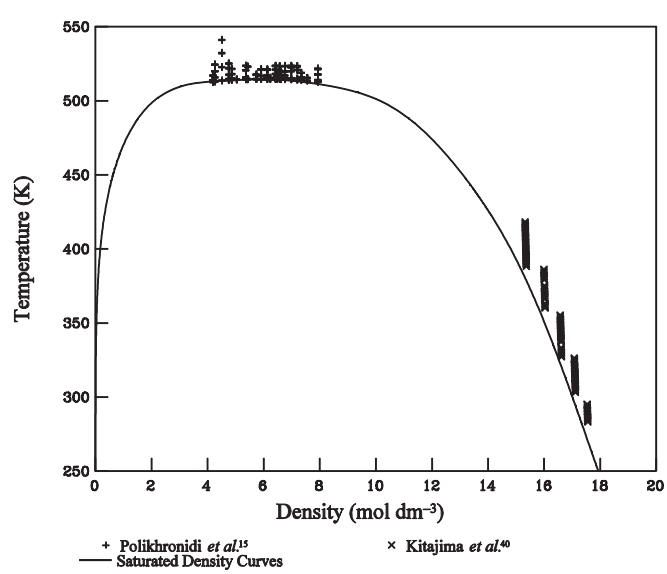

FIG. 5. Distribution of experimental isochoric heat capacity data.

This article is copyrighted as indicated in the article. Reuse of AIP content is subject to the terms at: http://scitation.aip.org/termsconditions. Downloaded to IP: 131.111.164.128 On: Tue, 21 Oct 2014 07:26:40

TABLE 6. Summary of sound speed data

Author	Points	p (MPa) Min	p (MPa) Max	T (K) Min	T (K) Max
Alexandrov and Kochetkov[98]	24	0.101	0.101	159	268
Álvarez *et al.*[17]	6	0.101	0.101	288	313
Brown *et al.*[99]	8	0.1	3190	298	298
Carnevale and Litovitz[100]	5	0.098	196	303	303
Dzida and Marczak[26]	90	0.101	91.5	293	318
Eden and Richardson[101]	3	49	98.1	293	293
Freyer *et al.*[102]	6	0.101	0.101	273	323
García-Miaja *et al.*[28]	6	0.101	0.101	293	318
Golik[29]	5	0.101	0.101	293	333
Gomez-Nieto and Thodos[5]	3	0.101	0.101	298	328
González *et al.*[32]	3	0.1	0.1	293	303
Hawley *et al.*[103]	8	0.098	479	303	303
Kadam *et al.*[37]	2	0.101	0.101	298	308
Khasanshin and Aleksandrov[39]	22	0.101	0.101	159	351
Langa *et al.*[42]	3	0.101	0.101	283	313
Onori[104]	7	0.101	0.101	283	313
Peleteiro *et al.*[55]	5	0.101	0.101	288	308
Rattan *et al.*[57]	2	0.101	0.101	298	308
Rodríguez *et al.*[58]	4	0.101	0.101	293	313
Sakurai *et al.*[105]	5	0.101	0.101	278	318
Sun *et al.*[106]	120	0.1	276	193	263
Sun *et al.*[107]	105	0.1	275	274	333
Vercher *et al.*[65]	6	0.101	0.101	278	328
Walsh and Rice[66]	2	4730	11000	294	299
Wankhede *et al.*[67]	3	0.101	0.101	298	308
Wilson and Bradley[108]	48	0.101	96.5	273	323
Zafarani-Moattar and Tohidifar[72]	5	0.101	0.101	288	328

measurement technique to collect data on reagent-grade ethanol. The measurement uncertainty was 0.2%.

Dzida and Marczak[26] measured sound speeds of ethanol using two vessels with the same acoustic path and construction, a ceramic transducer, and an acoustic mirror. One vessel was used for measurements at atmospheric pressure, the other was used for measurements under pressure. Measurements were based on the pulse-echo-overlap method. The sample purity of the ethanol was 99.8% by mass, before it was dried over 0.3 nm molecular sieves. The final mass fraction water content was less than 1.5×10^{-7}. Measurement uncertainty for the speed of sound was estimated to be 0.04% for pressures up to 60 MPa and 0.05% for higher pressures.

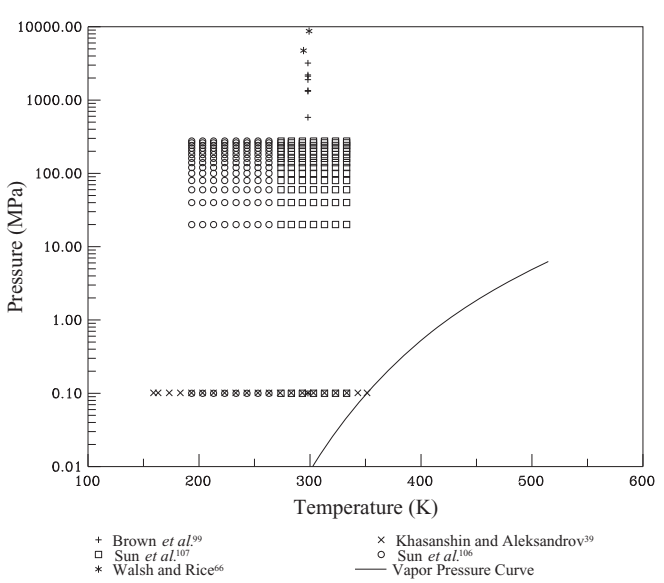

FIG. 6. Representative distribution of experimental sound speed data.

Eden and Richardson[101] measured speeds of sound in a refrigerated, pressurized vessel with an interferometer. Neither the sample purity nor the experimental accuracy was reported. Freyer *et al.*[102] also used a sonic interferometer to measure sound speeds with an accuracy of ± 1 m s^{-1}. The sample purity was checked by ensuring a boiling temperature within ± 0.1 °C of the accepted value from the literature. Garcia-Miaja *et al.*[28] used an Anton-Paar DSA48 sound analyzer to collect their data. The experimental uncertainty was not given. The sample was 99.9% pure by mass, before being dried over 0.3 nm molecular sieves. Golik *et al.*[29] used an ultrasonic interferometer to measure speed of sound data. Sample purity and experimental uncertainty were not specified.

Hawley *et al.*[103] used an acoustic chamber with a quartz transducer and a polished reflector to collect sound speed data. No sample purity or experimental uncertainty was reported. Khasanshin and Aleksandrov[39] report sound speed data over a broad range of temperatures, up to the atmospheric boiling point. However, all values have been calculated from a correlation based on data from other authors. Thus, this data set was not used for this work. Onori[104] measured ultrasonic velocities with a sing-around velocimeter. Measurements were reproducible to within ± 0.1 m s^{-1}; however, no sample purity was reported. Peleteiro *et al.*[55] used an Anton-Paar DSA–48 sound analyzer to determine sound speed data with an uncertainty of 1 m s^{-1}. The sample had a purity greater than 99.5% before being partially degassed and dried over 0.4 nm molecular sieves.

Sakurai *et al.*[105] used a sing-around velocimeter to measure sound speeds at a frequency of 5 MHz. Neither the experimental uncertainty nor the sample purity was given. However, the sample was purified by fractional distillation and stored over molecular sieves. Sun *et al.*[106,107] used a phase-comparison, pulse-echo technique to collect a large amount of liquid-phase sound speed data. Together, their measurements cover a very broad range of temperatures and extend to very high pressures. The experimental uncertainty for sound speed was 0.03% for temperatures above 273 K and 0.05% for temperatures below 273 K. Sample purity was better than 99.7 vol. %, with the main impurity being water (<0.2%).

Vercher *et al.*[65] used an Anton-Paar DSA–5000 to measure sound speed data at atmospheric pressure. The experimental uncertainty was estimated to be 0.05 m s^{-1}. Sample purity was 99.9% by mass, before being degassed and dried over molecular sieves. Walsh and Rice[66] used explosives to generate strong shock waves in liquid ethanol. This created extremely high pressure conditions, from which they collected two sound speed data points. The uncertainty was estimated to be 0.5%. No sample purity was given. Wilson and Bradley[108] collected sound speed data by measuring the time required for a pulse to travel between two crystal transducers. The experimental

This article is copyrighted as indicated in the article. Reuse of AIP content is subject to the terms at: http://scitation.aip.org/termsconditions. Downloaded to IP: 131.111.164.128 On: Tue, 21 Oct 2014 07:26:40

uncertainty was given as 0.56 m s^{-1} or better. The sample purity was 99.8 vol. %.

2.6. Second virial coefficient data

Twelve sources reported second virial coefficient data. No data were available for the third virial coefficient. The ranges of available data for the second virial coefficient are summarized in Table 7.

Abusleme and Vera[109] report second virial coefficients for ethanol with an estimated sample purity of 99.7%. They used a low-pressure Burnett-type apparatus with an estimated experimental uncertainty of 40 cm^3 mol^{-1}. Aucejo *et al.*[110] derived second virial coefficients for ethanol based on vapor-liquid equilibrium. The sample purity was 99.5 vol. %, and no experimental uncertainty was given. Barker *et al.*[111] determined second virial coefficients based solely on the experimental heat of vaporization data of Fiock *et al.*[80] Barrow[112] listed second virial coefficients for ethanol based on calculations from the Clapeyron equation.

Bich *et al.*[24] obtained second virial coefficient data for ethanol based on isochoric measurements of pressure as a function of temperature. The sample contained 0.02 wt. % water and 0.001 wt. % other impurities. No experimental uncertainty was listed; however, measurements above 493.15 K exhibited strong systematic deviations from the behavior they expected. The authors suggested that this deviation was due to decomposition. Knoebel and Edmister[113] determined second virial coefficient data for ethanol based on a least-squares analysis of their $p\rho T$ data. No experimental uncertainty or sample purity was listed.

Kretschmer and Wiebe[114] determined second virial coefficients for ethanol based on $p\rho T$ measurements. The sample was estimated to have less than 0.01% water content. The estimated uncertainty for the data was 5 cm^3 mol^{-1} at 393 K and 100 cm^3 mol^{-1} at 313 K. No information is given regarding the second virial coefficient data of Lambert.[115] Massucci *et al.*[116] determined second virial coefficient data for ethanol based on calorimetric measurements. The uncertainty of the data ranges from 50 cm^3 mol^{-1} at 300 K to 2 cm^3 mol^{-1} at 600 K. The sample purity was given as 99.7 mol. %. Noppe *et al.*[117] determined the second virial coefficient of ethanol based on pressure and temperature data. They listed no sample purity or experimental uncertainty.

Tsonopoulos *et al.*[118] recommended values based on the data of Kretschmer and Wiebe[114] and Bich *et al.*[24] They list uncertainties ranging from 15 cm^3 mol^{-1} (7.7%) at 540 K to 100 cm^3 mol^{-1} (8.3%) at 340 K. Wilson *et al.*[70] determined second virial coefficient data for ethanol based on $p\rho T$ data. They report using a sample of absolute 200 proof. The estimated uncertainty of the data is less than 100 cm^3 mol^{-1} for all but one data point (95% confidence limit).

TABLE 7. Summary of second virial coefficient data

Author	Points	T (K) Min	T (K) Max
Abusleme and Vera[109]	6	343	363
Aucejo *et al.*[110]	24	326	349
Barker *et al.*[111]	2	318	338
Barrow[112]	4	323	473
Bich *et al.*[24]	21	373	573
Knoebel and Edmister[113]	3	333	373
Kretschmer and Wiebe[114]	5	313	393
Lambert[115]	10	322	399
Massucci *et al.*[116]	16	300	600
Noppe *et al.*[117]	6	400	525
Tsonopoulos *et al.*[118]	11	340	540
Wilson *et al.*[70]	7	373	473

2.7. Vapor pressure data

Table 8 summarizes all vapor pressure data. Data were available over a range of temperatures from 174 K to the critical point. However, there is a great deal of scatter in the data below the normal boiling point. Timmermans[122] listed vapor pressure data from several authors. These included Bachmann, Crafts, Dreisbach and Shrader, Drucker *et al.*, Ferguson *et al.*, Kahlbaum and Wirkner, Konovalow, Schmidt,

TABLE 8. Summary of vapor pressure data

Author	Points	p (MPa) Min	p (MPa) Max	T (K) Min	T (K) Max
Ambrose and Sprake[119]	25	0.006	0.179	293	367
Ambrose *et al.*[120]	23	0.168	6.150	365	514
Amer *et al.*[121]	12	0.039	0.100	329	351
Aucejo *et al.*[110a]	22	0.030	0.130	324	358
Bachmann[b]	1	0.004	—	288	—
Bazaev *et al.*[2]	9	0.226	6.080	373	513
Crafts[b]	5	0.005	0.232	291	373
Deák *et al.*[123]	20	0.503	6.140	398	514
Devyatko and Stabnikov[124]	49	0.000	6.390	208	516
Dreisbach and Shrader[b]	3	0.016	0.068	311	342
Drucker *et al.*[b]	10	0.000	0.000	174	234
Dulitskaya[125]	3	0.008	0.089	298	348
Ferguson *et al.*[b]	1	0.010	—	303	—
Figurski and Malanowski[126]	17	0.013	0.098	307	351
Fiock *et al.*[80]	15	0.002	0.576	273	403
Kahlbaum and Wirkner[b]	38	0.003	0.101	281	351
Khurma *et al.*[127]	3	0.008	0.505	298	399
Konovalow[b]	5	0.006	0.102	292	352
Kretschmer and Wiebe[128a]	8	0.002	0.102	273	352
Lee and Hu[129]	6	0.075	0.159	344	363
Lydersen and Tsochev[130]	12	2.660	6.170	469	515
Merriman[131]	61	0.001	0.224	271	373
Mishchenko and Subbotina[132]	22	0.002	0.024	277	319
Mousa[133]	33	0.020	6.330	319	516
Pokki *et al.*[134]	13	0.021	0.101	316	351
Sauermann *et al.*[11]	21	0.048	2.960	334	473
Schmidt[b]	32	0.004	0.101	287	351
Schouteden and Deveux[b]	9	0.006	0.131	295	359
Swietoslawski and Zlotowski[b]	6	0.102	0.253	352	376
Takiguchi and Uematsu[61]	3	0.015	0.141	310	360
Takiguchi *et al.*[135]	27	0.015	0.524	310	400
Tower and Germann[b]	1	0.004	—	288	—
Watts and Louie[69]	12	0.010	0.320	308	384
Wilhoit and Zwolinski[136]	24	0.001	0.159	270	363
Wolff and Götz[137]	7	0.006	0.106	293	353
Young[b]	22	0.002	6.380	273	516

[a]Data used to fit Eq. (9).
[b]As reported by Timmermans.[122]

This article is copyrighted as indicated in the article. Reuse of AIP content is subject to the terms at: http://scitation.aip.org/termsconditions. Downloaded to IP: 131.111.164.128 On: Tue, 21 Oct 2014 07:26:40

Schouteden and Deveux, Swietoslawski and Zlotowski, Tower and Germann, and Young. Most of these sources were from 1925 or earlier, and the original sources were not retrieved for this work. Furthermore, their data exhibit substantial scatter. For these reasons, they are not discussed further or shown in deviation plots, for the sake of clarity.

Ambrose and Sprake[119] used comparative ebulliometry to determine vapor pressures of alcohol (99.95 mol. % purity). No measurement uncertainty was listed. Ambrose *et al.*[120] measured vapor pressures at higher pressures, up to the critical point. However, they listed no sample purity or measurement uncertainty. The data listed by Amer *et al.*[121] are based on an equation fit of data reported by Kretschmer and Wiebe[128] and Merriman.[131] Aucejo *et al.*[110] measured vapor pressures of ethanol (99.5 vol. %) using a dynamic recirculating still (all-glass Fischer LABODEST VLE apparatus model 602/D). The accuracy of temperature measurements was ±0.1 K. The uncertainty of lower pressure measurements is 0.01 kPa, while the uncertainty of higher pressure measurements is 0.1 kPa.

Bazaev *et al.*[2] reported vapor pressure of ethanol (99.8 mol. %) near the critical region. The data were acquired by using an analytical extrapolation technique, based on their $p\rho T$ data. Deák *et al.*[123] measured vapor pressure data of ethanol using a high-pressure capillary glass tube apparatus. The sample had a minimum purity of 99.0% before being dried over molecular sieve (3 Å). The final sample contained less than 0.01% water. The uncertainty of temperature measurements is 0.01 K, and the uncertainty of pressure measurements is 1 kPa.

Devyatko and Stabnikov[124] report vapor pressures, however they do not report any sample purity, experimental uncertainty, or methods. Dulitskaya[125] measured vapor pressures for ethanol (99.98 wt. %). The uncertainties of the temperature and pressure measurements were 0.03 K and 0.3 mmHg. Figurski and Malanowski[126] measured vapor pressures for ethanol (99.99 wt. %) using a van Ness ebulliometer. The uncertainties of the temperature and pressure were 0.01 K and 15 Pa. Fiock *et al.*[80] report vapor pressures for ethanol (99.95% wt. %) that were measured in a calorimeter. No experimental uncertainty was given.

Khurma *et al.*[127] report vapor pressure data for ethanol (99.98%), as measured in a multicell apparatus. The uncertainties of temperature and pressure measurements were 0.03 K and 0.10%, respectively. Kretschmer and Wiebe[128] used an equilibrium still to measure vapor pressures of ethanol. No sample purity was reported. The uncertainty of the data was 0.05 mmHg. Lee and Hu[129] used a static vapor-liquid equilibrium apparatus to measure vapor pressures of ethanol (99.8%). The uncertainties of temperature and pressure measurements were 0.02 K and 1.0%, respectively.

Merriman[131] reported vapor pressure data measured using a dynamic method. The purity was 99.5% before further purification; however, the final purity was not specified. No experimental uncertainty was listed. Mishchenko and Subbotina[132] measured vapor pressures for ethanol with an uncertainty of 0.3% for pressure. The sample contained no more than 0.1% water. Mousa[133] also measured vapor pressure data for ethanol. The sample purity was 99.99% before being dried over molecular sieve (5 Å) and degassed. The reported uncertainties for temperature and pressure measurements were 0.2 K and 1.0 kPa. However, the data reported deviate dramatically from all other vapor pressure data.

Pokki *et al.*[134] used a circulation still to measure vapor pressures of ethanol (99.7%). Estimated uncertainties of the temperature and pressure data were 0.05 K and 0.07 kPa. Sauermann *et al.*[11] measured vapor pressure data for ethanol using a Cailletet apparatus. The ethanol sample had an initial purity of 99.90% before being dried over molecular sieves and degassed. The measurement uncertainties for temperature and pressure were 0.02 K and 1 kPa. Takiguchi and Uematsu[61] and Takiguchi *et al.*[135] measured vapor pressures of ethanol with an initial sample purity of 99.5 vol. % before being dried over molecular sieve (4 Å). The estimated uncertainties of the temperature and pressure were 0.006 K and 0.4 kPa.

Watts and Louie[69] collected vapor pressure data for ethanol using an equilibrium cell with a recirculation pump. The sample had a stated purity of 99.5%. The estimated uncertainties of the temperature and pressure were 0.002 K and 0.01%. Wilhoit and Zwolinski[136] listed vapor pressure data, but these were generated from an Antoine equation fit to other sources. Wolff and Götz[137] measured vapor pressures of ethanol using a static method. The sample purity was 99% before being dried over molecular sieves. The experimental uncertainty is unknown; however, the data appear to be very inconsistent with other data.

2.8. Saturated liquid density data

Seven sources of experimental data were available for the saturated liquid density, as listed in Table 9. Timmermans[122] reported the data by Young, which are not discussed here for reasons discussed previously.

Bazaev *et al.*[2] determined saturated liquid densities for ethanol (99.8 mol. %) by extrapolating and intersecting $p\rho T$ measurements in the liquid and two-phase regions. No uncertainty for these data is listed, however it is noted that they had an absolute average deviation of 0.13% from the equation of state by Dillon and Penoncello.[13]

Hales and Ellender[138] measured saturated liquid densities of ethanol (99.95 mass%). The data were measured using a magnetic float device, and the results were corrected for water

TABLE 9. Summary of saturated liquid density data

		ρ (mol dm^{-3})		T (K)	
Author	Points	Min	Max	Min	Max
Bazaev *et al.*[2a]	9	7.84	15.5	373	513
Hales and Ellender[138a]	13	12.9	17.1	293	455
Mousa[133]	16	5.86	15.0	417	516
Polikhronidi *et al.*[15]	11	6.24	7.93	513	514
Takiguchi and Uematsu[61]	3	15.8	16.8	310	360
Takiguchi and Uematsu[3]	8	11.6	16.6	320	480
Young[b]	28	7.42	17.5	273	516

[a]Data used to fit Eq. (10).
[b]As reported by Timmermans.[122]

This article is copyrighted as indicated in the article. Reuse of AIP content is subject to the terms at: http://scitation.aip.org/termsconditions. Downloaded to IP: 131.111.164.128 On: Tue, 21 Oct 2014 07:26:40

content. The estimated uncertainty of the measurements was 0.15 kg m^{-3}. Mousa[133] measured saturated liquid densities for ethanol. The sample purity was 99.99% before being dried over molecular sieve (5 Å) and degassed. No experimental uncertainty was given for the saturated liquid density data. Furthermore, the data are inconsistent with other saturated liquid density data.

Polikhronidi *et al.*[15] measured saturated liquid densities of ethanol (99.97 mol. %) very near the critical point. Densities were measured using the same apparatus as was used for measuring isochoric heat capacities. The estimated uncertainties in density and saturation temperature measurements were 0.06% and 0.02 K, respectively. Takiguchi and Uematsu[3,61] measured saturated liquid density data for ethanol with an initial sample purity of 99.5 vol. % before being dried over molecular sieve (4 Å). The estimated uncertainty of the density was 0.1%.

2.9. Saturated vapor density data

Only five sources of data were available for the saturated vapor density, as shown in Table 10.

Bazaev *et al.*[2] determined saturated vapor densities for ethanol (99.8 mol. %) by extrapolating and intersecting $p\rho T$ measurements in the vapor and two-phase regions. No uncertainty for this data set is listed. Fiock *et al.*[80] list saturated vapor densities. However, these data are not experimental; they were calculated based on Young's[122] vapor pressure data. Mousa[133] measured saturated vapor densities for ethanol. The sample purity was 99.99% before being dried over molecular sieve (5 Å) and degassed. No experimental uncertainty was given for the saturated vapor density data. As with the saturated liquid density, the data are inconsistent with other saturated vapor density data.

Polikhronidi *et al.*[15] measured saturated vapor densities of ethanol (99.97 mol. %) very near the critical point. Densities were measured using the same apparatus as was used for measuring isochoric heat capacities. The estimated uncertainties in density and saturation temperature measurements were 0.06% and 0.02 K, respectively. Timmermans[122] reported the saturated vapor density data by Young. The paper by Young was not located, so the sample purity and experimental uncertainty are not known for this data set. However, the data are the most compatible with the fundamental equation, so this data set was used to establish a saturated vapor density curve.

Table 10. Summary of saturated vapor density data

Author	Points	ρ (mol dm^{-3}) Min	ρ (mol dm^{-3}) Max	T (K) Min	T (K) Max
Bazaev *et al.*[2a]	9	0.081	3.470	373	513
Fiock *et al.*[80]	15	0.001	0.193	273	403
Mousa[133]	16	0.653	5.920	417	516
Polikhronidi *et al.*[15]	11	4.2	6.13	513	514
Young[ab]	28	0.001	4.700	273	516

[a]Data used to fit Eq. (11).
[b]As reported by Timmermans.[122]

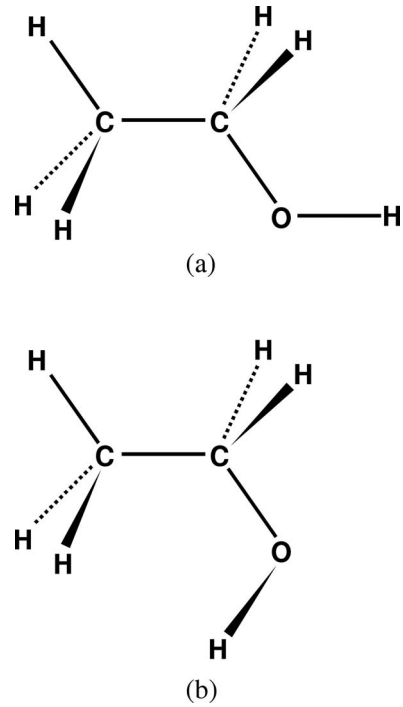

Fig. 7. The (a) *trans* and (b) *gauche* conformers of ethanol.

2.10. Ideal gas heat capacity data

Several authors report ideal gas heat capacity data calculated by extrapolating vapor-phase heat capacity data to zero pressure.[77,79,92,112,139] Other authors have reported vibrational wavenumbers that can be used to calculate ideal gas heat capacity behavior.[79,112,140–143]

Most recently, Chao *et al.*[144] reported ideal gas heat capacity data over a range of 100 K–1500 K. Their work was based on the best available spectroscopic data and accounted for an equilibrium mixture of *trans* and *gauche* conformers (see Fig. 7). Their data were calculated based on the wavenumber data of Barnes and Hallam,[140] Durig *et al.*,[142] and Green.[143] They also incorporated hydroxyl rotation barrier heights for the *trans* and *gauche* conformers from Durig *et al.*[142] and Kakar and Quade,[145] respectively, as well as the methyl group rotation barrier height suggested by Lovas.[146]

The equation presented by Chao and Hall[147] is nearly identical to that of Chao *et al.*[144] However, the Thermodynamics Research Center[148] selected the work of Chao *et al.*[144] to be their standard for ideal gas heat capacity data for ethanol. Thus, the data reported by Chao *et al.*[144] were used for this work.

3. The Ancillary Equations

The fundamental equation contains all thermodynamic information about a fluid, including the saturation properties. However, calculating the saturation boundaries is a highly iterative process of identifying equal pressures and Gibbs energies at constant temperature between the liquid and vapor phases. Though not used to calculate the saturation boundaries

This article is copyrighted as indicated in the article. Reuse of AIP content is subject to the terms at: http://scitation.aip.org/termsconditions. Downloaded to IP: 131.111.164.128 On: Tue, 21 Oct 2014 07:26:40

directly, three ancillary equations can be used as an initial estimate for this iterative process. These ancillary equations include a vapor pressure equation and saturated liquid and vapor density equations.

3.1. Comparison of data to equations

In the following sections, various equations are compared to the respective experimental data used in regression analysis. Comparisons were based on five statistical calculations—absolute average deviation (AAD), bias, standard deviation, σ, root-mean-square deviation (RMS), and maximum deviation (Max). These calculations are based upon the residuals between the data and corresponding calculated values. Residuals are defined as

$$\Delta X = X_{\text{data}} - X_{\text{calc}}, \tag{3}$$

where X is any given thermodynamic property, and ΔX is the residual value of that property at a specific data point. Comparisons are based on the percent deviation between the calculated and experimental value, according to Eq. (4):

$$\%\Delta X = \left(\frac{\Delta X}{X_{\text{data}}}\right) \times 100. \tag{4}$$

The AAD is used to determine the overall fitness of an equation relative to a given data set. The AAD is calculated by

$$\text{AAD} = \frac{1}{n}\sum_{i=1}^{n}|\%\Delta X_i|, \tag{5}$$

where n is the number of data points in the set. Equations (6)–(8) describe the remaining statistical calculations:

$$\text{Bias} = \frac{1}{n}\sum_{i=1}^{n}(\%\Delta X_i), \tag{6}$$

$$\sigma = \left[\frac{1}{n-1}\sum_{i=1}^{n}(\%\Delta X_i - \text{Bias})^2\right]^{\frac{1}{2}}, \tag{7}$$

$$\text{RMS} = \left[\frac{1}{n}\sum_{i=1}^{n}(\%\Delta X_i)^2\right]^{\frac{1}{2}}. \tag{8}$$

3.2. Ancillary equation fitting method

All ancillary equation fitting was performed by minimizing the weighted sum of the square of the residuals, using the MINIMIZE.EXE routine developed at the National Institute of Standards and Technology (NIST) and the University of Idaho Center for Applied Thermodynamic Studies (CATS). This routine has nonlinear fitting capabilities, allowing coefficients and exponents to be fit simultaneously.

3.3. The vapor pressure equation

The vapor pressure equation used in this work is the empirical form developed by Wagner *et al.*[149] The general equation form for this property is expressed as

$$\ln\left(\frac{p_\sigma}{p_c}\right) = \frac{T_c}{T}\sum_{i=1}^{4} N_i\left(1 - \frac{T}{T_c}\right)^{k_i}, \tag{9}$$

where p_σ is the vapor pressure, N_i are the coefficients of each term, and k_i are fitting exponents. Values for the critical parameters are given in Sec. 2.1. Lemmon and Goodwin[150] list several constraints for Eq. (9) that ensure proper behavior of the curve in the critical region. First, k_1 must equal 1 and k_2 must equal 1.5. All other k_i can be any value greater than 2. Additionally, N_1 should be negative, with values for most fluids falling between –6 and –8. N_2 is typically positive, with values for most fluids falling between 1 and 2.5.

The data from Aucejo *et al.*[110] and Bazaev *et al.*[2] were used to fit the vapor pressure equation. These data sets were selected because they produced an equation that most closely met the requirements discussed by Lemmon and Goodwin.[150] The coefficients and exponents of Eq. (9) are listed in Table 11.

Figure 8 shows the percent deviations of the vapor pressure data from the final form of the vapor pressure equation. The equation fits most experimental data to within 1%. The seemingly poor fit to certain data in the critical region is due to selecting a critical point that differs from those data sets (see Sec. 2.1). Data points whose deviations are outside the bounds of Fig. 8 are shown at the extremes of the plot. The same method is used for all subsequent plots in this work.

TABLE 11. Constants for the vapor pressure equation, Eq. (9)

i	N_i	k_i
1	−8.94161	1.0
2	1.61761	1.5
3	−51.1428	3.4
4	53.1360	3.7

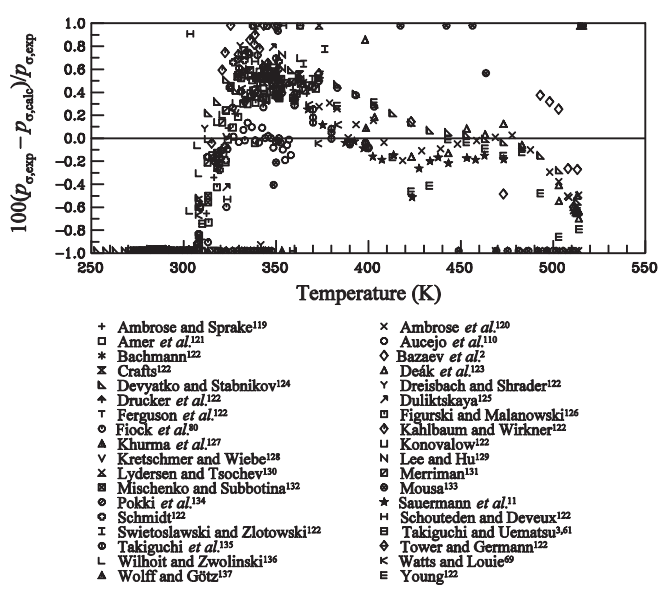

FIG. 8. Experimental deviations for the vapor pressure data.

This article is copyrighted as indicated in the article. Reuse of AIP content is subject to the terms at: http://scitation.aip.org/termsconditions. Downloaded to IP: 131.111.164.128 On: Tue, 21 Oct 2014 07:26:40

TABLE 12. Statistical calculations for the vapor pressure equation, Eq. (9)

Author	Points	AAD	Bias	σ	RMS	Max	$T > T_c$
Ambrose and Sprake[119]	25	0.795	−0.255	1.118	1.125	−3.297	0
Ambrose *et al.*[120]	23	0.222	−0.081	0.288	0.293	−0.633	0
Amer[121]	12	0.528	0.528	0.099	0.536	0.731	0
Aucejo *et al.*[110a]	22	0.059	−0.02	0.077	0.078	−0.189	0
Bachmann[b]	1	3.389	−3.389	—	3.389	−3.389	0
Bazaev *et al.*[2a]	9	0.363	0.003	0.415	0.391	−0.599	0
Crafts[b]	5	1.897	−0.717	2.242	2.13	−3.264	0
Deák *et al.*[123]	20	0.442	−0.314	0.415	0.512	0.857	0
Devyatko and Stabnikov[124]	49	12.513	−12.096	24.323	26.932	−96.309	2
Dreisbach and Shrader[b]	3	0.604	−0.013	0.871	0.711	−0.925	0
Drucker *et al.*[b]	10	48.719	−30.891	47.087	54.311	−83.031	0
Dulitskaya[125]	3	1.185	−0.66	1.58	1.449	−2.345	0
Ferguson *et al.*[b]	1	1.744	−1.744	—	1.744	−1.744	0
Figurski and Malanowski[126]	17	0.375	0.072	0.475	0.466	−1.285	0
Fiock[80]	15	1.609	−1.08	2.204	2.387	−5.606	0
Kahlbaum and Wirkner[b]	38	3.434	−2.718	3.405	4.322	−8.68	0
Khurma *et al.*[127]	3	0.803	−0.379	1.229	1.072	−1.773	0
Konovalow[b]	5	0.583	−0.439	0.796	0.836	−1.728	0
Kretschmer and Wiebe[128]	8	1.664	−1.419	3.114	3.24	−8.788	0
Lee and Hu[129]	6	0.554	0.554	0.139	0.568	0.728	0
Lydersen and Tsochev[130]	12	1.968	−1.968	0.279	1.985	−2.303	2
Merriman[131]	61	3.085	−2.699	3.293	4.237	−12.071	0
Mishchenko and Subbotina[132]	22	3.094	−3.094	2.772	4.112	−7.749	0
Mousa[133]	33	5.256	−4.293	5.647	7.023	−18.807	1
Pokki *et al.*[134]	13	0.513	0.482	0.228	0.53	0.746	0
Sauermann *et al.*[11]	21	0.238	−0.02	0.292	0.285	0.595	0
Schmidt[b]	32	1.535	−1.038	1.697	1.967	−3.977	0
Schouteden and Deveux[b]	9	1.611	−0.626	2.45	2.393	−5.776	0
Swietoslawski and Zlotowski[b]	6	0.574	0.574	0.119	0.584	0.775	0
Takiguchi and Uematsu[3,61]	3	0.535	0.04	0.686	0.561	−0.742	0
Takiguchi *et al.*[135]	27	0.322	0.094	0.47	0.471	−1.394	0
Tower and Germann[b]	1	4.739	−4.739	—	4.739	−4.739	0
Watts and Louie[69]	12	0.44	−0.075	0.495	0.48	−0.647	0
Wilhoit and Zwolinski[136]	24	1.378	−0.935	2.27	2.411	−7.316	0
Wolff[137]	7	4.702	−4.702	2.337	5.176	−8.983	0
Young[b]	22	1.130	−0.951	1.780	1.976	−6.189	3

[a]Data used to fit Eq. (9).
[b]As reported by Timmermans.[122]

Table 12 provides statistical calculations of the data compared to Eq. (9). Statistical calculations include the AAD, the standard deviation, σ, the RMS of the deviations, the maximum deviation, and the number of extraneous data points. These points are those whose temperatures exceed the critical temperature and cannot therefore be used in fitting the vapor pressure equation. These data points were not included in any of the statistical calculations.

3.4. The saturated liquid density equation

The saturated liquid density, ρ', is represented by

$$\frac{\rho'}{\rho_c} = 1 + \sum_{i=1}^{5} N_i \left(1 - \frac{T}{T_c}\right)^{k_i}. \tag{10}$$

TABLE 13. Constants for the saturated liquid density equation, Eq. (10)

i	N_i	k_i
1	9.00921	0.5
2	−23.1668	0.8
3	30.9092	1.1
4	−16.5459	1.5
5	3.64294	3.3

The density and temperature are reduced by the critical density and temperature. Values of the coefficients and exponents for Eq. (10) are given in Table 13.

The data of Bazaev *et al.*[2] and Hales and Ellender[138] were used to fit Eq. (10). Figure 9 shows the percent deviations of the saturated liquid density data from Eq. (10). The equation fits most data to within ±0.05% between 273–380 K, and ±0.1% between 380–450 K, and ±0.2% from 450 K to the critical point. The

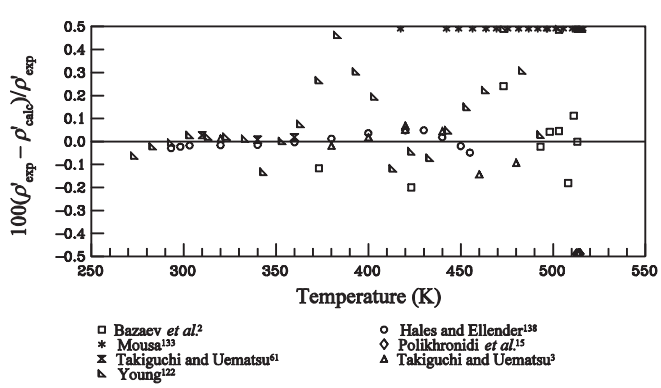

FIG. 9. Experimental deviations for the saturated liquid density data.

This article is copyrighted as indicated in the article. Reuse of AIP content is subject to the terms at: http://scitation.aip.org/termsconditions. Downloaded to IP: 131.111.164.128 On: Tue, 21 Oct 2014 07:26:40

TABLE 14. Statistical calculations for the saturated liquid density equation, Eq. (10)

Author	Points	AAD	Bias	σ	RMS	Max	$T > T_c$
Bazaev *et al.*[2a]	9	0.107	−0.009	0.142	0.134	0.241	0
Hales and Ellender[138a]	13	0.026	−0.001	0.031	0.03	−0.049	0
Mousa[133]	16	11.007	11.00	3.636	11.54	19.96	1
Polikhronidi *et al.*[15]	11	4.054	−4.054	3.001	4.962	−10.20	0
Takiguchi and Uematsu[61]	3	0.017	0.017	0.010	0.019	0.027	0
Takiguchi and Uematsu[3]	8	0.056	−0.008	0.074	0.07	−0.143	0
Young[b]	28	0.767	0.732	2.304	2.375	10.63	2

[a]Data used to fit Eq. (10).
[b]As reported by Timmermans.[122]

deviations of Mousa[133] and Polikhronidi *et al.*[15] were too large to fit within Fig. 9. Table 14 lists all statistical calculations comparing the saturated liquid density data to Eq. (10).

3.5. The saturated vapor density equation

The saturated vapor density, ρ'', is represented by

$$\ln\left(\frac{\rho''}{\rho_c}\right) = \sum_{i=1}^{4} N_i \left(1 - \frac{T}{T_c}\right)^{k_i}. \tag{11}$$

The density and temperature are again reduced by the critical density and temperature. Values for the coefficients and exponents of Eq. (11) are given in Table 15.

The data of Bazaev *et al.*[2] and Young[122] were used to fit Eq. (11). Figure 10 shows the percent deviations of the saturated vapor density data from Eq. (11). The equation fits most of the data to within ±0.7%. The deviations of the data from Mousa[133] and Polikhronidi *et al.*[15] are too large to fit within the range of Fig. 10. Table 16 lists all statistical calculations comparing the saturated vapor density data to Eq. (11).

4. Properties of the Ideal Gas

The ideal gas Helmholtz energy, a^0, can be expressed as

$$a^0 = h^0 - RT - Ts^0, \tag{12}$$

where h^0 is the ideal gas enthalpy and s^0 is the ideal gas entropy. Lemmon and Jacobsen[151] have shown that this can be expressed as a temperature-explicit equation:

$$a^0 = h_0^0 + \int_{T_0}^{T} c_p^0 \mathrm{d}T - RT - T\left[s_0^0 + \int_{T_0}^{T} \frac{c_p^0}{T}\mathrm{d}T - R\ln\left(\frac{\rho T}{\rho_0 T_0}\right)\right]. \tag{13}$$

TABLE 15. Constants for the saturated vapor density equation, Eq. (11)

i	N_i	k_i
1	−1.75362	0.21
2	−10.5323	1.1
3	−37.6407	3.4
4	−129.762	10.

Here, h_0^0 is a reference enthalpy, c_p^0 is the isobaric heat capacity of the ideal gas, s_0^0 is a reference entropy, T_0 is an arbitrary constant, and ρ_0 is the ideal gas density at T_0 and p_0, as given by Eq. (14):

$$\rho_0 = \frac{p_0}{RT_0}. \tag{14}$$

Equation (13) can be transformed to a dimensionless form. It then becomes

$$\alpha^0 = \frac{h_0^0\tau}{RT_c} - \frac{s_0^0}{R} - 1 + \ln\left(\frac{\delta\tau_0}{\delta_0\tau}\right) - \frac{\tau}{R}\int_{\tau_0}^{\tau}\frac{c_p^0}{\tau^2}\mathrm{d}\tau + \frac{1}{R}\int_{\tau_0}^{\tau}\frac{c_p^0}{\tau}\mathrm{d}\tau. \tag{15}$$

Thus, the ideal gas Helmholtz energy is only a function of temperature and pressure. However, the isobaric heat capacity of the ideal gas must be known, which is a function of temperature alone.

4.1. The ideal gas heat capacity equation

The ideal gas heat capacity is determined by statistical mechanics. It includes contributions from molecular translation, rotation, and vibration. Based on Prausnitz *et al.*,[152] the ideal gas heat capacity for ethanol is described by Eq. (16):

$$\frac{c_p^0}{R} = 4 + \sum_{i=1}^{21} \frac{\left(\frac{\theta}{T}\right)^2 \exp\left(\frac{\theta}{T}\right)}{\left[\exp\left(\frac{\theta}{T}\right) - 1\right]^2} + \Delta c_v^0. \tag{16}$$

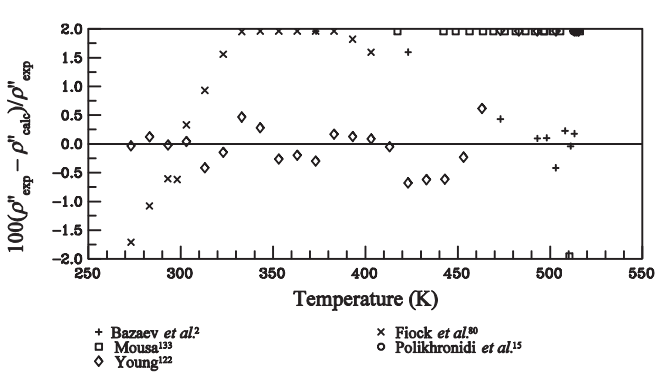

FIG. 10. Experimental deviations for the saturated vapor density data.

This article is copyrighted as indicated in the article. Reuse of AIP content is subject to the terms at: http://scitation.aip.org/termsconditions. Downloaded to IP: 131.111.164.128 On: Tue, 21 Oct 2014 07:26:40

TABLE 16. Statistical calculations for the saturated vapor density equation, Eq. (11)

Author	Points	AAD	Bias	σ	RMS	Max	$T > T_c$
Bazaev *et al.*[2a]	9	1.014	0.912	2.001	2.095	6.041	0
Fiock *et al.*[80]	15	1.552	1.019	1.390	1.686	2.328	0
Mousa[133]	16	19.20	17.90	14.215	22.56	57.16	1
Polikhronidi *et al.*[15]	11	24.91	24.91	4.022	25.21	32.60	0
Young[ab]	28	1.273	1.002	2.270	2.441	7.071	2

[a]Data used to fit Eq. (11).
[b]As reported by Timmermans.[122]

Here, Δc_v^0 is a correction term that accounts for any deviation from theory, and θ is the characteristic temperature, defined as

$$\theta = \left(\frac{hc}{k_B}\right)\nu_i, \tag{17}$$

where h is the Planck constant, c is the speed of light in a vacuum, k_B is the Boltzmann constant, and ν_i is the wavenumber of the ith vibrational frequency.

There are 21 vibrational frequencies for ethanol. However, only 19 of these frequencies can be determined using spectroscopic methods. The remaining two frequencies result from internal rotations of the methyl and hydroxyl groups. To reduce the number of terms that results from Eq. (16), an empirical equation was fit to the ideal gas heat capacity data of Chao *et al.*[144] Their work was selected because it appears to be the most accurate and up-to-date work available. The form of the ideal gas heat capacity equation used in this work retains the proper theoretical form shown in Eq. (16) and is expressed as

$$\frac{c_p^0}{R} = d_1 + \sum_{i=2}^{5} d_i \frac{\left(\frac{\theta_i}{T}\right)^2 \exp\left(\frac{\theta_i}{T}\right)}{\left[\exp\left(\frac{\theta_i}{T}\right) - 1\right]^2}. \tag{18}$$

In this equation, θ_i and d_i are empirical constants, determined by minimizing the sum of the weighted and squared residuals between the data and the correlated equation. The constants θ_i and d_i are listed in Table 17. The values of θ_i do not correspond to actual vibrational frequencies of ethanol.

As shown in Fig. 11, Eq. (18) fits all ideal gas heat capacity data reported by Chao *et al.*[144] within less than ±0.02%.

4.2. The ideal gas Helmholtz energy equation

Once the ideal gas heat capacity equation has been developed, it is useful to express α^0 in terms of that equation.

TABLE 17. Constants of the ideal gas heat capacity equation, Eq. (18)

i	d_i	θ_i (K)
1	4.430 69	—
2	2.143 26	420.4
3	5.092 06	1334
4	6.601 38	1958
5	5.707 77	4420

Combining Eqs. (15)–(19) yields the form

$$\alpha^0 = \ln\delta + x_1 \ln\tau + x_2 + x_3\tau + \sum_{i=4}^{7} x_i \ln[1 - \exp(-y_i\tau)], \tag{19}$$

where x_3 and the x_i and y_i in the summation are computed from the d_i and θ_i of Eq. (18) and x_1 and x_2 are chosen to satisfy the selected EOS reference state. For this fundamental equation, the ideal gas reference states are $T_0 = 273.15$ K, $p_0 = 0.001$ MPa, $h_0^0 = 52\ 811.79$ J mol^{-1}, and $s_0^0 = 209.5830$ J mol^{-1} K^{-1}. This reference state is calculated such that enthalpy and entropy values of the saturated-liquid state at 0 °C are 200 kJ kg^{-1} and 1 kJ kg^{-1} K^{-1}, respectively. Constants of Eq. (19) are listed in Table 18.

5. Properties of the Real Fluid

5.1. The functional form of the residual portion of the fundamental equation

The equation form used in this work was developed by Setzmann and Wagner[153] for methane. It has been used for many other correlations, such as the propane equation of state by Lemmon *et al.*[154] The residual contribution to the Helmholtz energy is given by an empirical equation in the following form:

$$\alpha^r(\delta,\tau) = \sum N_i \delta^{d_i}\tau^{t_i} + \sum N_i \delta^{d_i}\tau^{t_i}\exp(-\delta^{l_i}) + \sum N_i \delta^{d_i}\tau^{t_i}\exp[-\eta_i(\delta-\varepsilon_i)^2 - \beta_i(\tau-\gamma_i)^2]. \tag{20}$$

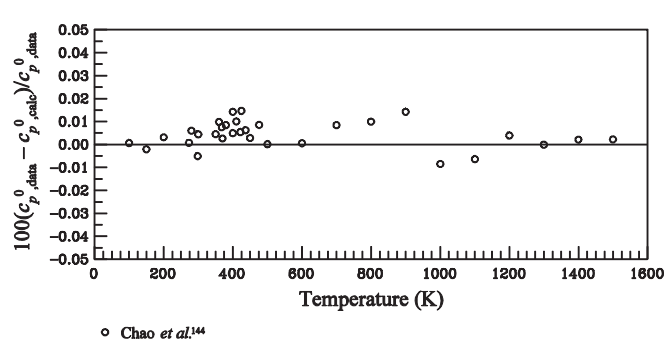

FIG. 11. Experimental deviations for the ideal gas heat capacity data.

This article is copyrighted as indicated in the article. Reuse of AIP content is subject to the terms at: http://scitation.aip.org/termsconditions. Downloaded to IP: 131.111.164.128 On: Tue, 21 Oct 2014 07:26:40

TABLE 18. Constants of the ideal gas Helmholtz energy equation, Eq. (19)

i	x_i	y_i
1	3.430 69	—
2	−12.7531	—
3	9.390 94	—
4	2.143 26	0.816 771
5	5.092 06	2.591 75
6	6.601 38	3.804 08
7	5.707 77	8.587 36

For Eq. (20), N_i, d_i, t_i, l_i, η_i, ε_i, β_i, and γ_i are constants. Although these constants are arbitrary, some values must fall within reasonable bounds in order to obtain proper limiting behavior. Except for N_i, constants are expected to be positive. All d_i and l_i are positive integers. Functions for calculating thermodynamic properties from the Helmholtz energy formulation are presented in Appendix A.

5.2. Fitting procedure and results

The residual portion of the fundamental equation of state presented in this work was developed by using a Levenberg-Marquardt algorithm in a package developed by NIST. This nonlinear algorithm optimizes the equation by minimizing the weighted and summed square of the residuals. The algorithm is useful because it allows both coefficients and exponents to be fit. Also, a broad variety of data forms can be used to fit the equation. Data forms utilized in this work include density, sound speed, isobaric heat capacity, vapor pressure, and saturated liquid density.

In addition to using experimental data to fit the equation, several constraints can be imposed on it. These force proper behavior of the thermodynamic surface by adding a penalty to the sum of the square of the residuals when the conditions of the constraint are not met. For example, constraints can force the first and second derivatives of pressure with respect to density at constant temperature to be zero at the critical point.

The final form of the residual portion of the fundamental equation of state is given by Eq. (21). Constants of Eq. (21) are listed in Table 19:

$$\alpha^{r}(\delta,\tau) = \sum_{i=1}^{6} N_i \delta^{d_i} \tau^{t_i} + \sum_{i=7}^{16} N_i \delta^{d_i} \tau^{t_i} \exp(-\delta^{l_i}) + \sum_{i=17}^{25} N_i \delta^{d_i} \tau^{t_i} \exp[-\eta_i(\delta-\varepsilon_i)^2 - \beta_i(\tau-\gamma_i)^2] \tag{21}$$

Tabulated saturation properties calculated from the fundamental equation are provided in Appendix B.

5.3. Data selection

Data were selected in an attempt to provide coverage of the full range of the thermodynamic surface of liquid- and gas-phase ethanol. Other factors included the quality and reputation of the data source, sample purity, measurement accuracy, and compatibility with the rest of the thermodynamic surface. In fitting the fundamental equation, high-accuracy data were weighted heavily, and less accurate data were weighted

TABLE 19. Constants of the residual portion of the fundamental equation of state, Eq. (21)

i	N_i	t_i	d_i	l_i	η_i	β_i	γ_i	ε_i
1	0.058200796	1.00	4					
2	0.94391227	1.04	1					
3	−0.80941908	2.72	1					
4	0.55359038	1.174	2					
5	−1.4269032	1.329	2					
6	0.13448717	0.195	3					
7	0.42671978	2.43	1	1				
8	−1.1700261	1.274	1	1				
9	−0.92405872	4.16	1	2				
10	0.34891808	3.30	3	1				
11	−0.91327720	4.177	3	2				
12	0.022629481	2.50	2	1				
13	−0.15513423	0.81	2	2				
14	0.21055146	2.02	6	1				
15	−0.21997690	1.606	6	1				
16	−0.0065857238	0.86	8	1				
17	0.75564749	2.50	1		1.075	1.207	1.194	0.779
18	0.10694110	3.72	1		0.463	0.0895	1.986	0.805
19	−0.069533844	1.19	2		0.876	0.581	1.583	1.869
20	−0.24947395	3.25	3		1.108	0.947	0.756	0.694
21	0.027177891	3.00	3		0.741	2.356	0.495	1.312
22	−0.00090539530	2.00	2		4.032	27.01	1.002	2.054
23	−0.12310953	2.00	2		2.453	4.542	1.077	0.441
24	−0.089779710	1.00	2		2.300	1.287	1.493	0.793
25	−0.39512601	1.00	1		3.143	3.090	1.542	0.313

This article is copyrighted as indicated in the article. Reuse of AIP content is subject to the terms at: http://scitation.aip.org/termsconditions. Downloaded to IP: 131.111.164.128 On: Tue, 21 Oct 2014 07:26:40

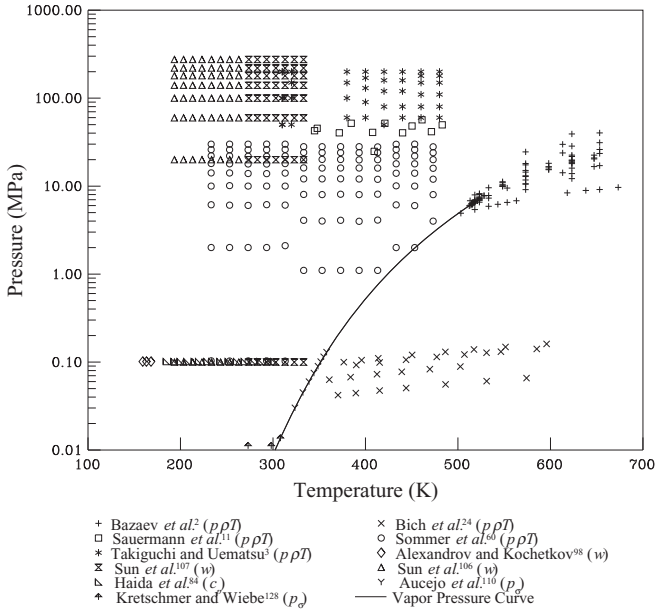

FIG. 12. Pressure-temperature plot of data used to fit the fundamental equation.

lightly. All data used to fit the fundamental equation are shown in Figs. 12 and 13.

5.3.1. Pressure–density–temperature data selection

Several works reporting $p\rho T$ data were used to fit the fundamental equation. For the near-atmospheric and subatmospheric gas-phase region, the data by Bich *et al.*[24] were fit. Their data were selected for their high sample purity and apparent accuracy. Watts and Louie[69] also collected data in this region. Though their data were not used in this work, they demonstrated excellent agreement with the data of Bich *et al.*[24] and could be considered for use in future work. The only other $p\rho T$ data source in this region was Wilson *et al.*[70] Their data were clearly less accurate than that of Bich *et al.*[24] and were incompatible with the rest of the data used in the fit.

The fit in the liquid regions relied heavily on the data of Sommer *et al.*,[60] whose data appear to be highly accurate and consistent with other reliable data sets. To expand the fundamental equation to higher pressures ranges, the data from Sauermann *et al.*[11] and Takiguchi and Uematsu[3] were also included. These three data sources appeared to be in strong agreement with each other, except at very high temperatures, where the data of Sommer *et al.*[60] and Takiguchi and Uematsu[3] begin to deviate systematically from one another.

Finally, the data from Bazaev *et al.*[2] were used to fit the near-critical and supercritical regions of the $p\rho T$ surface. This data set provided the most recent and accurate experimental data in the critical region. Kalafati *et al.*[38] also reported a significant amount of data in the critical region; however, their data were rejected due to the large percentage (4%) of water in the sample. Both Golubev *et al.*[30] and Lo and Stiel[45] reported a large amount of data in the critical region, but their data had been smoothed and were therefore not considered to be appropriate for this work. Tammann and Ruhenbeck[62] report a wide range of supercritical data, but the data proved to be highly incompatible with more accurate data sets.

Lower temperature, liquid-phase $p\rho T$ data could have been added to the fit by including the data from Hugo *et al.*[36] However, their data showed strong systematic deviations from other data, so it was not used for this work. Khasanshin and Aleksandrov[39] also reported low-temperature $p\rho T$ data, but their data were calculated, not experimental. The equation of state produced in this work relies on low-temperature isobaric heat capacity and sound speed data to fit the low-temperature regions of the thermodynamic surface.

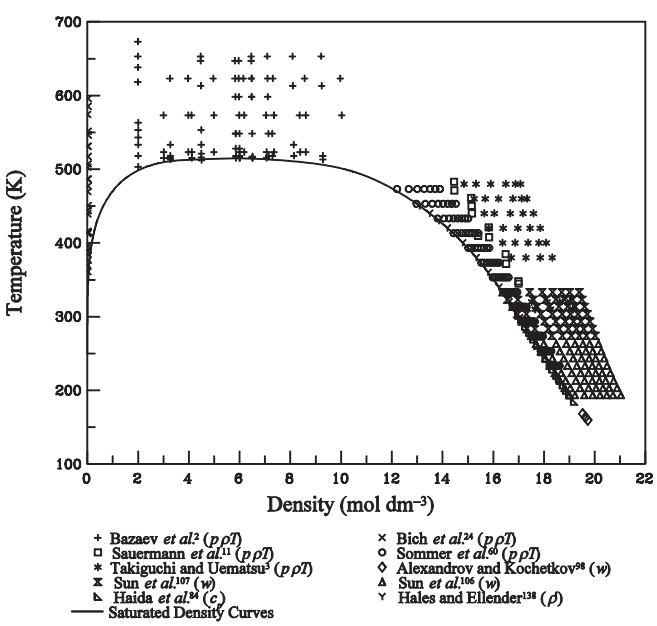

FIG. 13. Temperature-density plot of data used to fit the fundamental equation.

5.3.2. Isobaric heat capacity data selection

The data from Haida *et al.*[84] were selected for fitting the isobaric heat capacities. Their data were located only at atmospheric pressure. However, this data set, combined with other data types over the rest of the thermodynamic surface, proved to be sufficient for correctly modeling most of the isobaric heat capacity surface. The data of Hwa and Ziegler[85] were in very close agreement with the data of Haida *et al.*,[84] but were not used in fitting the equation.

No other isobaric heat capacity data were included in the fit. The data from Sun *et al.*[106,107] were excluded from the fit because they were derived from sound speed data.

While the data of Dong *et al.*,[78] Counsell *et al.*,[77] and Strömsöe *et al.*[94] appear to be of good quality, fitting other data types in the low-pressure vapor-phase region is sufficient to model most of the data from these authors. However, large, systematic deviations occur very near the saturated vapor curve. An attempt was made to fit the near-saturation data of Dong *et al.*,[78] but this resulted in distorting other regions of the surface without significantly improving the near-saturation heat capacity correlation. Therefore, the data from these

This article is copyrighted as indicated in the article. Reuse of AIP content is subject to the terms at: http://scitation.aip.org/termsconditions. Downloaded to IP: 131.111.164.128 On: Tue, 21 Oct 2014 07:26:40

authors were not included in the fit. This discrepancy in the near-saturation vapor phase heat capacity should be explored further in future work.

The heat capacity data of Fulem *et al.*[82] were also considered for the fit. The data were reported as saturation heat capacity data, though they appeared to be isobaric heat capacity data. Nonetheless, these two data types are almost identical at the conditions where these data were reported. An attempt was made to fit these data in both forms. In both cases, only slight improvements to the fit of these data were observed, while other regions of the surface were negatively affected. Thus, the data from Fulem *et al.*[82] were not used in this work.

5.3.3. Sound speed data selection

The sound speed data of Sun *et al.*[106,107] were selected to fit the fundamental equation. These data were chosen not only because of their high experimental accuracy and sample purity, but also because of their broad coverage of the liquid phase. The more recent data of Dzida and Marczak[26] appear to be of excellent quality and could be considered for future work. The data of Wilson and Bradley[108] were not used because the reported experimental uncertainty was greater than that reported by other authors measuring data in the same region. However, these data also appear to be of excellent quality and could be considered for future work. The low-temperature data of Alexandrov and Kochetkov[98] were also weighted slightly in order to extend the range of the fundamental equation for sound speeds.

Two sources report sound speed data at very high pressures —Brown *et al.*[99] and Walsh and Rice.[66] With the exception of these two sources, no other author reports any type of data over 500 MPa. However, neither source reported any sample purity. For this reason, as well as the fact that their data were well beyond the limits of the fundamental equation, their data were not used in this work. Similarly, the data of Hawley *et al.*[103] extend to pressures as high as 479 MPa, yet no sample purity or experimental uncertainty is given. So this data set was also not considered appropriate for this work. Eden and Richardson[101] did not report sample purity or experimental uncertainty either. The data of Carnevale and Litovitz[100] did not exhibit good agreement with other data in the same region and were not used in this work.

All other authors only reported data at atmospheric pressure. To maintain consistency across the thermodynamic surface, the same authors whose data were used at higher pressures were also used at atmospheric pressure. No authors reported sound speed values for ethanol in the vapor phase.

5.3.4. Vapor pressure data selection

Vapor pressure data from Aucejo *et al.*[110] were used to fit the fundamental equation. Their measurements were of high quality, and using their data to fit the vapor pressure ancillary equation yielded the most physically correct results for Eq. (9). For these reasons, this data set was selected for both the vapor pressure equation and the fundamental equation. The data of Bazaev *et al.*[2] were selected for fitting the vapor pressure ancillary equation, but were not necessary for fitting the fundamental equation.

Many other sources of vapor pressure data appeared to be of good quality, including: Ambrose and Sprake,[119] Ambrose *et al.*,[120] Deák *et al.*,[123] Figurski and Malanowski,[126] Sauermann *et al.*,[11] Takiguchi and Uematsu,[61] and Takiguchi *et al.*[135] Nonetheless, using their data did not produce a vapor pressure curve that was as physically correct as that produced by fitting the data of Aucejo *et al.*[110] and Bazaev *et al.*[2] Thus, the vapor pressure data from these authors were not used for this work.

5.3.5. Saturated liquid density data selection

The saturated liquid density data of Hales and Ellender[138] were selected for use in fitting both the saturated liquid density ancillary equation and the fundamental equation. This data set was selected for its range and apparent accuracy. The data of Bazaev *et al.*[2] were used to improve the fit near the critical point of the saturated liquid density equation, but were not used to fit the fundamental equation. The data from Takiguchi and Uematsu[3,61] showed excellent agreement with the data used to fit the correlations in this work.

The data from Young[122] demonstrate systematic deviations from other data in the same region and were not considered to be appropriate for this work. The data of Polikhronidi *et al.*[15] and Mousa[133] deviate substantially from all other data and were not considered to be appropriate for this work.

5.3.6. Saturated vapor density data selection

A very limited set of data was available for the saturated vapor density. The data of Young[122] are the only available experimental data over most of the range of the saturated density curve, so their data were used to fit the saturated vapor density ancillary equation. The data of Bazaev *et al.*[2] were also used to help fit the saturated vapor density equation near the critical point. However, no saturated vapor density data were used to fit the fundamental equation due to the high level of uncertainty inherent in this data form.

The data of Fiock *et al.*[80] were not experimental and were therefore considered to be inappropriate for this work. The data of Polikhronidi *et al.*[15] and Mousa[133] deviate substantially from all other data and were not considered to be appropriate for this work.

5.3.7. Unused data forms

Some data forms were not used to fit the fundamental equation due to the uncertainty of their measurements. This was the case with saturated vapor density data and isochoric heat capacity data. These data forms were occasionally incorporated into the fitting process, but this resulted in only slight improvements to the fit of those data forms, while worsening the fit of more reliable data forms. These data may nevertheless

This article is copyrighted as indicated in the article. Reuse of AIP content is subject to the terms at: http://scitation.aip.org/termsconditions. Downloaded to IP: 131.111.164.128 On: Tue, 21 Oct 2014 07:26:40

be useful for future work, and should not necessarily be disregarded. Virial coefficient data were not utilized, since sufficient $p\rho T$ data were available.

6. Comparison of the Fundamental Equation to the Data

This section presents the deviations between the fundamental equation and all available data. All deviation plots have been created for both the fundamental equation developed in this work and the equation reported by Dillon and Penoncello.[13] This allows for a quick comparison of the two equations. The fit statistics for both fundamental equations are likewise presented. Statistical information is presented in tabular form for all data sets, including those not included in the deviation plots. The fundamental equation was evaluated in part by considering the same five statistical calculations as discussed in Sec. 3.1, and whose equations are given by Eqs. (5)–(8).

6.1. Comparison to $p\rho T$ data

The fundamental equation compares very well to most of the experimental $p\rho T$ data. In general, the equation predicts density data to within ±0.2%. In the critical region, the equation predicts density data to within about ±2%.

Table 20 lists all statistical calculations for the $p\rho T$ data. For comparison, statistics were calculated for the fundamental

TABLE 20. Statistical comparisons of $p\rho T$ data to the fundamental equations developed in this work (italic) and by Dillon and Penoncello[13] (bold)

Author	Points	AAD	Bias	σ	RMS	Max
Álvarez *et al.*[17]	6	*0.018*	*−0.018*	*0.021*	*0.026*	*−0.061*
		0.061	**−0.061**	**0.031**	**0.068**	**−0.118**
Aminabhavi and Patil[18]	3	*0.037*	*0.037*	*0.009*	*0.038*	*0.047*
		0.016	**−0.013**	**0.016**	**0.019**	**−0.028**
Aralaguppi *et al.*[19]	3	*0.071*	*0.071*	*0.033*	*0.076*	*0.093*
		0.027	**0.021**	**0.026**	**0.030**	**0.036**
Aralaguppi and Baragi[20]	3	*0.067*	*0.067*	*0.000*	*0.067*	*0.067*
		0.016	**0.016**	**0.008**	**0.017**	**0.024**
Arbusow[21]	5	*0.201*	*0.187*	*0.185*	*0.250*	*0.479*
		0.213	**0.208**	**0.185**	**0.265**	**0.499**
Bazaev *et al.*[2]	102	*2.961*	*2.002*	*6.026*	*6.322*	*26.638*
		1.091	**0.385**	**3.290**	**3.297**	**30.994**
Benson and D'Arcy[22]	2	*0.015*	*−0.015*	*0.009*	*0.017*	*−0.022*
		0.053	**−0.053**	**0.019**	**0.055**	**−0.067**
Bhagwat and Subnis[23]	7	*1.812*	*1.812*	*0.660*	*1.912*	*3.109*
		1.757	**1.757**	**0.660**	**1.861**	**3.055**
Bich *et al.*[24]	34	*0.060*	*−0.024*	*0.113*	*0.114*	*−0.474*
		0.071	**−0.017**	**0.122**	**0.121**	**−0.453**
Bridgman[25]	126	*7.493*	*7.493*	*2.918*	*8.037*	*11.274*
		7.395	**7.394**	**2.886**	**7.933**	**10.984**
Dzida and Marczak[26]	6	*0.038*	*0.038*	*0.009*	*0.039*	*0.047*
		0.013	**−0.013**	**0.007**	**0.014**	**−0.020**
Easteal and Woolf[27]	6	*0.076*	*0.076*	*0.030*	*0.081*	*0.099*
		0.050	**0.042**	**0.038**	**0.054**	**0.077**
García-Miaja *et al.*[28]	6	*0.023*	*0.023*	*0.004*	*0.024*	*0.029*
		0.027	**−0.027**	**0.011**	**0.029**	**−0.042**
Golik *et al.*[29]	8	*0.017*	*0.012*	*0.024*	*0.025*	*0.065*
		0.046	**−0.007**	**0.062**	**0.059**	**0.139**
Golubev *et al.*[30]	106	*0.646*	*0.558*	*1.671*	*1.754*	*9.700*
		0.621	**0.586**	**1.572**	**1.671**	**9.277**
Gómez *et al.*[31]	3	*0.020*	*0.008*	*0.030*	*0.025*	*0.042*
		0.043	**−0.043**	**0.037**	**0.053**	**−0.072**
Gonçalves *et al.*[1]	175	*0.176*	*0.149*	*0.133*	*0.200*	*0.489*
		0.160	**0.112**	**0.145**	**0.183**	**0.511**
González *et al.*[32]	3	*0.042*	*0.042*	*0.000*	*0.042*	*0.043*
		0.007	**0.000**	**0.010**	**0.008**	**0.010**
Gupta and Hanks[33]	24	*0.078*	*0.045*	*0.077*	*0.087*	*0.194*
		0.067	**0.046**	**0.074**	**0.085**	**0.143**
Hilczer and Goc[34]	7	*0.357*	*0.095*	*0.412*	*0.393*	*−0.584*
		0.353	**0.055**	**0.414**	**0.387**	**−0.541**
Hu *et al.*[35]	5	*0.012*	*−0.011*	*0.010*	*0.015*	*−0.026*
		0.058	**−0.058**	**0.012**	**0.059**	**−0.069**
Hugo *et al.*[36]	195	*0.213*	*0.049*	*0.281*	*0.285*	*0.766*
		0.280	**−0.059**	**0.381**	**0.385**	**−1.243**
Kadam *et al.*[37]	2	*0.114*	*−0.114*	*0.015*	*0.114*	*−0.124*
		0.164	**−0.164**	**0.025**	**0.165**	**−0.182**

This article is copyrighted as indicated in the article. Reuse of AIP content is subject to the terms at: http://scitation.aip.org/termsconditions. Downloaded to IP: 131.111.164.128 On: Tue, 21 Oct 2014 07:26:40

TABLE 20. Statistical comparisons of $p\rho T$ data to the fundamental equations developed in this work (italic) and by Dillon and Penoncello[13] (bold)—Continued

Author	Points	AAD	Bias	σ	RMS	Max
Kalafati *et al.*[38]	216	*7.529*	*−5.700*	*7.103*	*9.094*	*−36.733*
		8.408	**−6.602**	**8.362**	**10.639**	**−51.907**
Khasanshin and Aleksandrov[39]	22	*0.047*	*−0.047*	*0.056*	*0.072*	*−0.185*
		0.166	**0.095**	**0.370**	**0.374**	**1.454**
Kitajima *et al.*[40]	116	*0.031*	*0.027*	*0.024*	*0.036*	*0.059*
		0.049	**0.039**	**0.054**	**0.066**	**0.153**
Kubota *et al.*[41]	46	*0.240*	*−0.239*	*0.142*	*0.278*	*−0.563*
		0.305	**−0.305**	**0.172**	**0.349**	**−0.674**
Langa *et al.*[42]	3	*0.020*	*0.018*	*0.033*	*0.033*	*0.057*
		0.017	**−0.017**	**0.024**	**0.026**	**−0.045**
Lasarte *et al.*[43]	15	*0.019*	*0.009*	*0.022*	*0.023*	*0.043*
		0.034	**−0.023**	**0.034**	**0.040**	**−0.073**
Ling and Van Winkle[44]	3	*0.069*	*0.040*	*0.107*	*0.096*	*0.161*
		0.103	**0.009**	**0.140**	**0.115**	**0.169**
Lo and Stiel[45]	162	*0.531*	*0.275*	*0.972*	*1.008*	*7.796*
		0.286	**0.128**	**0.738**	**0.747**	**5.875**
Matkowska *et al.*[46]	117	*0.029*	*−0.028*	*0.015*	*0.032*	*−0.055*
		0.074	**−0.074**	**0.031**	**0.080**	**−0.129**
Mutalik *et al.*[47]	3	*0.100*	*0.100*	*0.001*	*0.100*	*0.101*
		0.049	**0.049**	**0.006**	**0.050**	**0.056**
Nikam *et al.*[48]	7	*0.015*	*−0.014*	*0.012*	*0.018*	*−0.030*
		0.066	**−0.066**	**0.009**	**0.066**	**−0.080**
Ormanoudis *et al.*[49]	12	*0.047*	*−0.045*	*0.032*	*0.055*	*−0.081*
		0.084	**−0.084**	**0.033**	**0.089**	**−0.119**
Ortega[50]	6	*0.023*	*−0.020*	*0.021*	*0.028*	*−0.049*
		0.071	**−0.071**	**0.031**	**0.077**	**−0.109**
Ozawa *et al.*[51]	44	*0.115*	*0.085*	*0.124*	*0.149*	*0.448*
		0.091	**0.002**	**0.119**	**0.117**	**0.364**
Papaioannou *et al.*[52]	12	*0.046*	*−0.044*	*0.034*	*0.055*	*−0.082*
		0.083	**−0.083**	**0.034**	**0.089**	**−0.120**
Papaioannou *et al.*[53]	10	*0.056*	*−0.054*	*0.035*	*0.064*	*−0.087*
		0.093	**−0.093**	**0.034**	**0.098**	**−0.126**
Pečar and Določek[54]	15	*0.043*	*0.032*	*0.038*	*0.049*	*0.072*
		0.028	**−0.019**	**0.033**	**0.037**	**−0.080**
Peleteiro *et al.*[55]	5	*0.022*	*0.010*	*0.030*	*0.029*	*0.057*
		0.031	**−0.031**	**0.019**	**0.035**	**−0.047**
Peleteiro *et al.*[56]	7	*0.017*	*0.006*	*0.026*	*0.025*	*0.057*
		0.026	**−0.021**	**0.023**	**0.030**	**−0.047**
Rattan *et al.*[57]	2	*0.035*	*0.012*	*0.049*	*0.037*	*0.047*
		0.042	**−0.038**	**0.059**	**0.056**	**−0.080**
Rodríguez *et al.*[58]	4	*0.012*	*−0.012*	*0.009*	*0.014*	*−0.017*
		0.058	**−0.058**	**0.008**	**0.059**	**−0.067**
Sauermann *et al.*[11]	97	*0.035*	*−0.025*	*0.037*	*0.044*	*0.135*
		0.078	**−0.028**	**0.090**	**0.093**	**−0.257**
Schroeder *et al.*[59]	25	*0.011*	*−0.011*	*0.005*	*0.012*	*−0.020*
		0.064	**0.054**	**0.044**	**0.069**	**0.099**
Sommer *et al.*[60]	222	*0.009*	*0.000*	*0.013*	*0.013*	*0.076*
		0.073	**0.042**	**0.078**	**0.089**	**0.226**
Takiguchi and Uematsu[61]	116	*0.040*	*0.038*	*0.032*	*0.050*	*0.140*
		0.058	**−0.042**	**0.057**	**0.071**	**−0.145**
Takiguchi and Uematsu[3]	259	*0.054*	*0.014*	*0.079*	*0.080*	*−0.355*
		0.149	**−0.079**	**0.165**	**0.183**	**−0.439**
Tammann and Ruhenbeck[62]	113	*3.783*	*−2.495*	*5.874*	*6.358*	*−17.499*
		3.910	**−2.711**	**5.887**	**6.458**	**−17.460**
Tanaka *et al.*[63]	44	*0.247*	*−0.247*	*0.139*	*0.283*	*−0.563*
		0.314	**−0.314**	**0.169**	**0.356**	**−0.674**
Tu *et al.*[64]	3	*0.018*	*0.018*	*0.003*	*0.019*	*0.021*
		0.035	**−0.035**	**0.011**	**0.036**	**−0.042**
Vercher *et al.*[65]	6	*0.005*	*−0.005*	*0.000*	*0.005*	*−0.005*
		0.043	**−0.040**	**0.028**	**0.048**	**−0.064**
Walsh and Rice[66]	2	*0.635*	*0.635*	*0.643*	*0.781*	*1.090*
		—	—	—	—	—
Wankhede *et al.*[67]	4	*0.006*	*−0.006*	*0.005*	*0.007*	*−0.010*
		0.052	**−0.052**	**0.011**	**0.053**	**−0.062**
Watson *et al.*[68]	70	*0.035*	*−0.023*	*0.036*	*0.043*	*−0.095*
		0.087	**−0.087**	**0.054**	**0.102**	**−0.202**

This article is copyrighted as indicated in the article. Reuse of AIP content is subject to the terms at: http://scitation.aip.org/termsconditions. Downloaded to IP: 131.111.164.128 On: Tue, 21 Oct 2014 07:26:40

TABLE 20. Statistical comparisons of $p\rho T$ data to the fundamental equations developed in this work (italic) and by Dillon and Penoncello[13] (bold)—Continued

Author	Points	AAD	Bias	σ	RMS	Max
Watts and Louie[69]	37	*0.061*	*−0.061*	*0.009*	*0.062*	*−0.080*
		0.088	**−0.076**	**0.060**	**0.097**	**−0.122**
Wilson *et al.*[70]	65	*0.558*	*0.104*	*0.711*	*0.713*	*1.886*
		0.627	**0.122**	**0.805**	**0.808**	**2.139**
Yusa *et al.*[71]	24	*0.321*	*−0.104*	*0.432*	*0.435*	*−1.052*
		0.324	**−0.181**	**0.436**	**0.464**	**−1.152**
Zafarani-Moattar and Tohidifar[72]	5	*0.009*	*−0.009*	*0.001*	*0.009*	*−0.011*
		0.055	**−0.055**	**0.018**	**0.057**	**−0.071**
Zéberg-Mikkelsen *et al.*[57]	79	*0.079*	*−0.077*	*0.161*	*0.178*	*−0.613*
		0.126	**−0.125**	**0.174**	**0.214**	**−0.673**

equation developed in this work as well as for the equation of Dillon and Penoncello.[13]

Figure 14 shows the percent deviations of the $p\rho T$ data. Again, for comparison, deviations are plotted for the fundamental equation developed in this work and the equation of Dillon and Penoncello.[13] For the sake of clarity, those authors who reported only seven or fewer data points, exclusively at atmospheric pressure, are not included in Fig. 14. However, statistics for the data reported by these authors are still provided in Table 20. Also note that those data points with an AAD > 100 are not included in the statistical calculations, but the number of excluded points is listed.

6.2. Comparison to near-critical and supercritical pressure data

Due to the very small slope of isotherms in the critical region, the fitness of a fundamental equation in the critical region is not easily discerned from the deviation of density. A more useful measure is the deviation of pressure. Thus, the percent deviation in pressure is used for the five authors reporting $p\rho T$ data in the critical and supercritical regions.

Despite improving the behavior of the critical region, the fundamental equation developed in this work does not compare to $p\rho T$ data as well as the equation of Dillon and Penoncello.[13] In particular, the equation does not fit the data of Bazaev *et al.*[2] and Lo and Stiel[45] as well as the existing formulation. The fundamental equation fits most of the data of Bazaev *et al.*[2] within ±2% in pressure.

Table 21 lists all statistical calculations for the near-critical and supercritical pressure data. Figure 15 shows the percent deviations of the near-critical and supercritical pressure data.

6.3. Comparison to isobaric heat capacity data

The fundamental equation compares well to most of the experimental isobaric heat capacity data. The equation predicts most experimental liquid-phase data to within ±1%. The equation predicts vapor-phase heat capacity data to within ±2%, except near saturation. The near-saturation vapor heat capacity data exhibit strong systematic deviations from the fundamental equation.

Table 22 lists all statistical calculations for the isobaric heat capacity data. Figure 16 shows the percent deviations of the isobaric heat capacity data. For the sake of clarity, those authors who reported only two or fewer data points, exclusively at atmospheric pressure, are not included in Fig. 16. However, statistics for the data reported by these authors are still provided in Table 22. Since the available experimental isobaric heat capacity data only covered a limited range of the thermodynamic surface, the calculated data of Sun *et al.*[106,107] were included in the statistical calculations and deviation plots. These data were calculated from sound speed data and were therefore not used to fit the equation. However, they have been included below for comparison.

6.4. Comparison to isochoric heat capacity data

The fundamental equation demonstrates substantial improvements in the comparison to the available isochoric heat capacity data. Almost all of the data from Kitajima *et al.*[40] fall within ±3%. The fundamental equation does not fit the data of Polikhronidi *et al.*[15] very well. This is expected, however, since their data are near the critical point, and the critical point chosen for this work is different from the critical point they recommended. Nonetheless, the new fundamental equation represents their data more closely than the equation of Dillon and Penoncello.[13]

Table 23 lists all statistical calculations for the isochoric heat capacity data. Statistics were calculated for the fundamental equation developed in this work as well as for the equation of Dillon and Penoncello.[13] Figure 17 shows the percent deviations of the isochoric heat capacity data. Deviations are plotted for the fundamental equation developed in this work and the equation of Dillon and Penoncello.[13]

6.5. Comparison to sound speed data

The fundamental equation compares reasonably well to most of the experimental sound speed data. The equation predicts most experimental data to within ±1%. Some systematic deviations remain between the equation and the sound speed data. However, deviations of the data have been

This article is copyrighted as indicated in the article. Reuse of AIP content is subject to the terms at: http://scitation.aip.org/termsconditions. Downloaded to IP: 131.111.164.128 On: Tue, 21 Oct 2014 07:26:40

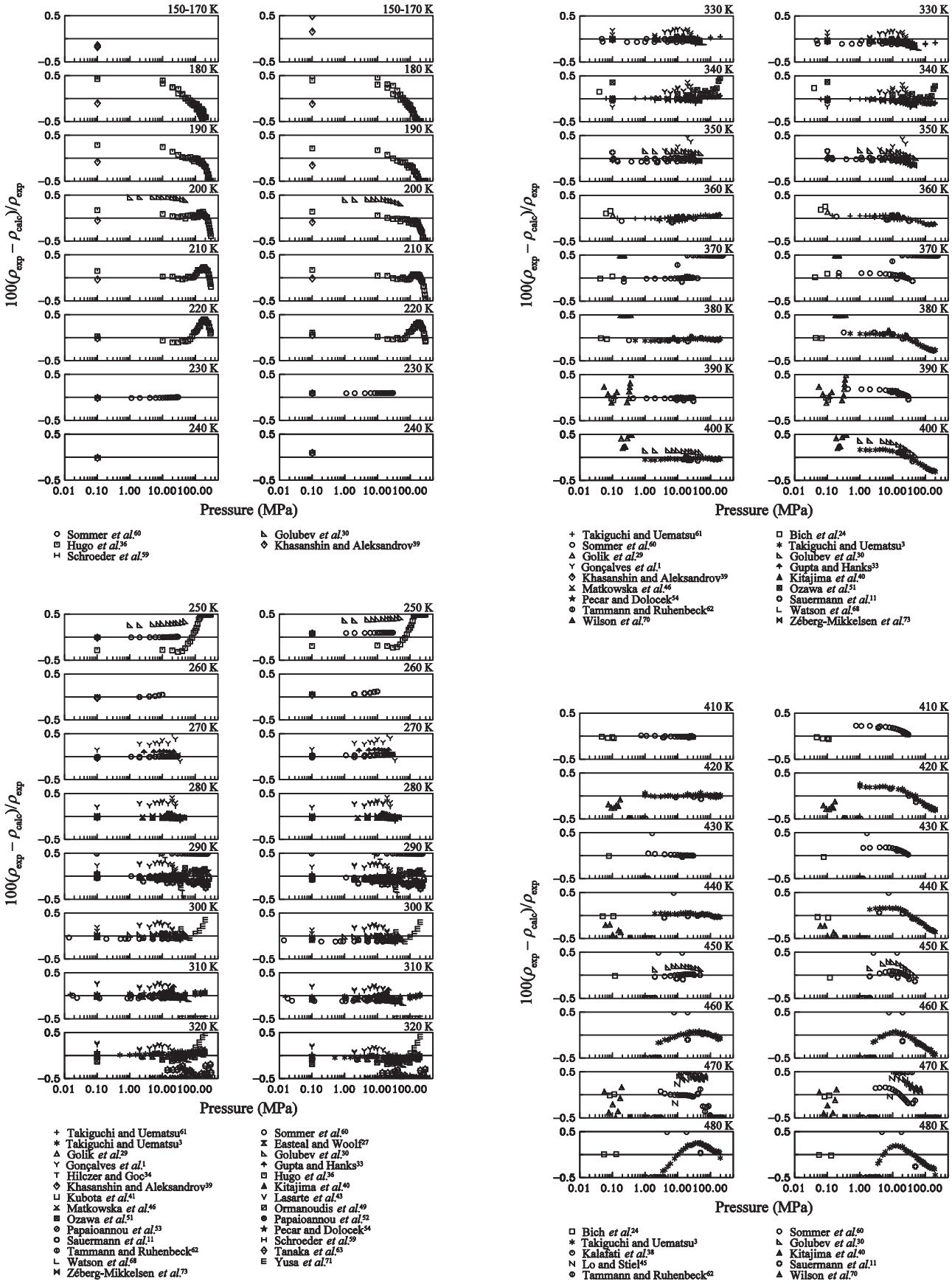

FIG. 14. Comparisons of $p\rho T$ data to the fundamental equations developed in this work (left) and by Dillon and Penoncello[13] (right).

This article is copyrighted as indicated in the article. Reuse of AIP content is subject to the terms at: http://scitation.aip.org/termsconditions. Downloaded to IP: 131.111.164.128 On: Tue, 21 Oct 2014 07:26:40

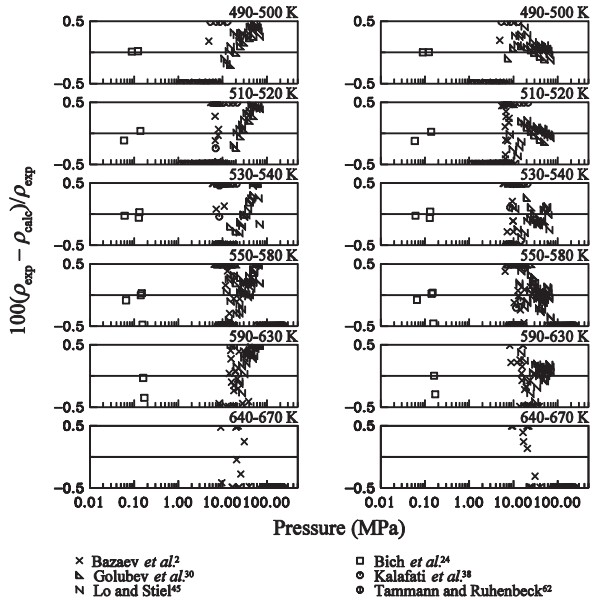

FIG. 14. (*Continued.*)

substantially reduced compared to the equation of Dillon and Penoncello.[13]

Table 24 lists all statistical calculations for the sound speed data. Figure 18 shows the percent deviations of the sound speed data.

6.6. Comparison to second virial coefficient data

Due to the nature of the second virial coefficient, B, statistical comparisons are not made by percent deviation, but rather by a difference (in $dm^3\ mol^{-1}$) multiplied by a factor of 10^3. In general, most of the data lie within $\pm 40\ dm^3\ mol^{-1}$. The fundamental equation developed in this work fits almost all data better than the equation of Dillon and Penoncello,[13] with the exception of the data from Barrow *et al.*[112]

Table 25 lists all statistical calculations for the second virial coefficient data. Figure 19 shows the scaled deviations of the second virial coefficient data.

6.7. Comparison to vapor pressure data

The fundamental equation predicts most vapor pressure data to within ±1%. Both this equation and the equation of Dillon and Penoncello[13] exhibit strong systematic deviations with most of the vapor pressure data. The equation developed in this work does not predict most vapor pressure data as well as the equation of Dillon and Penoncello.[13] Most previous research has considered the data of Ambrose and Sprake[119] and Ambrose *et al.*[120] to be the standard for experimental vapor pressure data. It is possible that this has resulted in most of the experimental data reflecting that data. However, the experimental work of Aucejo *et al.*[110] appears to be of very high accuracy. Even when using the data of Ambrose and Sprake[119] and Ambrose *et al.*[120] to fit the fundamental equation, the equation tended to fit the data of Aucejo *et al.*[110] better. Thus, it was accepted that the fundamental equation would fit the data of Aucejo *et al.*,[110] despite disagreement with most of the other experimental data.

Table 26 lists all statistical calculations for the vapor pressure data. Figure 20 shows the percent deviations of the vapor pressure data.

6.8. Comparison to saturated liquid density data

The fundamental equation compares well to most of the experimental saturated liquid density data. The equation predicts most experimental data to within ±0.3%, except near the critical point, where the data are more scattered. Deviations of the data show minor improvements over the equation of Dillon and Penoncello[13] for most of the saturated liquid curve. However, the equation of Dillon and Penoncello[13] fits critical region data more closely than the equation developed in this work.

Table 27 lists all statistical calculations for the saturated liquid density data. Figure 21 shows the percent deviations of the saturated liquid density data.

6.9. Comparison to saturated vapor density data

There is a great deal of scatter in the saturated vapor density data. The equation predicts most of the data of Young[122] to within ±1%. In this case, the fundamental equation predicts

TABLE 21. Comparisons of near-critical and supercritical pressure data to the fundamental equations developed in this work (italic) and by Dillon and Penoncello[13] (bold)

Author	Points	AAD	Bias	σ	RMS	Max	AAD > 100
Bazaev *et al.*[2]	158	*0.454*	*−0.021*	*0.727*	*0.725*	*4.400*	*0*
		0.371	**−0.042**	**0.595**	**0.595**	**3.135**	**0**
Golubev *et al.*[30]	106	*10.514*	*−10.074*	*17.794*	*20.370*	*−94.934*	*6*
		10.778	**−10.153**	**19.810**	**22.171**	**−95.811**	**7**
Kalafati *et al.*[38]	216	*5.847*	*0.397*	*10.897*	*10.879*	*−85.836*	*2*
		6.398	**0.278**	**11.584**	**11.561**	**−89.411**	**2**
Lo and Stiel[45]	162	*2.436*	*−1.484*	*3.448*	*3.744*	*−32.000*	*0*
		1.246	**−0.647**	**3.209**	**3.264**	**−35.520**	**0**
Tammann and Ruhenbeck[62]	113	*21.896*	*0.493*	*26.099*	*25.985*	*−72.266*	*3*
		22.192	**2.147**	**26.094**	**26.063**	**−70.846**	**3**

This article is copyrighted as indicated in the article. Reuse of AIP content is subject to the terms at: http://scitation.aip.org/termsconditions. Downloaded to IP: 131.111.164.128 On: Tue, 21 Oct 2014 07:26:40

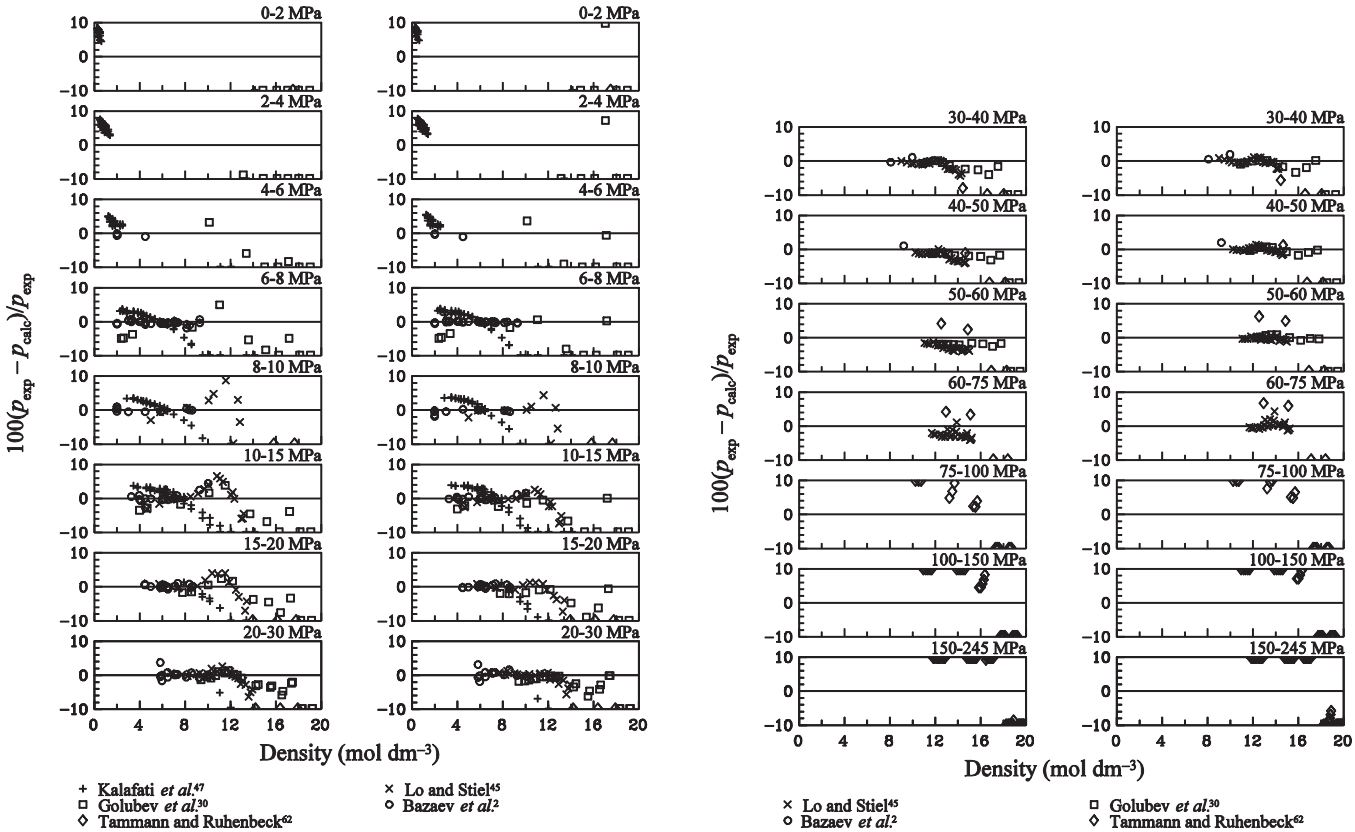

FIG. 15. Comparisons of near-critical and supercritical pressure data to the fundamental equations developed in this work (left) and by Dillon and Penoncello[13] (right).

the data of Polikhronidi *et al.*[15] more accurately, and the data of Bazaev *et al.*[2] less accurately, than the equation of Dillon and Penoncello.[13]

Table 28 lists all statistical calculations for the saturated vapor density data. Figure 22 shows the percent deviations of the saturated vapor density data.

6.10. Comparison to the ancillary equations

The fundamental equation was compared to the three ancillary equations discussed in Sec. 3. Comparisons were made in terms of percent deviation and are shown in Fig. 23.

The fundamental equation replicates the vapor pressure ancillary equation within ±0.7% over the temperature range from 320 K to the critical point. However, the fundamental equation deviates sharply from the vapor pressure equation at temperatures below 320 K. This deviation at low temperatures is due in part to the fact that vapor pressures below 300 K are very small. Thus, even a large percent deviation corresponds to a very small difference in pressure. Nonetheless, the agreement between these two equations leaves room for improvement. It should also be mentioned that vapor pressures predicted by the fundamental equation do not produce a vapor pressure equation that adheres very well to the guidelines required by Lemmon and Goodwin,[150] as discussed in Sec. 3.3.

The fundamental equation demonstrates excellent agreement with the saturated liquid density ancillary equation. The fundamental equation agrees with the saturated liquid density curve to within ±0.1% over a range of 260–460 K. Larger deviations near the critical point are a result of the near-zero slope in this area.

The fundamental equation agrees with the saturated vapor density ancillary equation within ±1% over a range of 275–500 K. Again, the larger deviations near the critical point are a result of the near-zero slope of the saturation curve in this area. Given the amount of scatter in the saturated vapor density data and the limited number of data sources, the fundamental equation is considered to be in reasonable agreement with the saturated vapor equation.

7. Behavior of the Fundamental Equation

While it is important to fit experimental data well, a fundamental equation must also demonstrate theoretically correct behavior. The behavior of a fundamental equation is important in the range of available data and even beyond the physical limits of the fluid. This section presents the behavior of several properties that demonstrate the overall behavior of the fundamental equation presented in this work. This behavior is also compared with the behavior of Dillon and Penoncello's[13] equation. Though not exhaustive, this section provides a representative overview of the thermodynamic behavior of certain properties that indicate the quality of a fundamental equation.

This article is copyrighted as indicated in the article. Reuse of AIP content is subject to the terms at: http://scitation.aip.org/termsconditions. Downloaded to IP: 131.111.164.128 On: Tue, 21 Oct 2014 07:26:40

TABLE 22. Comparisons of isobaric heat capacity data to the fundamental equations developed in this work (italic) and by Dillon and Penoncello[13] (bold)

Author	Points	AAD	Bias	σ	RMS	Max
Bennewitz and Rossner[74]	2	*8.413*	*−5.377*	*11.898*	*9.985*	*−13.790*
		36.755	**−36.756**	**18.337**	**38.975**	**−49.722**
Benson and D'Arcy[22]	2	*1.064*	*0.505*	*1.504*	*1.178*	*1.569*
		4.962	**−4.962**	**0.727**	**4.989**	**−5.477**
Blacet *et al.*[75]	9	*5.367*	*5.367*	*2.629*	*5.911*	*9.757*
		2.729	**−2.355**	**2.101**	**3.077**	**−4.938**
Bose[76]	8	*0.404*	*−0.170*	*0.468*	*0.470*	*−0.808*
		5.106	**−5.106**	**3.298**	**5.965**	**−8.637**
Counsell *et al.*[77]	25	*2.862*	*1.938*	*4.608*	*4.914*	*17.350*
		6.746	**−5.449**	**4.817**	**7.209**	**12.117**
Dong *et al.*[78]	24	*7.788*	*6.802*	*9.587*	*11.591*	*26.974*
		8.811	**−0.270**	**10.641**	**10.420**	**22.849**
Eucken and Franck[79]	7	*0.460*	*−0.184*	*0.627*	*0.609*	*−1.275*
		5.532	**−3.497**	**5.743**	**6.364**	**−10.139**
Fiock *et al.*[80]	8	*23.554*	*23.554*	*23.822*	*32.425*	*48.368*
		24.669	**17.580**	**26.405**	**30.317**	**44.651**
Fortier *et al.*[81]	2	*0.160*	*0.160*	*0.013*	*0.160*	*0.169*
		5.549	**−5.549**	**0.013**	**5.549**	**−5.559**
Fulem *et al.*[82]	16	*3.954*	*3.954*	*1.521*	*4.219*	*7.228*
		3.559	**−0.947**	**4.200**	**4.175**	**−7.344**
García-Miaja *et al.*[28]	6	*1.272*	*1.272*	*0.351*	*1.312*	*1.785*
		5.322	**−5.322**	**0.875**	**5.382**	**−6.236**
Gibson *et al.*[83]	11	*1.345*	*−1.345*	*0.782*	*1.538*	*−2.536*
		8.487	**−8.120**	**6.947**	**10.479**	**−16.114**
Haida *et al.*[84]	46	*0.155*	*−0.033*	*0.183*	*0.184*	*0.394*
		12.020	**9.383**	**12.210**	**15.294**	**24.838**
Hwa and Ziegler[85]	41	*0.332*	*0.131*	*0.644*	*0.649*	*3.048*
		9.683	**−7.047**	**13.822**	**15.363**	**−45.973**
Kelley[86]	20	*0.736*	*−0.179*	*0.932*	*0.926*	*2.498*
		15.517	**−14.609**	**16.772**	**21.924**	**−52.125**
Khasanshin and Aleksandrov[39]	22	*0.914*	*0.787*	*1.486*	*1.636*	*5.414*
		12.675	**−10.962**	**18.546**	**21.177**	**−67.093**
Mazur[87]	34	*1.141*	*0.424*	*1.216*	*1.271*	*2.326*
		3.553	**−1.604**	**5.540**	**5.689**	**−19.487**
Mitsukuri and Hara[88]	25	*4.225*	*4.225*	*1.266*	*4.403*	*7.114*
		8.075	**2.611**	**9.185**	**9.371**	**−22.417**
Parks[89]	7	*1.115*	*1.033*	*1.895*	*2.036*	*5.192*
		12.932	**−10.223**	**23.546**	**24.077**	**−62.278**
Pedersen *et al.*[90]	16	*2.369*	*2.367*	*1.226*	*2.648*	*5.173*
		5.626	**−5.626**	**0.867**	**5.688**	**−6.939**
Peleteiro *et al.*[55]	4	*0.199*	*−0.197*	*0.168*	*0.245*	*−0.374*
		5.437	**−5.437**	**0.959**	**5.500**	**−6.489**
Peleteiro *et al.*[56]	5	*0.253*	*−0.248*	*0.199*	*0.305*	*−0.480*
		5.005	**−5.005**	**1.258**	**5.130**	**−6.480**
Rivkin and Vinnikova[91]	6	*1.108*	*0.550*	*1.312*	*1.318*	*2.234*
		6.701	**−6.701**	**1.626**	**6.863**	**−9.977**
Sinke and De Vries[92]	9	*6.113*	*5.845*	*9.508*	*10.702*	*27.928*
		7.654	**−0.528**	**10.418**	**9.837**	**23.858**
Stephens and Olson[93]	11	*2.909*	*2.909*	*0.809*	*3.010*	*4.051*
		2.135	**−1.293**	**2.155**	**2.428**	**−3.783**
Strömsöe *et al.*[94]	12	*5.198*	*2.999*	*8.379*	*8.565*	*22.862*
		7.527	**−2.507**	**8.549**	**8.560**	**18.297**
Sun *et al.*[106]	120	*0.966*	*−0.358*	*1.733*	*1.763*	*−8.415*
		2.759	**−0.495**	**3.894**	**3.910**	**−16.905**
Sun *et al.*[107]	105	*1.674*	*0.993*	*1.931*	*2.164*	*4.840*
		4.456	**−4.456**	**1.339**	**4.651**	**−7.519**
Vercher *et al.*[65]	6	*1.758*	*−1.008*	*2.472*	*2.471*	*−4.933*
		7.606	**−7.606**	**3.627**	**8.295**	**−13.030**
Veselý *et al.*[95]	3	*0.307*	*0.307*	*0.229*	*0.360*	*0.567*
		6.683	**−6.683**	**1.008**	**6.734**	**−7.552**
Williams and Daniels[96]	7	*3.435*	*3.328*	*2.955*	*4.308*	*8.027*
		4.127	**−4.127**	**2.335**	**4.659**	**−7.235**
Yu *et al.*[97]	4	*1.480*	*−0.736*	*1.563*	*1.541*	*−2.017*
		6.740	**−6.740**	**0.880**	**6.783**	**−7.292**

This article is copyrighted as indicated in the article. Reuse of AIP content is subject to the terms at: http://scitation.aip.org/termsconditions. Downloaded to IP: 131.111.164.128 On: Tue, 21 Oct 2014 07:26:40

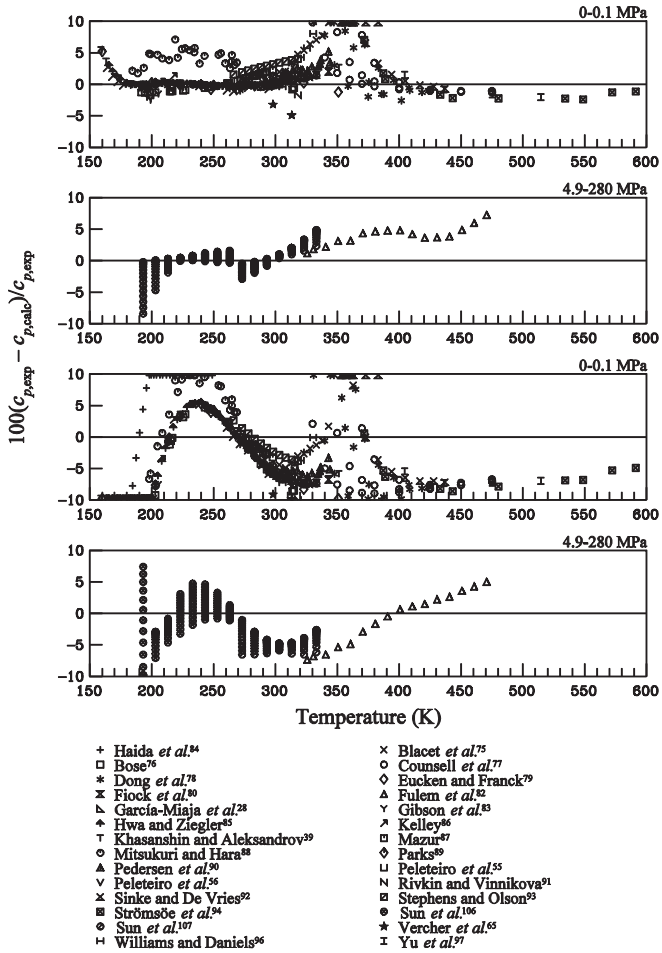

FIG. 16. Comparisons of isobaric heat capacity data to the fundamental equations developed in this work (top two panels) and by Dillon and Penoncello[13] (bottom two panels).

7.1. Behavior of the $p\rho T$ surface

One key aspect of a high-quality fundamental equation is that it must extrapolate well beyond available experimental data. For the $p\rho T$ surface, this means that, at high pressures and densities, isotherms should eventually converge to a single line on a pressure-density plot. Isotherms should not become parallel or cross each other. As shown in Fig. 24, the equation developed in this work extrapolates very well. This is the result of the first term of Eq. (21) being fixed, such that $t_1 = 1.00$ and $d_1 = 4.00$, as recommended by Lemmon and Jacobsen.[151]

The extrapolation behavior of the equation developed in this work is a substantial improvement over the behavior of the equation of Dillon and Penoncello,[13] which is shown in Fig. 25.

TABLE 23. Comparisons of isochoric heat capacity data to the fundamental equations developed in this work (italic) and by Dillon and Penoncello[13] (bold)

Author	Points	AAD	Bias	σ	RMS	Max
Polikhronidi *et al.*[15]	371	*15.95*	*15.95*	*8.36*	*18.00*	*46.80*
		25.56	**25.56**	**8.13**	**26.82**	**53.58**
Kitajima *et al.*[40]	116	*0.94*	*0.57*	*1.12*	*1.25*	*3.03*
		7.47	**−7.47**	**2.50**	**7.88**	**−10.65**

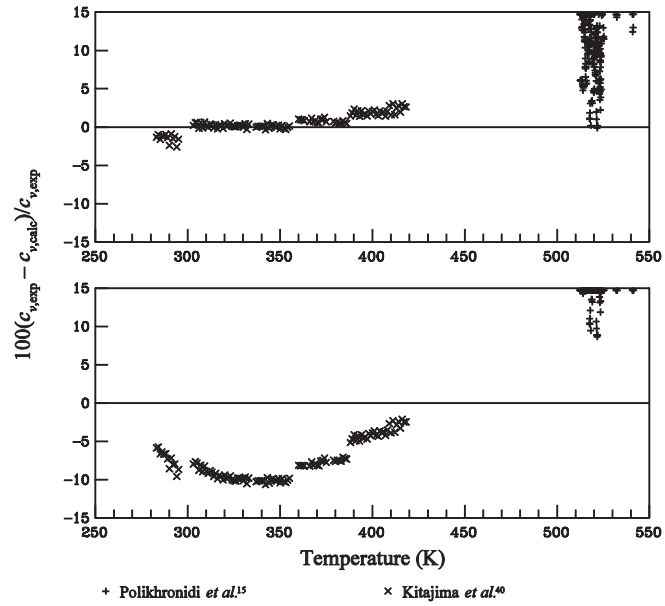

FIG. 17. Comparison of isochoric heat capacity data to the fundamental equations developed in this work (top) and by Dillon and Penoncello[13] (bottom).

Note that all properties in this section have been calculated using the REFPROP software from NIST.[155]

7.2. Behavior of the vapor densities

One model for describing the behavior of a fluid is the virial equation of state, given as

$$p = \rho RT\left(1 + B\rho + C\rho^2 + D\rho^3 + E\rho^4 + \ldots\right), \qquad (22)$$

where B is the second virial coefficient, C is the third, D is the fourth, and so on. In the dilute-gas region, only the first three terms of Eq. (22) contribute substantially to the behavior of the virial equation. Thus, for low densities, the virial equation may be truncated as

$$p = \rho RT\left(1 + B\rho + C\rho^2\right). \qquad (23)$$

After some algebraic manipulation, Eq. (23) may be expressed as

$$\frac{Z-1}{\rho} = B + C\rho, \qquad (24)$$

where Z is the compressibility factor. Based on Eq. (24), the virial coefficients may be derived from the fundamental equation by extrapolating isotherms to zero density. Plotting the left-hand side of Eq. (24) against density, B is simply the intercept of a given isotherm, and C is its slope at zero density. Therefore, B and C can be expressed as functions of temperature only. The second and third virial coefficients can be calculated from the fundamental equation, as shown in Appendix A.

This article is copyrighted as indicated in the article. Reuse of AIP content is subject to the terms at: http://scitation.aip.org/termsconditions. Downloaded to IP: 131.111.164.128 On: Tue, 21 Oct 2014 07:26:40

TABLE 24. Comparisons of sound speed data to the fundamental equations developed in this work (italic) and by Dillon and Penoncello[13] (bold)

Author	Points	AAD	Bias	σ	RMS	Max
Alexandrov and Kochetkov[98]	24	*0.361*	*0.053*	*0.467*	*0.461*	*−1.300*
		2.561	**1.142**	**3.665**	**3.765**	**8.805**
Álvarez *et al.*[17]	6	*0.264*	*0.264*	*0.038*	*0.266*	*0.301*
		0.525	**0.525**	**0.051**	**0.527**	**0.573**
Brown *et al.*[99]	8	*22.923*	*−22.742*	*10.456*	*24.756*	*−33.255*
		5.786	**−3.696**	**7.623**	**8.031**	**−18.134**
Carnevale and Litovitz[100]	5	*0.450*	*−0.412*	*0.483*	*0.597*	*−0.931*
		0.671	**0.427**	**0.640**	**0.714**	**0.996**
Dzida *et al.*[26]	90	*0.219*	*−0.196*	*0.137*	*0.239*	*−0.334*
		0.868	**0.868**	**0.200**	**0.890**	**1.185**
Eden and Richardson[101]	3	*6.703*	*6.703*	*8.423*	*9.603*	*16.403*
		6.520	**6.520**	**6.432**	**8.372**	**13.927**
Freyer *et al.*[102]	6	*0.844*	*0.844*	*0.129*	*0.852*	*1.064*
		1.075	**1.075**	**0.073**	**1.077**	**1.172**
García-Miaja *et al.*[28]	6	*0.053*	*0.021*	*0.061*	*0.059*	*0.086*
		0.328	**0.328**	**0.026**	**0.329**	**0.354**
Golik *et al.*[29]	5	*0.239*	*−0.218*	*0.216*	*0.291*	*−0.516*
		0.164	**0.164**	**0.107**	**0.190**	**0.335**
Gómez *et al.*[31]	3	*0.164*	*0.150*	*0.227*	*0.239*	*0.408*
		0.530	**0.530**	**0.107**	**0.537**	**0.647**
González *et al.*[32]	3	*0.289*	*0.289*	*0.016*	*0.290*	*0.302*
		0.529	**0.529**	**0.028**	**0.529**	**0.553**
Hawley *et al.*[103]	8	*0.811*	*−0.350*	*1.014*	*1.011*	*−2.292*
		1.383	**1.219**	**1.114**	**1.604**	**3.213**
Kadam *et al.*[37]	2	*0.218*	*0.218*	*0.015*	*0.218*	*0.229*
		0.501	**0.501**	**0.076**	**0.504**	**0.555**
Khasanshin and Aleksandrov[39]	22	*0.264*	*0.043*	*0.322*	*0.318*	*0.750*
		1.810	**1.046**	**2.999**	**3.112**	**8.750**
Langa *et al.*[42]	3	*0.161*	*0.161*	*0.018*	*0.162*	*0.182*
		0.399	**0.399**	**0.123**	**0.412**	**0.528**
Onori[104]	7	*0.742*	*0.727*	*1.622*	*1.668*	*4.400*
		0.964	**0.964**	**1.673**	**1.824**	**4.757**
Peleteiro *et al.*[55]	5	*0.299*	*0.299*	*0.124*	*0.319*	*0.453*
		0.538	**0.538**	**0.182**	**0.562**	**0.740**
Rattan *et al.*[57]	2	*0.951*	*0.951*	*0.895*	*1.143*	*1.584*
		1.232	**1.232**	**0.832**	**1.366**	**1.821**
Rodríguez *et al.*[58]	4	*0.084*	*0.084*	*0.040*	*0.091*	*0.129*
		0.357	**0.357**	**0.077**	**0.364**	**0.455**
Sakurai *et al.*[105]	5	*0.091*	*0.039*	*0.104*	*0.101*	*0.139*
		0.275	**0.275**	**0.056**	**0.280**	**0.310**
Sun *et al.*[106]	120	*0.288*	*0.128*	*0.322*	*0.345*	*1.114*
		0.662	**0.438**	**0.872**	**0.973**	**2.911**
Sun *et al.*[107]	105	*0.233*	*−0.126*	*0.330*	*0.351*	*1.721*
		0.863	**0.863**	**0.309**	**0.916**	**2.853**
Vercher *et al.*[65]	6	*0.093*	*0.072*	*0.091*	*0.110*	*0.175*
		0.357	**0.357**	**0.096**	**0.368**	**0.467**
Walsh and Rice[66]	2	*86.615*	*86.615*	*4.547*	*86.675*	*89.830*
		—	—	—	—	—
Wankhede *et al.*[67]	3	*0.381*	*−0.184*	*0.421*	*0.390*	*−0.495*
		0.257	**0.100**	**0.380**	**0.326**	**0.535**
Wilson and Bradley[108]	48	*0.144*	*−0.008*	*0.207*	*0.205*	*0.991*
		0.923	**0.923**	**0.310**	**0.972**	**1.617**
Zafarani-Moattar and Tohidifar[72]	5	*0.077*	*0.052*	*0.083*	*0.091*	*0.138*
		0.386	**0.386**	**0.067**	**0.390**	**0.466**

The behavior of the second and third virial coefficients can be a useful indicator of the quality of a fundamental equation —both in the range of experimental data and in extrapolation of the equation. According to Iglesias-Silva and Hall,[156] B should meet at least three criteria. First, B must approach $-\infty$ as temperature approaches absolute zero. Second, B must pass through a maximum value at some temperature greater than the Boyle temperature (at which $B = 0$). Third, B should approach zero as T approaches ∞. According to Lemmon and Jacobsen,[151] the behavior of C should be similar to that of B, though the location of their maxima and zero values will differ.

This article is copyrighted as indicated in the article. Reuse of AIP content is subject to the terms at: http://scitation.aip.org/termsconditions. Downloaded to IP: 131.111.164.128 On: Tue, 21 Oct 2014 07:26:40

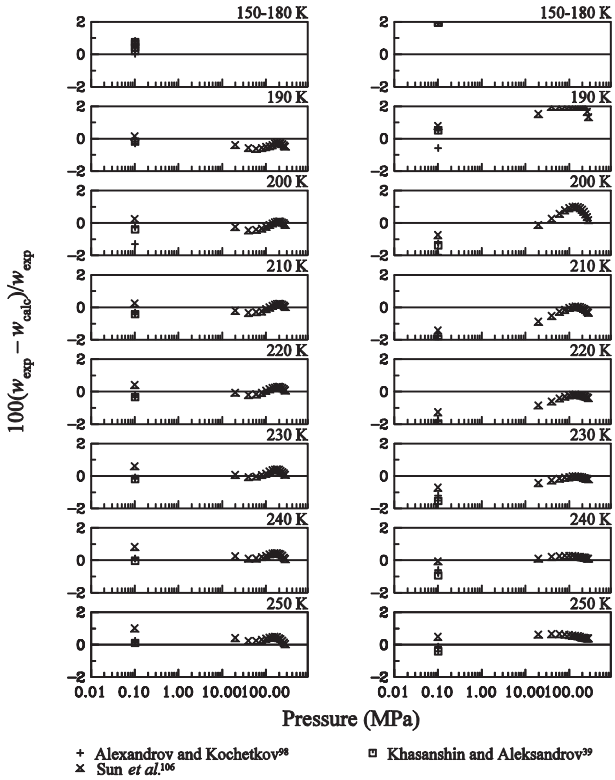

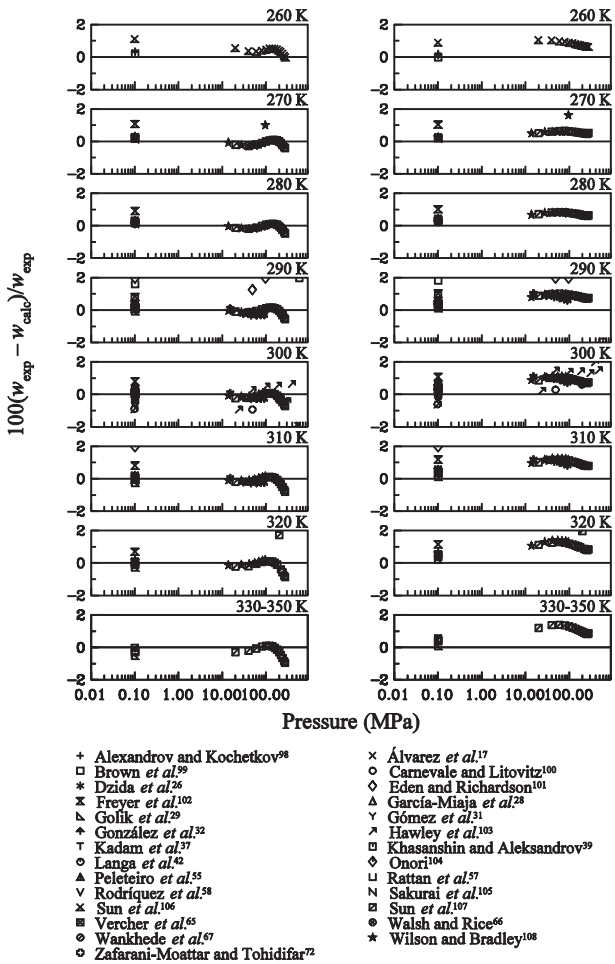

FIG. 18. Comparisons of sound speed data to the fundamental equations developed in this work (left) and by Dillon and Penoncello[13] (right).

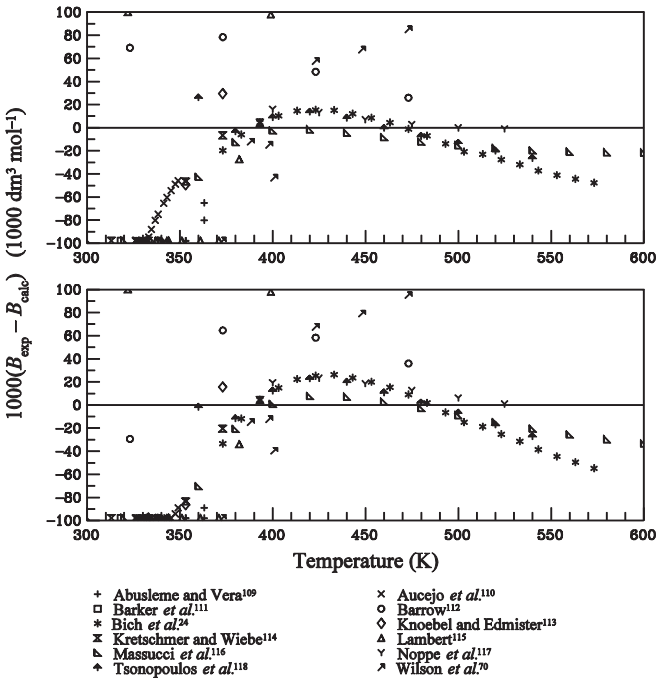

FIG. 19. Comparison of second virial coefficient data to the fundamental equations developed in this work (top) and by Dillon and Penoncello[13] (bottom).

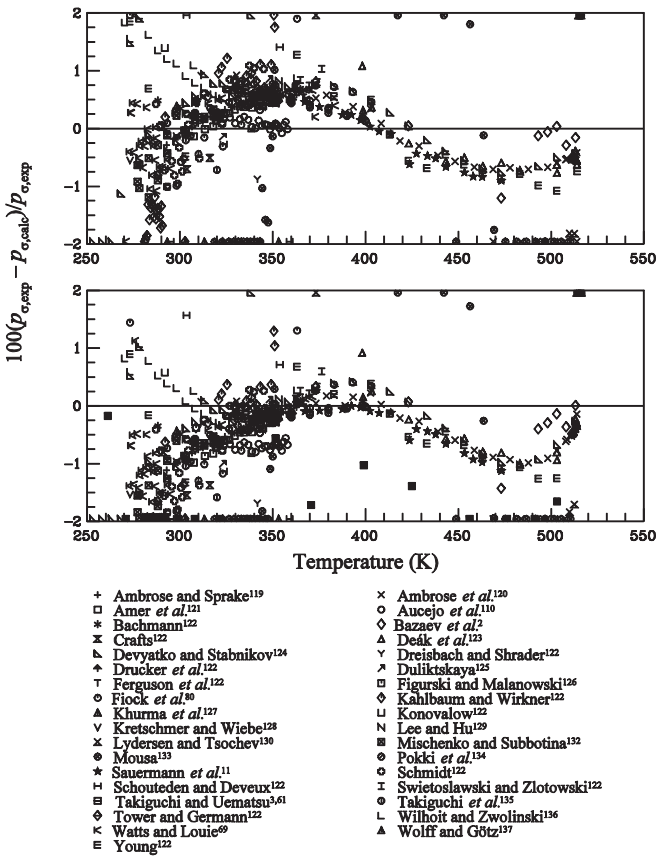

FIG. 20. Comparison of vapor pressure data to the fundamental equations developed in this work (top) and by Dillon and Penoncello[13] (bottom).

This article is copyrighted as indicated in the article. Reuse of AIP content is subject to the terms at: http://scitation.aip.org/termsconditions. Downloaded to IP: 131.111.164.128 On: Tue, 21 Oct 2014 07:26:40

TABLE 25. Comparisons of second virial coefficient data to the fundamental equations developed in this work (italic) and by Dillon and Penoncello[13] (bold)

Author	Points	$\Delta B \times 10^3$	Bias	σ	RMS	Max
Abusleme and Vera[109]	6	*179.28*	*−179.28*	*123.09*	*211.58*	*−336.99*
		217.31	**−217.31**	**135.81**	**250.19**	**−390.16**
Aucejo *et al.*[110]	24	*102.12*	*−102.12*	*29.68*	*106.17*	*−130.54*
		177.84	**−177.84**	**45.72**	**183.38**	**−220.84**
Barker *et al.*[111]	2	*590.76*	*−590.76*	*42.21*	*591.51*	*−620.60*
		678.81	**−678.81**	**77.95**	**681.04**	**−733.93**
Barrow[112]	4	*55.41*	*55.41*	*23.34*	*58.99*	*78.28*
		47.02	**32.30**	**42.95**	**49.27**	**64.50**
Bich *et al.*[24]	21	*19.33*	*−11.30*	*21.31*	*23.67*	*−47.64*
		23.46	**−7.98**	**26.87**	**27.41**	**−54.74**
Knoebel and Edmister[113]	3	*159.08*	*−139.56*	*227.57*	*232.38*	*−398.35*
		191.28	**−180.95**	**257.01**	**277.09**	**−471.82**
Kretschmer and Wiebe[114]	5	*183.17*	*−181.45*	*295.50*	*320.59*	*−696.87*
		233.97	**−232.19**	**345.03**	**386.20**	**−826.55**
Lambert[115]	10	*374.06*	*−328.22*	*333.96*	*456.19*	*−850.81*
		407.90	**−361.47**	**361.16**	**498.05**	**−926.90**
Massucci *et al.*[116]	16	*77.15*	*−77.15*	*165.02*	*177.43*	*−638.77*
		101.73	**−99.41**	**216.64**	**232.12**	**−820.54**
Noppe *et al.*[117]	6	*6.62*	*6.10*	*7.06*	*8.87*	*15.83*
		13.31	**13.31**	**8.57**	**15.44**	**23.10**
Tsonopoulos *et al.*[118]	11	*26.51*	*−16.25*	*51.24*	*51.48*	*−163.72*
		32.29	**−20.06**	**69.01**	**68.79**	**−222.82**
Wilson *et al.*[70]	7	*75.54*	*−15.66*	*113.39*	*106.14*	*−248.11*
		81.51	**−12.62**	**121.96**	**113.62**	**−261.97**

The behavior of the second and third virial coefficients for this work is shown in Fig. 26. Both coefficients correctly approach $-\infty$ in the zero-temperature limit. B also behaves correctly as temperature approaches infinity, remaining positive but approaching zero. The behavior of C in this limit is correct insofar as it approaches zero; however, it does descend into the negative region, which is theoretically incorrect. B reaches its maximum at about 3200 K—just over $6 \times T_c$. C reaches its maximum at roughly 530 K, which is close to the critical temperature.

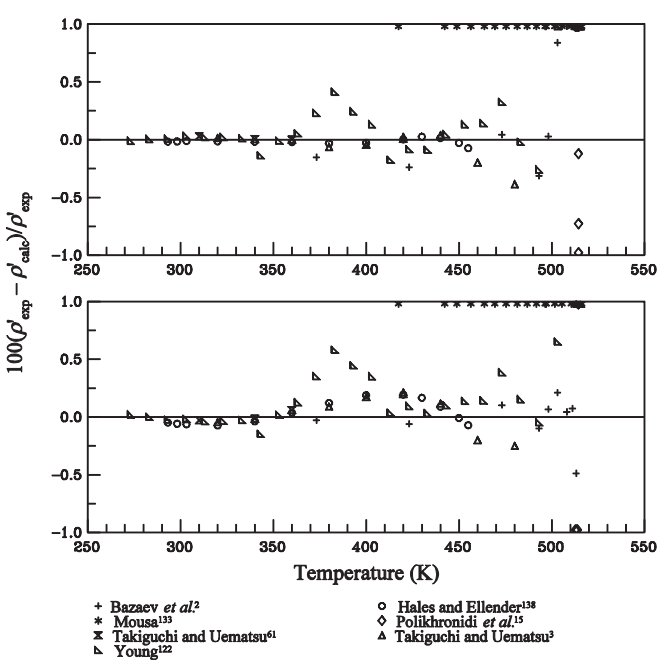

FIG. 21. Comparison of saturated liquid density data to the fundamental equations developed in this work (top) and by Dillon and Penoncello[13] (bottom).

Despite these issues, the behavior of the second and third virial coefficients has been improved over the equation by Dillon and Penoncello,[13] as shown in Fig. 27. In their equation, both virial coefficients approached infinity at both extremes of the temperature scale. Neither curve demonstrated any maximum—local or global—at any point. This indicates that the new equation developed here is much more theoretically sound than its predecessor. The effect of these differing virial coefficients is evident in the behavior of the vapor densities, as shown in Fig. 28.

Note that behavior in the ranges discussed here is purely theoretical. Real ethanol begins to decompose at temperatures just beyond the range of experimental data. While extrapolation behavior is important, the equation of state presented in this work is only considered to be valid up to a temperature of 650 K. When extrapolating the equation beyond 650 K, the reader should bear in mind the possibility of molecular decomposition of the real fluid.

7.3. Behavior in the critical region

The difference between the critical point selected for this work and the critical point calculated from the fundamental equation is extremely small—well within the experimental uncertainty of the data of Bazaev *et al.*[2] These differences are highlighted in Table 29.

The behavior of the critical region appears to be very good, as shown by Fig. 29. The critical isotherm (514.71 K) appears to have an inflection point with zero slope at the critical point.

This article is copyrighted as indicated in the article. Reuse of AIP content is subject to the terms at: http://scitation.aip.org/termsconditions. Downloaded to IP: 131.111.164.128 On: Tue, 21 Oct 2014 07:26:40

TABLE 26. Comparisons of vapor pressure data to the fundamental equations developed in this work (italic) and by Dillon and Penoncello[13] (bold)

Author	Points	AAD	Bias	σ	RMS	Max	$T > T_c$
Ambrose and Sprake[119]	25	*0.396*	*0.340*	*0.291*	*0.444*	*0.609*	*0*
		0.439	**−0.437**	**0.352**	**0.557**	**−1.115**	**0**
Ambrose *et al.*[120]	23	*0.485*	*−0.177*	*0.497*	*0.517*	*−0.708*	*0*
		0.415	**−0.339**	**0.419**	**0.532**	**−0.992**	**0**
Amer *et al.*[121]	12	*0.597*	*0.597*	*0.103*	*0.605*	*0.811*	*0*
		0.201	**−0.201**	**0.089**	**0.219**	**−0.307**	**0**
Aucejo *et al.*[110]	22	*0.083*	*0.074*	*0.072*	*0.102*	*0.201*	*0*
		0.694	**−0.694**	**0.059**	**0.696**	**−0.801**	**0**
Bachmann[a]	1	*0.482*	*0.482*	*—*	*0.482*	*0.482*	*0*
		0.349	**−0.349**	**—**	**0.349**	**−0.349**	**0**
Bazaev *et al.*[2]	9	*0.360*	*−0.163*	*0.532*	*0.528*	*−1.208*	*0*
		0.391	**−0.302**	**0.496**	**0.557**	**−1.429**	**0**
Crafts[a]	5	*0.920*	*0.436*	*1.350*	*1.284*	*2.638*	*0*
		1.202	**−0.286**	**1.519**	**1.388**	**2.169**	**0**
Deák *et al.*[123]	20	*0.570*	*−0.425*	*0.424*	*0.593*	*1.082*	*0*
		0.530	**−0.413**	**0.426**	**0.586**	**−0.998**	**0**
Devyatko and Stabnikov[124]	49	*2.400*	*−1.513*	*4.659*	*4.852*	*−22.367*	*1*
		3.207	**−2.977**	**6.321**	**6.927**	**−28.743**	**1**
Dreisbach and Shrader[a]	3	*0.905*	*0.318*	*1.038*	*0.906*	*0.921*	*0*
		0.613	**−0.513**	**1.018**	**0.976**	**−1.688**	**0**
Drucker *et al.*[a]	10	*47.750*	*37.693*	*45.014*	*56.960*	*90.584*	*0*
		46.105	**33.055**	**46.044**	**54.779**	**88.789**	**0**
Dulitskaya[125]	3	*0.388*	*0.180*	*0.582*	*0.508*	*0.852*	*0*
		0.703	**−0.634**	**0.638**	**0.821**	**−1.008**	**0**
Ferguson *et al.*[a]	1	*0.175*	*−0.175*	*—*	*0.175*	*−0.175*	*0*
		1.013	**–1.013**	**—**	**1.013**	**–1.013**	**0**
Figurski and Malanowski[126]	17	*0.317*	*0.299*	*0.180*	*0.347*	*0.470*	*0*
		0.515	**−0.515**	**0.214**	**0.555**	**−0.983**	**0**
Fiock *et al.*[80]	15	*0.644*	*0.397*	*0.853*	*0.914*	*2.394*	*0*
		0.829	**−0.280**	**0.942**	**0.952**	**−1.826**	**0**
Kahlbaum and Wirkner[a]	38	*1.246*	*−0.367*	*1.334*	*1.366*	*−2.896*	*0*
		1.410	**−1.200**	**1.365**	**1.804**	**−3.796**	**0**
Khurma *et al.*[127]	3	*0.439*	*0.439*	*0.155*	*0.457*	*0.613*	*0*
		0.240	**−0.140**	**0.292**	**0.277**	**−0.434**	**0**
Konovalow[a]	5	*0.481*	*0.481*	*0.551*	*0.689*	*1.396*	*0*
		0.563	**−0.331**	**0.561**	**0.601**	**−0.817**	**0**
Kretschmer and Wiebe[128]	8	*0.317*	*0.148*	*0.342*	*0.353*	*−0.547*	*0*
		0.697	**−0.697**	**0.400**	**0.791**	**−1.529**	**0**
Lee and Hu[129]	6	*0.661*	*0.661*	*0.149*	*0.675*	*0.825*	*0*
		0.128	**−0.035**	**0.195**	**0.182**	**−0.403**	**0**
Lydersen and Tsochev[130]	12	*2.252*	*−2.252*	*0.379*	*2.281*	*−2.899*	*2*
		2.439	**−2.439**	**0.487**	**2.482**	**−3.090**	**3**
Merriman[131]	61	*0.572*	*0.124*	*0.702*	*0.707*	*−2.820*	*0*
		0.748	**−0.684**	**0.765**	**1.022**	**−3.865**	**0**
Mishchenko and Subbotina[132]	22	*0.408*	*−0.206*	*0.491*	*0.522*	*−1.192*	*0*
		1.065	**−1.065**	**0.509**	**1.175**	**−2.061**	**0**
Mousa[133]	33	*5.311*	*−4.441*	*5.462*	*6.973*	*−18.286*	*1*
		5.793	**−4.973**	**5.671**	**7.476**	**−19.304**	**1**
Pokki *et al.*[134]	13	*0.589*	*0.589*	*0.107*	*0.598*	*0.809*	*0*
		0.195	**−0.195**	**0.133**	**0.233**	**−0.503**	**0**
Sauermann *et al.*[11]	21	*0.474*	*−0.114*	*0.541*	*0.540*	*−0.903*	*0*
		0.367	**−0.367**	**0.351**	**0.503**	**−1.124**	**0**
Schmidt[a]	32	*0.572*	*0.142*	*0.644*	*0.650*	*1.091*	*0*
		0.741	**−0.690**	**0.654**	**0.944**	**−1.843**	**0**
Schouteden and Deveux[a]	9	*1.465*	*−0.075*	*1.986*	*1.874*	*−3.604*	*0*
		1.368	**−0.862**	**1.978**	**2.055**	**−4.280**	**0**
Swietoslawski and Zlotowski[a]	6	*0.767*	*0.767*	*0.168*	*0.782*	*1.035*	*0*
		0.265	**0.203**	**0.266**	**0.317**	**0.598**	**0**
Takiguchi and Uematsu[61]	3	*0.420*	*0.420*	*0.196*	*0.449*	*0.579*	*0*
		0.345	**−0.345**	**0.264**	**0.407**	**−0.647**	**0**
Takiguchi *et al.*[135]	27	*0.408*	*0.322*	*0.328*	*0.455*	*0.771*	*0*
		0.214	**−0.209**	**0.381**	**0.428**	**−1.584**	**0**
Tower and Germann[a]	1	*0.817*	*−0.817*	*—*	*0.817*	*−0.817*	*0*
		1.659	**−1.659**	**—**	**1.659**	**−1.659**	**0**

This article is copyrighted as indicated in the article. Reuse of AIP content is subject to the terms at: http://scitation.aip.org/termsconditions. Downloaded to IP: 131.111.164.128 On: Tue, 21 Oct 2014 07:26:40

TABLE 26. Comparisons of vapor pressure data to the fundamental equations developed in this work (italic) and by Dillon and Penoncello[13] (bold)—Continued

Author	Points	AAD	Bias	σ	RMS	Max	$T > T_c$
Watts and Louie[69]	12	*0.471*	*0.471*	*0.120*	*0.485*	*0.717*	*0*
		0.268	**−0.242**	**0.183**	**0.299**	**−0.407**	**0**
Wilhoit and Zwolinski[136]	24	*0.896*	*0.896*	*0.468*	*1.007*	*1.956*	*0*
		0.355	**0.078**	**0.435**	**0.433**	**1.070**	**0**
Wolff and Götz[137]	7	*3.841*	*−3.841*	*1.247*	*4.010*	*−5.873*	*0*
		4.690	**−4.690**	**1.290**	**4.840**	**−6.748**	**0**
Young[a]	22	*0.716*	*−0.202*	*0.812*	*0.815*	*1.855*	*3*
		0.718	**−0.478**	**0.677**	**0.813**	**−1.324**	**4**

[a]As reported by Timmermans.[122]

Higher temperature isotherms increase monotonically, while lower temperature isotherms exhibit some negative slope in the two-phase region.

This behavior is a substantial improvement over that of the equation of Dillon and Penoncello,[13] shown in Fig. 30. The critical point as calculated by their equation is far away from the reference values chosen for that work. The result is that the saturated vapor and saturated liquid curves do not meet at the critical point. Rather, the vapor dome ends abruptly at a pressure of 6.148 MPa and a temperature of 513.9 K. Furthermore, the slope and curvature of the critical and near critical isotherms are highly uncharacteristic of real fluid behavior.

7.4. Behavior of the isobaric and isochoric heat capacities

The behavior of the isobaric heat capacity, shown in Fig. 31, appears to be good over most of its range. The fundamental equation correctly models a peak tending toward infinity at the critical point. Vapor-phase heat capacities appear to be theoretically correct. However, systematic deviations occur between the experimental data[77,94] and the fundamental equation near the saturated vapor curve. As shown by Fig. 32, the experimental data indicate that the saturated vapor heat capacity curve should be higher than predicted by the equation. It is unclear whether this is a result of experimental error or a failure of the equation of state to model real fluid behavior. The fact that $(\partial^2 c_p/\partial T^2)_p$ is negative in the liquid region around 420 K may also indicate some uncharacteristic behavior in the equation. Also, for very high pressures, $(\partial c_p/\partial T)_p$ is negative at very low temperatures (e.g., the 300 MPa isobar below about 200 K in Fig. 31). This is also uncharacteristic of the real fluid behavior. Fitting the heat capacity data of Sun *et al.*[106,107] may improve this behavior.

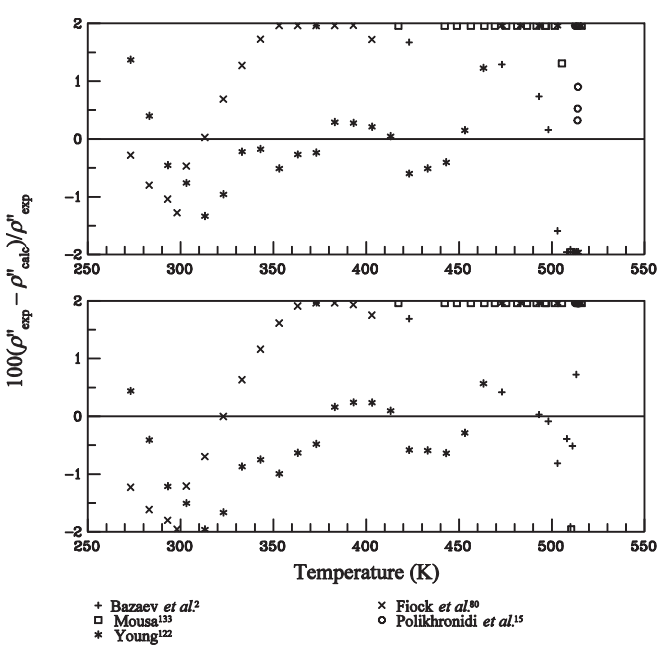

FIG. 22. Comparison of saturated vapor density data to the fundamental equations developed in this work (top) and by Dillon and Penoncello[13] (bottom).

The equation developed in this work shows substantial improvements over the equation of Dillon and Penoncello[13] in terms of the isobaric heat capacity behavior. The isobaric heat capacity behavior of Dillon and Penoncello's[13] equation is shown in Fig. 33. Though imperfect, the equation developed in this work has improved the behavior of $(\partial^2 c_p/\partial T^2)_p$ below the critical point. Furthermore, the behavior of low-temperature heat capacities of this work demonstrates a significant improvement over the previous equation.

The behavior of the isochoric heat capacity, shown in Fig. 34, is not as good as the isobaric heat capacity. The isochoric heat capacity exhibits the same problems with $(\partial^2 c_p/\partial T^2)_p$ and $(\partial c_p/\partial T)_p$ as the isobaric heat capacity. Nonetheless, the equation developed in this work demonstrates improved isochoric heat capacity behavior over the equation of Dillon and Penoncello,[13] shown in Fig. 35.

7.5. Behavior of the sound speed

The sound speed behavior of the fundamental equation is shown in Fig. 36. The behavior is generally good. Theoretically, sound speed should approach zero at the critical point. However, few, if any, fundamental equations achieve this in practice. Generally, it is sufficient for the speed of sound to demonstrate a minimum at the critical point. The equation developed in this work properly exhibits this behavior.

The sound speed behavior of this work demonstrates improvement over that of the equation of Dillon and Penoncello[13] near the triple-point temperature. The equation of Ref. 13, shown in Fig. 37, demonstrates highly uncharacteristic behavior below

This article is copyrighted as indicated in the article. Reuse of AIP content is subject to the terms at: http://scitation.aip.org/termsconditions. Downloaded to IP: 131.111.164.128 On: Tue, 21 Oct 2014 07:26:40

TABLE 27. Comparisons of saturated liquid density data to the fundamental equations developed in this work (italic) and by Dillon and Penoncello[13] (bold)

Author	Points	AAD	Bias	σ	RMS	Max	$T > T_c$
Bazaev *et al.*[2]	9	*1.993*	*1.837*	*2.967*	*3.346*	*7.546*	*0*
		0.131	**−0.020**	**0.199**	**0.188**	**−0.489**	**0**
Hales and Ellender[138]	13	*0.023*	*−0.017*	*0.024*	*0.029*	*−0.074*	*0*
		0.089	**0.033**	**0.105**	**0.106**	**0.193**	**0**
Mousa[133]	16	*11.276*	*11.276*	*4.549*	*12.102*	*24.024*	*1*
		10.986	**10.986**	**3.653**	**11.539**	**20.011**	**1**
Polikhronidi *et al.*[15]	11	*3.681*	*2.869*	*3.400*	*4.329*	*6.334*	*0*
		1.691	**−1.691**	**0.226**	**1.701**	**−1.884**	**8**
Takiguchi and Uematsu[61]	3	*0.011*	*0.011*	*0.016*	*0.017*	*0.029*	*0*
		0.035	**0.004**	**0.047**	**0.039**	**0.058**	**0**
Takiguchi and Uematsu[3]	8	*0.097*	*−0.077*	*0.146*	*0.157*	*−0.386*	*0*
		0.160	**0.036**	**0.181**	**0.173**	**−0.251**	**0**
Young[a]	28	*1.293*	*1.233*	*4.066*	*4.173*	*16.912*	*2*
		0.368	**0.341**	**1.041**	**1.076**	**5.238**	**3**

[a]As reported by Timmermans.[122]

about 220 K. Sharp discontinuities are also apparent at high pressures, caused by the negative heat capacities. Though isobars of the sound speed calculated from this work have some minor inflection points at low temperatures, their behavior is a substantial improvement over the existing equation.

7.6. Behavior of the characteristic equations

Four characteristic curves were plotted as a means of determining the quality of the fundamental equation. These include the Boyle curve

$$\left(\frac{\partial Z}{\partial v}\right)_T = 0, \tag{25}$$

the Joule-Thomson inversion curve,

$$\left(\frac{\partial Z}{\partial T}\right)_p = 0, \tag{26}$$

the Joule inversion curve,

$$\left(\frac{\partial Z}{\partial T}\right)_v = 0, \tag{27}$$

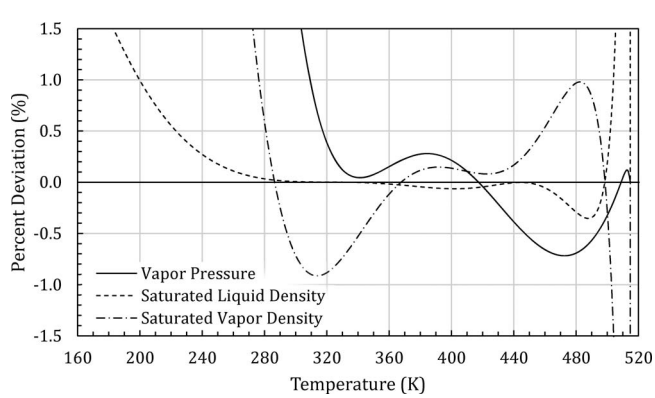

FIG. 23. Deviations of the ancillary equations from the fundamental equation developed in this work.

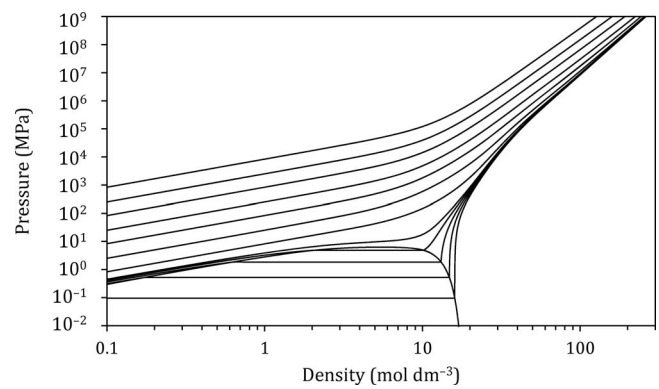

FIG. 24. Isothermal behavior of the fundamental equation developed in this work at extreme conditions (from bottom to top, isotherms are shown at 350, 400, 450, 500, 550, 1×10^3, 3×10^3, 1×10^4, 3×10^4, 1×10^5, 3×10^5, and 1×10^6 K).

and the ideal curve

$$\frac{p}{\rho RT} = 1. \tag{28}$$

These four curves describe the thermodynamic surface in regions well beyond the limits of the experimental data. Thus,

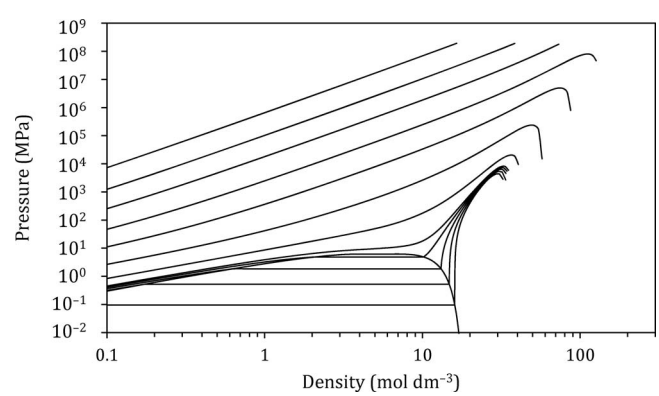

FIG. 25. Isothermal behavior of the fundamental equation of Dillon and Penoncello[13] at extreme conditions (from bottom to top, isotherms are shown at 350, 400, 450, 500, 550, 1×10^3, 3×10^3, 1×10^4, 3×10^4, 1×10^5, 3×10^5, and 1×10^6 K).

This article is copyrighted as indicated in the article. Reuse of AIP content is subject to the terms at: http://scitation.aip.org/termsconditions. Downloaded to IP: 131.111.164.128 On: Tue, 21 Oct 2014 07:26:40

TABLE 28. Comparisons of saturated vapor density data to the fundamental equations developed in this work (italic) and by Dillon and Penoncello[13] (bold)

Author	Points	AAD	Bias	σ	RMS	Max	$T > T_c$
Bazaev *et al.*[2]	9	*4.789*	*−2.577*	*7.452*	*7.484*	*−19.319*	*0*
		1.171	**0.768**	**2.054**	**2.084**	**5.868**	**0**
Fiock *et al.*[80]	15	*1.341*	*0.823*	*1.335*	*1.530*	*2.332*	*0*
		1.447	**0.300**	**1.590**	**1.565**	**2.092**	**0**
Mousa[133]	16	*19.886*	*17.568*	*15.539*	*23.108*	*57.194*	*1*
		19.166	**17.781**	**14.357**	**22.551**	**57.211**	**1**
Polikhronidi *et al.*[15]	11	*5.482*	*5.482*	*4.284*	*6.837*	*12.805*	*0*
		21.888	**21.888**	**1.149**	**21.911**	**23.402**	**7**
Young[a]	28	*2.647*	*−0.808*	*6.173*	*6.107*	*−26.793*	*2*
		1.596	**0.580**	**2.551**	**2.566**	**7.262**	**3**

[a]As reported by Timmermans.[122]

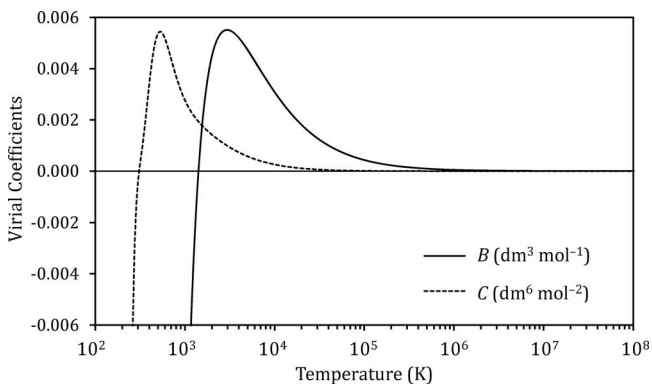

FIG. 26. Virial coefficient behavior of the fundamental equation developed in this work.

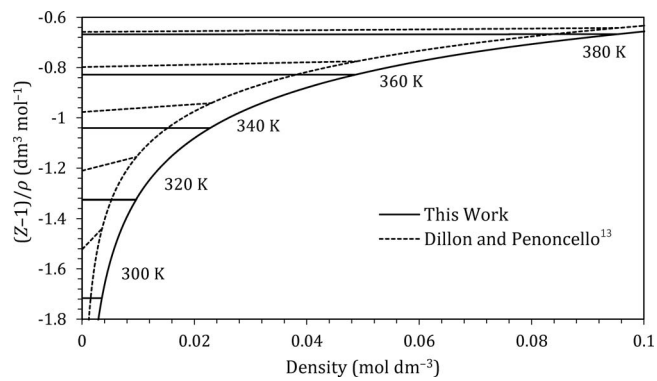

FIG. 28. Isothermal behavior of the vapor density of ethanol.

they provide a way to observe the quality of the fundamental equation's extrapolation behavior. The zero-pressure intercept of the Boyle and ideal curves corresponds to the Boyle temperature —the temperature at which the second virial coefficient is zero. The zero-pressure intercept of the Joule inversion curve corresponds to the temperature where the second virial coefficient reaches its maximum. The fundamental equation for R-125 (pentafluoroethane) published by Lemmon and Jacobsen[151] displays exemplary characteristic curves.

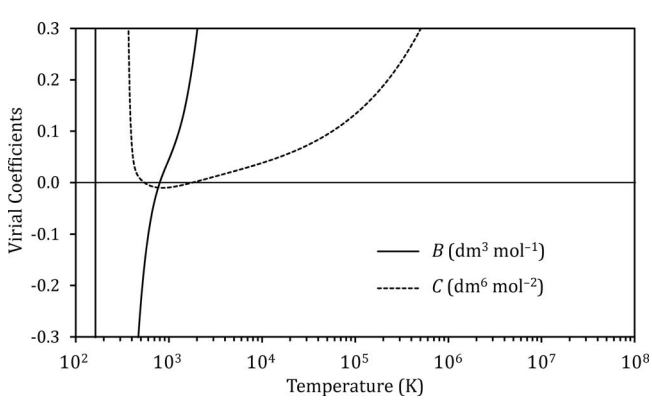

FIG. 27. Virial coefficient behavior of the fundamental equation of Dillon and Penoncello.[13]

Figure 38 compares the characteristic curves of R-125 with those of the fundamental equation presented in this work. The Boyle curve and ideal curve for ethanol both appear to be theoretically correct. However, the Joule-Thomson inversion curve exhibits negative curvature near its top. This is uncharacteristic of real fluid behavior. The Joule-Inversion curve also exhibits uncharacteristic behavior across its length. Thus, the equation of state presented in this work does not extrapolate as well as that for R-125.

Nevertheless, the new ethanol equation is a substantial improvement over the behavior of the fundamental equation of Dillon and Penoncello.[13] The characteristic curves for their equation are shown in Fig. 39. All curves demonstrate highly unphysical behavior. No Joule-Thomson inversion curve could be calculated from their equation. Therefore, despite some uncharacteristic behavior, the equation developed in this work is a significant improvement over the equation of Dillon and

TABLE 29. Comparison of the selected critical point to the fundamental equation

	Reference (Bazaev *et al.*[2])	Fundamental equation	$\left(\frac{\text{Fund.eq.}}{\text{Reference}}\right)$
Critical temperature (K)	514.71 ± 0.2	514.709 285	99.999 861%
Critical pressure (MPa)	6.268 ± 0.008	6.267 915	99.998 637%
Critical density (mol dm^{-3})	5.93 ± 0.04	5.930 686	100.011 574%

This article is copyrighted as indicated in the article. Reuse of AIP content is subject to the terms at: http://scitation.aip.org/termsconditions. Downloaded to IP: 131.111.164.128 On: Tue, 21 Oct 2014 07:26:40

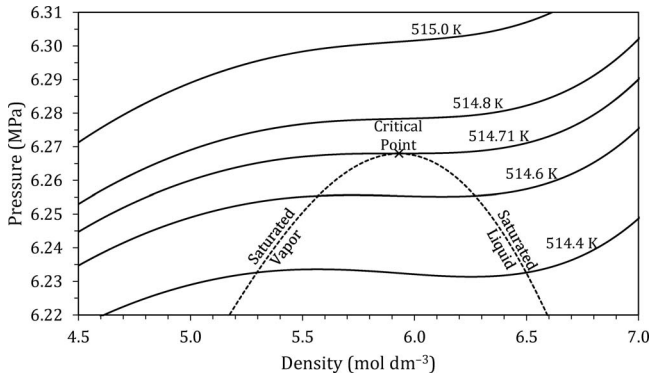

FIG. 29. Isothermal behavior near the critical point of the fundamental equation developed in this work.

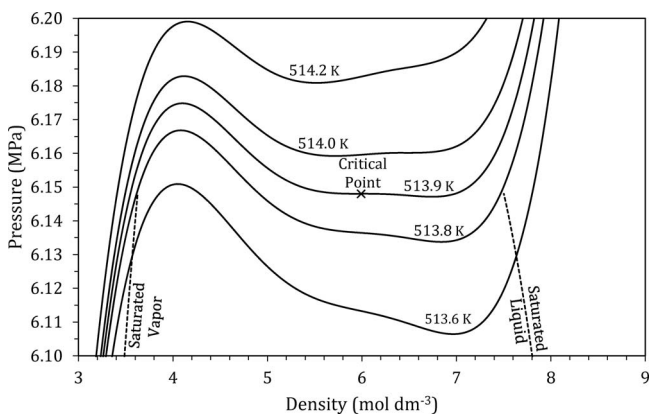

FIG. 30. Isothermal behavior near the critical point of the fundamental equation of Dillon and Penoncello.[13]

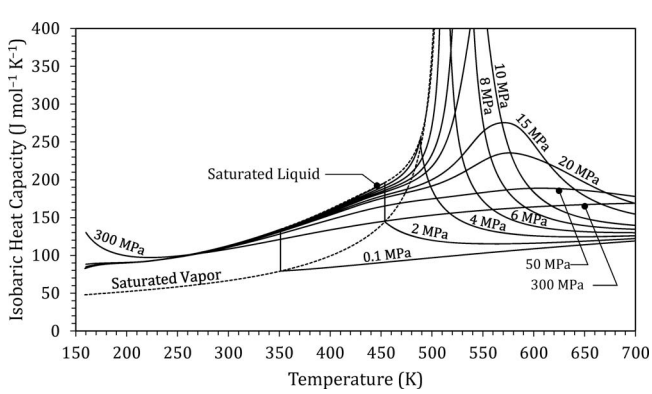

FIG. 31. Isobaric heat capacity behavior of the fundamental equation developed in this work.

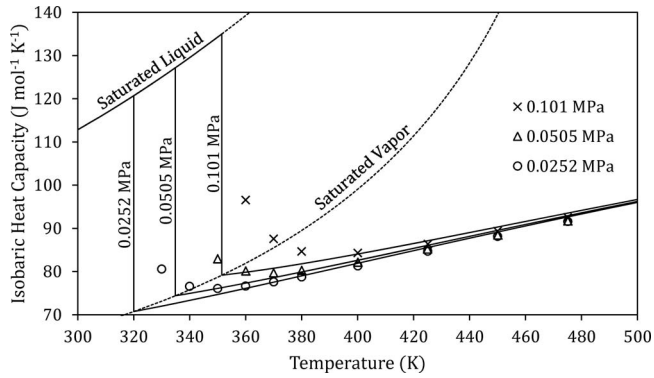

FIG. 32. Comparison of vapor-phase heat capacity data from Counsell *et al.*[77] to the fundamental equation presented in this work.

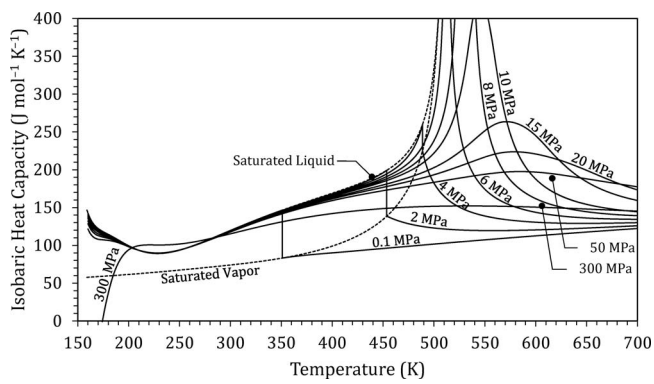

FIG. 33. Isobaric heat capacity behavior of the fundamental equation of Dillon and Penoncello.[13]

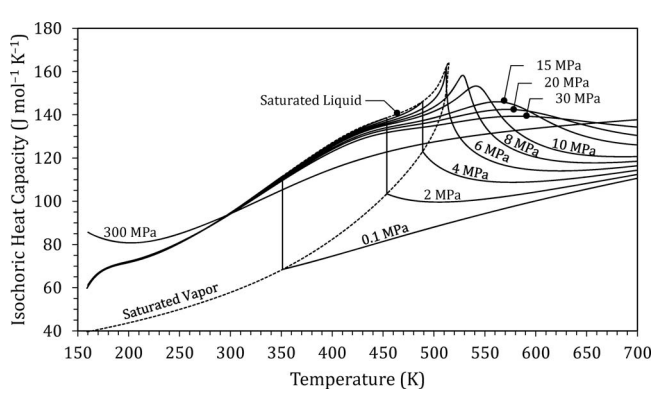

FIG. 34. Isochoric heat capacity behavior of the fundamental equation developed in this work.

This article is copyrighted as indicated in the article. Reuse of AIP content is subject to the terms at: http://scitation.aip.org/termsconditions. Downloaded to IP: 131.111.164.128 On: Tue, 21 Oct 2014 07:26:40

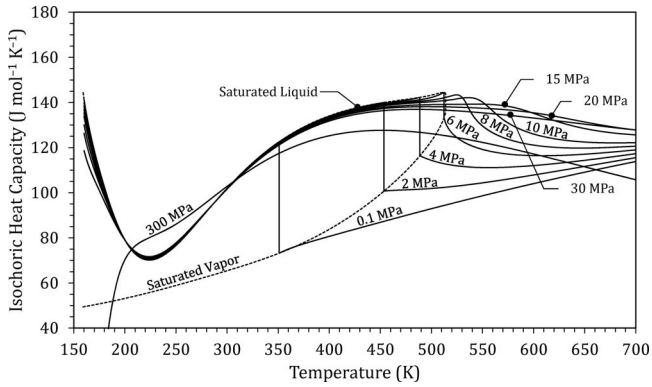

FIG. 35. Isochoric heat capacity behavior of the fundamental equation of Dillon and Penoncello.[13]

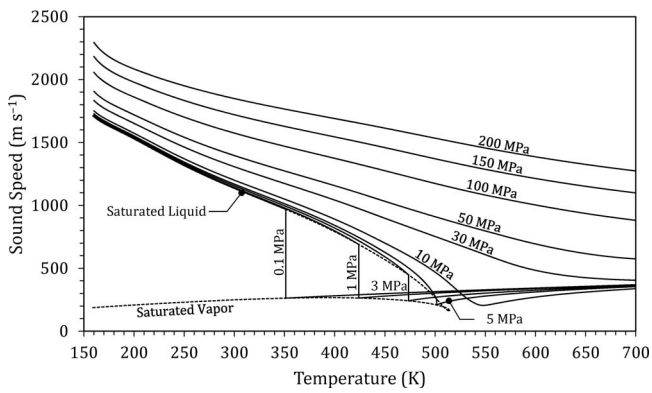

FIG. 36. Sound speed behavior of the fundamental equation developed in this work.

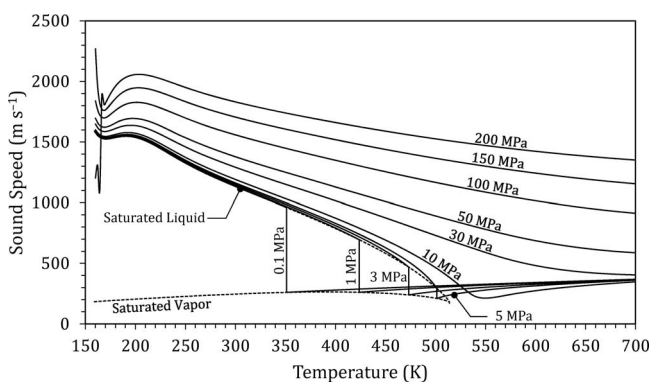

FIG. 37. Sound speed behavior of the fundamental equation of Dillon and Penoncello.[13]

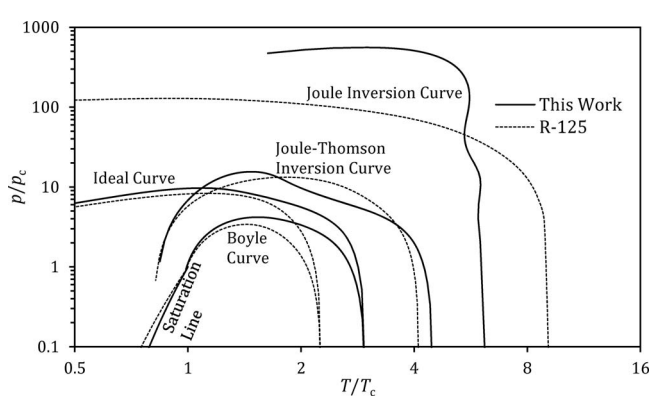

FIG. 38. Characteristic curves for ethanol and R-125.

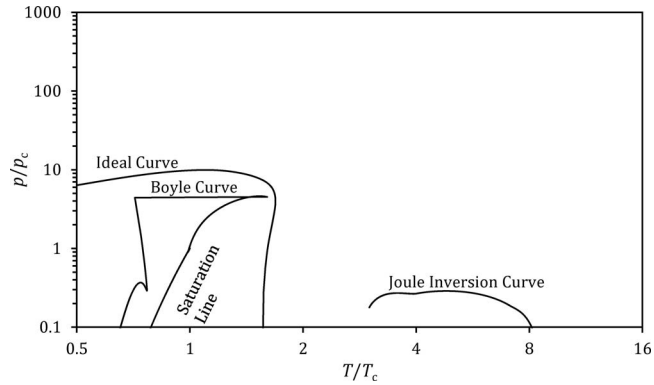

FIG. 39. Characteristic curves of the fundamental equation of Dillon and Penoncello.[13]

Penoncello[13] in this regard. Note that Dillon and Penoncello[13] did not have the ability to plot these curves when they developed their equation.

7.7. Behavior of the saturated densities

The behavior of the saturated density curves is an important parameter for determining the quality of a fundamental equation. The curve that bisects the saturated vapor curve and the saturated liquid curve is called the rectilinear diameter. The rectilinear diameter for density, Φ, is calculated as

$$\Phi = \frac{1}{2}(\rho' + \rho''). \tag{29}$$

Wang and Anisimov[157] have shown that the rectilinear diameter of a real fluid should bend slightly in the direction of the saturated vapor curve near the critical point. Bazaev *et al.*[2] have shown that ethanol follows this behavior. However, Fig. 40 shows that the rectilinear diameter predicted by the equation of state does bend correctly at first, but then turns back toward the saturated liquid curve to get to the critical point. This behavior is inconsistent with real fluid behavior and is indicative of some shortcomings of the fundamental equation near the critical point.

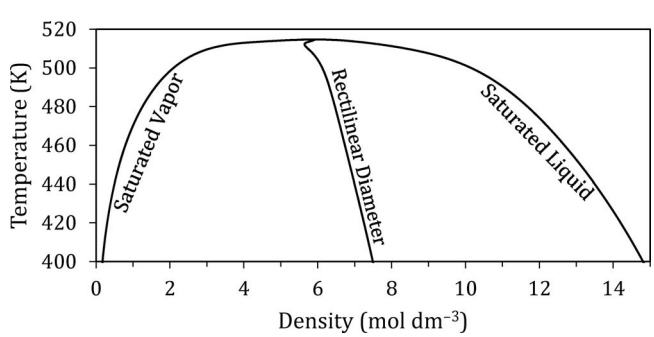

FIG. 40. Behavior of the rectilinear diameter for the fundamental equation developed in this work.

This article is copyrighted as indicated in the article. Reuse of AIP content is subject to the terms at: http://scitation.aip.org/termsconditions. Downloaded to IP: 131.111.164.128 On: Tue, 21 Oct 2014 07:26:40

8. Conclusions and Recommendations

8.1. Conclusions

The purpose of this work was to utilize nonlinear fitting techniques and new experimental data to develop a more accurate and theoretically correct fundamental equation for ethanol than was previously available. For most of the parts, this equation exceeds the fundamental equation of Dillon and Penoncello[13] in the representation of available data and theoretical correctness of the thermodynamic surface. In particular, the heat capacity, critical region, and extrapolation behavior of the equation presented in this work demonstrate significant improvements over the equation of Dillon and Penoncello.[13]

The fundamental equation presented in this work is valid for single-phase and saturation states for temperatures from 160 to 650 K and pressures up to 280 MPa. The formulation may be used to calculate thermodynamic properties anywhere within this range.

The uncertainty of the fundamental equation in calculating thermodynamic properties is 0.2% for density (2% in the critical region), 1% for speed of sound, 1% for liquid-phase heat capacities, and 2% for vapor heat capacities. Values of the vapor pressure and saturated vapor density are represented to within ±1% at temperatures of 300 K and above. Values of the saturated liquid density are represented to within 0.3% at temperatures of 200 K and above.

8.2. Recommendations

Though the equation presented in this work resolves some of the problems of Dillon and Penoncello's[13] equation, some issues remain unresolved. First of all, the fit of the equation in the critical region does not sufficiently represent the experimental data within their stated accuracy. The fundamental equation of Dillon and Penoncello[13] fits the data more closely, despite significant flaws in the critical region. Whether the discrepancy is due to experimental error or inaccuracy of the fundamental equation remains unknown. This should be elucidated in future work. It may be beneficial to reconsider the location of the critical point.

Second, the discrepancy between the near-saturation, vapor-phase isobaric heat capacity data, and the fundamental equation should be resolved. Future work should investigate whether the difference is due to experimental error or some insufficiency of the fundamental equation. The behavior of the methanol equation of de Reuck and Craven[158] appears to be more in line with the behavior of the experimental data of Counsell *et al.*[77] rather than that of the equation presented in this work. Therefore, the discrepancy that arises in this work likely indicates a deficiency of the equation rather than the experimental data.

Third, the uncertainty and disagreement of vapor pressure data, particularly at low pressures, has historically plagued work on the fundamental equation of ethanol. High-accuracy experimental work across the entire range of the vapor pressure curve would be a tremendous help in developing a more accurate fundamental equation.

Saturated vapor density data were also extremely limited and demonstrated a high degree of scatter. High-accuracy experimental work for this property may also improve the accuracy of a future equation.

Very limited isochoric heat capacity data were available. Additional data, particularly in the liquid region, may be helpful.

Further development of the fundamental equation should continue in order to achieve an equation that produces more theoretically sound characteristic curves, second and third virial coefficient curves, heat capacity curves, rectilinear diameter, and two-phase behavior. This will be a necessary step toward obtaining a reference-quality fundamental equation for ethanol.

Finally, the scope of this work was limited to the liquid, vapor, two-phase, and supercritical regions. Future work to review the melting curve and glassy-phase data would complement this work well. Since this work did not include a melting curve, the melting curve of Sun *et al.*[159] is provided below for reference. They used a Simon-Glatzel equation in the form

$$\frac{p}{N} = \left(\frac{T}{T_0}\right)^k - 1, \tag{30}$$

where N, T_0, and k are the fit parameters. According to Sun *et al.*,[159] $N = 436.9$ MPa, $T_0 = 158.37$ K, and $k = 2.6432$.

9. Appendix A: Thermodynamic Equations

This Appendix documents the equations used to calculate thermodynamic properties from the fundamental EOS. Table 30 contains calculated properties for computer-program verification.

Pressure (p):

$$p = \rho RT\left[1 + \delta\left(\frac{\partial \alpha^{\mathrm{r}}}{\partial \delta}\right)_\tau\right]. \tag{A1}$$

Compressibility factor (Z)

$$Z = \frac{p}{\rho RT} = 1 + \delta\left(\frac{\partial \alpha^{\mathrm{r}}}{\partial \delta}\right)_\tau. \tag{A2}$$

Internal energy (u):

$$\frac{u}{RT} = \tau\left[\left(\frac{\partial \alpha^0}{\partial \tau}\right)_\delta + \left(\frac{\partial \alpha^{\mathrm{r}}}{\partial \tau}\right)_\delta\right]. \tag{A3}$$

Enthalpy (h):

$$\frac{h}{RT} = \tau\left[\left(\frac{\partial \alpha^0}{\partial \tau}\right)_\delta + \left(\frac{\partial \alpha^{\mathrm{r}}}{\partial \tau}\right)_\delta\right] + \delta\left(\frac{\partial \alpha^{\mathrm{r}}}{\partial \delta}\right)_\tau + 1. \tag{A4}$$

Entropy (s):

$$\frac{s}{RT} = \tau\left[\left(\frac{\partial \alpha^0}{\partial \tau}\right)_\delta + \left(\frac{\partial \alpha^{\mathrm{r}}}{\partial \tau}\right)_\delta\right] - \alpha^0 - \alpha^{\mathrm{r}}. \tag{A5}$$

This article is copyrighted as indicated in the article. Reuse of AIP content is subject to the terms at: http://scitation.aip.org/termsconditions. Downloaded to IP: 131.111.164.128 On: Tue, 21 Oct 2014 07:26:40

TABLE 30. Calculated values of properties for algorithm verification

T (K)	ρ (mol dm^{-3})	p (MPa)	c_v (J mol^{-1} K^{-1})	c_p (J mol^{-1} K^{-1})	w (m s^{-1})
300.0	18.0	65.640 781	94.211 739	110.342 95	1454.8360
450.0	13.2	2.921 546 0	137.367 90	191.289 01	588.678 33
450.0	0.5	1.554 077 1	97.346 133	125.531 09	263.572 31
550.0	6.0	10.315 533	151.001 69	440.131 87	207.740 32
514.8	6.0	6.278 417 6	163.950 41	115 623.88	159.345 83

Gibbs energy (g):

$$\frac{g}{RT} = 1 + \alpha^0 + \alpha^{\mathrm{r}} + \delta\left(\frac{\partial\alpha^{\mathrm{r}}}{\partial\delta}\right)_\tau. \tag{A6}$$

Isochoric heat capacity (c_v):

$$\frac{c_v}{R} = -\tau^2\left[\left(\frac{\partial^2\alpha^0}{\partial\tau^2}\right)_\delta + \left(\frac{\partial^2\alpha^{\mathrm{r}}}{\partial\tau^2}\right)_\delta\right]. \tag{A7}$$

Isobaric heat capacity (c_p):

$$\frac{c_p}{R} = \frac{c_v}{R} + \frac{\left[1 + \delta\left(\frac{\partial\alpha^{\mathrm{r}}}{\partial\delta}\right)_\tau - \delta\tau\left(\frac{\partial^2\alpha^{\mathrm{r}}}{\partial\delta\partial\tau}\right)\right]^2}{\left[1 + 2\delta\left(\frac{\partial\alpha^{\mathrm{r}}}{\partial\delta}\right)_\tau + \delta^2\left(\frac{\partial^2\alpha^{\mathrm{r}}}{\partial\delta^2}\right)_\tau\right]}. \tag{A8}$$

Speed of sound (w):

$$\frac{w^2M}{RT} = 1 + 2\delta\left(\frac{\partial\alpha^{\mathrm{r}}}{\partial\delta}\right)_\tau + \delta^2\left(\frac{\partial^2\alpha^{\mathrm{r}}}{\partial\delta^2}\right)_\tau - \frac{\left[1 + \delta\left(\frac{\partial\alpha^{\mathrm{r}}}{\partial\delta}\right)_\tau - \delta\tau\left(\frac{\partial^2\alpha^{\mathrm{r}}}{\partial\delta\partial\tau}\right)_\tau\right]^2}{\tau^2\left[\left(\frac{\partial^2\alpha^0}{\partial\tau^2}\right)_\delta + \left(\frac{\partial^2\alpha^{\mathrm{r}}}{\partial\tau^2}\right)_\delta\right]}. \tag{A9}$$

Fugacity coefficient (φ):

$$\varphi = \exp[Z - 1 - \ln(Z) + \alpha^{\mathrm{r}}]. \tag{A10}$$

Second virial coefficient (B):

$$B(T) = \lim_{\delta\to 0}\left[\frac{1}{\rho_{\mathrm{c}}}\left(\frac{\partial\alpha^{\mathrm{r}}}{\partial\delta}\right)_\tau\right]. \tag{A11}$$

Third virial coefficient (C):

$$C(T) = \lim_{\delta\to 0}\left[\frac{1}{\rho_{\mathrm{c}}^2}\left(\frac{\partial^2\alpha^{\mathrm{r}}}{\partial\delta^2}\right)_\tau\right]. \tag{A12}$$

First derivative of pressure with respect to density at constant temperature

$$\left(\frac{\partial p}{\partial\rho}\right)_T = RT\left[1 + 2\delta\left(\frac{\partial\alpha^{\mathrm{r}}}{\partial\delta}\right)_\tau + \delta^2\left(\frac{\partial^2\alpha^{\mathrm{r}}}{\partial\delta^2}\right)_\tau\right]. \tag{A13}$$

Second derivative of pressure with respect to density at constant temperature

$$\left(\frac{\partial^2 p}{\partial\rho^2}\right)_T = \frac{RT}{\rho}\left[2\delta\left(\frac{\partial\alpha^{\mathrm{r}}}{\partial\delta}\right)_\tau + 4\delta^2\left(\frac{\partial^2\alpha^{\mathrm{r}}}{\partial\delta^2}\right)_\tau + \delta^3\left(\frac{\partial^3\alpha^{\mathrm{r}}}{\partial\delta^3}\right)_\tau\right]. \tag{A14}$$

First derivative of pressure with respect to temperature at constant density

$$\left(\frac{\partial p}{\partial T}\right)_\rho = R\rho\left[1 + \delta\left(\frac{\partial\alpha^{\mathrm{r}}}{\partial\delta}\right)_\tau - \delta\tau\left(\frac{\partial^2\alpha^{\mathrm{r}}}{\partial\delta\partial\tau}\right)\right]. \tag{A15}$$

The derivatives of the ideal gas Helmholtz energy required by the equations for the thermodynamic properties are

$$\tau\left(\frac{\partial\alpha^0}{\partial\tau}\right)_\delta = a_1 + a_3\tau + \tau\sum_{i=4}^{7} a_i b_i \frac{1}{\exp(b_i\tau) - 1}. \tag{A16}$$

$$\tau^2\left(\frac{\partial^2\alpha^0}{\partial\tau^2}\right)_\delta = -a_1 - \tau^2\sum_{i=4}^{7} a_i b_i^2 \frac{\exp(b_i\tau)}{[\exp(b_i\tau) - 1]^2}. \tag{A17}$$

The derivatives of the residual Helmholtz energy required by the equations for the thermodynamic properties are

$$\begin{aligned}\delta\left(\frac{\partial\alpha^{\mathrm{r}}}{\partial\delta}\right)_\tau = &\sum_{i=1}^{6} N_i\delta^{d_i}\tau^{t_i}d_i + \sum_{i=7}^{16} N_i\delta^{d_i}\tau^{t_i}\exp(-\delta^{l_i})(d_i - l_i\delta^{l_i}) \\ &+ \sum_{i=17}^{25} N_i\delta^{d_i}\tau^{t_i}\exp[-\eta_i(\delta - \varepsilon_i)^2 - \beta_i(\tau - \gamma_i)^2] \\ &\times [d_i - 2\eta_i\delta(\delta - \varepsilon_i)],\end{aligned} \tag{A18}$$

$$\begin{aligned}\delta^2\left(\frac{\partial^2\alpha^{\mathrm{r}}}{\partial\delta^2}\right)_\tau = &\sum_{i=1}^{6} N_i\delta^{d_i}\tau^{t_i}[d_i(d_i - 1)] + \sum_{i=7}^{16} N_i\delta^{d_i}\tau^{t_i}\exp(-\delta^{l_i}) \\ &\times [(d_i - l_i\delta^{l_i})(d_i - 1 - l_i\delta^{l_i}) - l_i^2\delta^{l_i}] \\ &+ \sum_{i=17}^{25} N_i\delta^{d_i}\tau^{t_i}\exp[-\eta_i(\delta - \varepsilon_i)^2 - \beta_i(\tau - \gamma_i)^2] \\ &\times \{[d_i - 2\eta_i\delta(\delta - \varepsilon_i)]^2 - d_i - 2\eta_i\delta^2\},\end{aligned} \tag{A19}$$

$$\begin{aligned}\tau\left(\frac{\partial\alpha^{\mathrm{r}}}{\partial\tau}\right)_\delta = &\sum_{i=1}^{6} N_i\delta^{d_i}\tau^{t_i}t_i + \sum_{i=7}^{16} N_i\delta^{d_i}\tau^{t_i}\exp(-\delta^{l_i})t_i \\ &+ \sum_{i=17}^{25} N_i\delta^{d_i}\tau^{t_i}\exp[-\eta_i(\delta - \varepsilon_i)^2 \\ &- \beta_i(\tau - \gamma_i)^2][t_i - 2\beta_i\tau(\tau - \gamma_i)],\end{aligned} \tag{A20}$$

This article is copyrighted as indicated in the article. Reuse of AIP content is subject to the terms at: http://scitation.aip.org/termsconditions. Downloaded to IP: 131.111.164.128 On: Tue, 21 Oct 2014 07:26:40

$$\tau^2\left(\frac{\partial^2\alpha^{\mathrm{r}}}{\partial\tau^2}\right)_\delta = \sum_{i=1}^{6} N_i\delta^{d_i}\tau^{t_i}[t_i(t_i-1)] + \sum_{i=7}^{16} N_i\delta^{d_i}\tau^{t_i}\exp(-\delta^{l_i})[t_i(t_i-1)] + \sum_{i=17}^{25} N_i\delta^{d_i}\tau^{t_i}\exp[-\eta_i(\delta-\varepsilon_i)^2-\beta_i(\tau-\gamma_i)^2] \times \{[t_i-2\beta_i\tau(\tau-\gamma_i)]^2-t_i-2\beta_i\tau^2\}, \quad \text{(A21)}$$

$$\tau\delta\left(\frac{\partial^2\alpha^{\mathrm{r}}}{\partial\tau\partial\delta}\right) = \sum_{i=1}^{6} N_i\delta^{d_i}\tau^{t_i}(d_it_i) + \sum_{i=7}^{16} N_i\delta^{d_i}\tau^{t_i}\exp(-\delta^{l_i})[t_i(d_i-l_i\delta^{l_i})] + \sum_{i=17}^{25} N_i\delta^{d_i}\tau^{t_i}\exp[-\eta_i(\delta-\varepsilon_i)^2-\beta_i(\tau-\gamma_i)^2] \times [d_i-2\eta_i\delta(\delta-\varepsilon_i)][t_i-2\beta_i\tau(\tau-\gamma_i)], \quad \text{(A22)}$$

$$\delta\tau^2\left(\frac{\partial^3\alpha^{\mathrm{r}}}{\partial\delta\partial\tau^2}\right) = \sum_{i=1}^{6} N_i\delta^{d_i}\tau^{t_i}[d_it_i(t_i-1)] + \sum_{i=7}^{16} N_i\delta^{d_i}\tau^{t_i}\exp(-\delta^{l_i})[t_i(t_i-1)(d_i-l_i\delta^{l_i})] + \sum_{i=17}^{25} N_i\delta^{d_i}\tau^{t_i}\exp[-\eta_i(\delta-\varepsilon_i)^2-\beta_i(\tau-\gamma_i)^2] \times [d_i-2\eta_i\delta(\delta-\varepsilon_i)] \times \{[t_i-2\beta_i\tau(\tau-\gamma_i)]^2-t_i-2\beta_i\tau^2\}, \quad \text{(A23)}$$

$$\delta^3\left(\frac{\partial^3\alpha^{\mathrm{r}}}{\partial\delta^3}\right) = \sum_{i=1}^{6} N_i\delta^{d_i}\tau^{t_i}[d_i(d_i-1)(d_i-2)] + \sum_{i=7}^{16} N_i\delta^{d_i}\tau^{t_i}\exp(-\delta^{l_i})[d_i(d_i-1)(d_i-2) + l_i\delta^{l_i}(-2+6d_i-3d_i^2-3d_il_i+3l_i-l_i^2) + 3l_i^2\delta^{2l_i}(d_i-1+l_i)-l_i^3\delta^{3l_i}] + \sum_{i=17}^{25} N_i\delta^{d_i}\tau^{t_i}\exp[-\eta_i(\delta-\varepsilon_i)^2-\beta_i(\tau-\gamma_i)^2] \times \{[d_i-2\eta_i\delta(\delta-\varepsilon_i)]^3-3d_i^2+2d_i-6d_i\eta_i\delta^2 + 6\eta_i\delta(\delta-\varepsilon_i)(d_i+2\eta_i\delta^2)\}. \quad \text{(A24)}$$

10. Appendix B: Thermodynamic Property Tables of Ethanol at Saturation

T (K)	p (MPa)	$\hat{\rho}$ (kg m^{-3})	$\hat{h}$ (kJ kg^{-1})	$\hat{s}$ (kJ kg^{-1} K^{-1})	$\hat{c}_v$ (kJ kg^{-1} K^{-1})	$\hat{c}_p$ (kJ kg^{-1} K^{-1})	w (m s^{-1})
200	1.1017×10^{-6}	869.47	–353.22	–1.2888	1.5555	1.9536	1528.4
		3.0523×10^{-5}	655.31	3.7539	0.9487	1.1291	207.28
210	4.1456×10^{-6}	860.56	–333.59	–1.1930	1.5807	1.9734	1486.0
		1.0938×10^{-4}	666.72	3.5704	0.9732	1.1537	211.96
220	1.3694×10^{-5}	851.77	–313.73	–1.1006	1.6127	2.0006	1442.8
		3.4489×10^{-4}	678.38	3.4090	0.9990	1.1795	216.51
230	4.0404×10^{-5}	843.09	–293.56	–1.0109	1.6518	2.0355	1399.7
		9.7344×10^{-4}	690.30	3.2667	1.0259	1.2065	220.93
240	1.0804×10^{-4}	834.49	–273.00	–0.92344	1.6970	2.0773	1357.5
		2.4948×10^{-3}	702.47	3.1410	1.0541	1.2349	225.22
250	2.6500×10^{-4}	825.96	–251.99	–0.83769	1.7472	2.1251	1316.7
		5.8757×10^{-3}	714.90	3.0299	1.0837	1.2648	229.38
260	6.0229×10^{-4}	817.47	–230.48	–0.75332	1.8016	2.1785	1277.4
		0.012846	727.58	2.9315	1.1146	1.2963	233.42
270	1.2795×10^{-3}	809.00	–208.40	–0.67001	1.8599	2.2374	1239.7
		0.026297	740.51	2.8445	1.1470	1.3297	237.32
280	2.5597×10^{-3}	800.53	–185.71	–0.58749	1.9218	2.3020	1203.5
		0.050778	753.64	2.7673	1.1810	1.3651	241.09
290	4.8529×10^{-3}	792.03	–162.34	–0.50550	1.9874	2.3726	1168.6
		0.093087	766.96	2.6990	1.2167	1.4029	244.69
300	8.7679×10^{-3}	783.45	–138.23	–0.42380	2.0562	2.4492	1134.8
		0.16292	780.41	2.6383	1.2542	1.4436	248.12
310	0.015169	774.77	–113.32	–0.34217	2.1276	2.5318	1101.8
		0.27356	793.95	2.5845	1.2939	1.4875	251.35
320	0.025238	765.93	–87.559	–0.26042	2.2009	2.6200	1069.3
		0.44260	807.50	2.5367	1.3359	1.5353	254.35
330	0.040531	756.89	–60.884	–0.17841	2.2752	2.7134	1036.9
		0.69267	821.01	2.4940	1.3804	1.5875	257.08

This article is copyrighted as indicated in the article. Reuse of AIP content is subject to the terms at: http://scitation.aip.org/termsconditions. Downloaded to IP: 131.111.164.128 On: Tue, 21 Oct 2014 07:26:40

TABLE . —Continued

T (K)	p (MPa)	$\hat{\rho}$ (kg m^{-3})	$\hat{h}$ (kJ kg^{-1})	$\hat{s}$ (kJ kg^{-1} K^{-1})	$\hat{c}_v$ (kJ kg^{-1} K^{-1})	$\hat{c}_p$ (kJ kg^{-1} K^{-1})	w (m s^{-1})
340	0.063033	747.59	–33.246	–0.09599	2.3498	2.8116	1004.5
		1.0521	834.39	2.4559	1.4278	1.6448	259.51
350	0.095207	737.96	–4.5946	–0.01307	2.4239	2.9147	971.63
		1.5557	847.57	2.4217	1.4782	1.7081	261.60
360	0.14003	727.93	25.119	0.07045	2.4971	3.0228	938.02
		2.2455	860.46	2.3908	1.5321	1.7781	263.32
370	0.20099	717.44	55.951	0.15469	2.5690	3.1367	903.36
		3.1715	872.97	2.3629	1.5895	1.8559	264.62
380	0.28215	706.37	87.960	0.23974	2.6393	3.2569	867.39
		4.3929	885.03	2.3373	1.6508	1.9428	265.46
390	0.38803	694.64	121.21	0.32571	2.7069	3.3837	829.84
		5.9787	896.54	2.3137	1.7161	2.0402	265.80
400	0.52368	682.11	155.76	0.41267	2.7707	3.5162	790.52
		8.0099	907.42	2.2918	1.7856	2.1501	265.58
410	0.69452	668.67	191.64	0.50065	2.8289	3.6525	749.32
		10.581	917.55	2.2711	1.8596	2.2749	264.77
420	0.90636	654.21	228.87	0.58958	2.8801	3.7898	706.25
		13.804	926.83	2.2514	1.9382	2.4184	263.30
430	1.1653	638.60	267.42	0.67934	2.9238	3.9255	661.46
		17.813	935.14	2.2322	2.0219	2.5857	261.12
440	1.4776	621.78	307.23	0.76971	2.9610	4.0600	615.14
		22.773	942.30	2.2131	2.1109	2.7848	258.14
450	1.8499	603.62	348.26	0.86055	2.9941	4.2005	567.36
		28.895	948.12	2.1936	2.2061	3.0283	254.25
460	2.2890	583.95	390.56	0.95188	3.0274	4.3654	517.75
		36.466	952.25	2.1730	2.3085	3.3386	249.29
470	2.8023	562.33	434.36	1.0442	3.0654	4.5923	465.32
		45.907	954.22	2.1502	2.4199	3.7583	243.00
480	3.3976	537.83	480.27	1.1385	3.1132	4.9593	408.14
		57.899	953.15	2.1237	2.5438	4.3811	234.97
490	4.0839	508.25	529.65	1.2376	3.1773	5.6740	343.18
		73.735	947.29	2.0900	2.6868	5.4635	224.46
500	4.8719	467.38	586.15	1.3485	3.2735	7.6477	266.01
		96.617	932.30	2.0408	2.8662	8.0519	210.09
510	5.7767	386.14	666.74	1.5038	3.4620	21.626	180.23
		141.92	887.92	1.9374	3.1586	26.346	188.28
514.71	6.2680	273.19	758.74	1.6803			
239.18	0.0001	835.19	–274.70	–0.93055	1.6931	2.0736	1360.9
		2.3171×10^{-3}	701.46	3.1507	1.0518	1.2326	224.87
246.77	0.0002	828.71	–258.84	–0.86525	1.7304	2.1090	1329.7
		4.4923×10^{-3}	710.85	3.0643	1.0740	1.2550	228.05
254.91	0.0004	821.79	–241.50	–0.79614	1.7734	2.1507	1297.2
		8.7000×10^{-3}	721.09	2.9801	1.0987	1.2801	231.38
259.95	0.0006	817.51	–230.58	–0.75372	1.8013	2.1783	1277.6
		0.012799	727.52	2.9320	1.1145	1.2962	233.40
263.67	0.0008	814.36	–222.44	–0.72264	1.8225	2.1995	1263.4
		0.016829	732.30	2.8984	1.1263	1.3083	234.86
266.64	0.001	811.85	–215.89	–0.69794	1.8398	2.2170	1252.2
		0.020806	736.13	2.8726	1.1359	1.3182	236.02
276.35	0.002	803.63	–194.07	–0.61756	1.8988	2.2778	1216.6
		0.040183	748.82	2.7944	1.1684	1.3519	239.73
286.89	0.004	794.67	–169.67	–0.53093	1.9667	2.3500	1179.3
		0.077517	762.81	2.7193	1.2054	1.3909	243.59
293.50	0.006	789.04	–153.99	–0.47689	2.0111	2.3987	1156.7
		0.11379	771.65	2.6769	1.2296	1.4168	245.92
298.40	0.008	784.83	–142.14	–0.43687	2.0450	2.4366	1140.1
		0.14939	778.25	2.6476	1.2481	1.4368	247.59
302.33	0.01	781.44	–132.50	–0.40477	2.0726	2.4680	1127.0
		0.18449	783.56	2.6252	1.2633	1.4535	248.90
315.34	0.02	770.08	–99.676	–0.29854	2.1665	2.5782	1084.4
		0.35524	801.19	2.5583	1.3160	1.5125	252.98
323.57	0.03	762.74	–78.152	–0.23121	2.2273	2.6527	1057.7
		0.52116	812.33	2.5209	1.3514	1.5533	255.35
329.71	0.04	757.16	–61.666	–0.18077	2.2731	2.7106	1037.9
		0.68408	820.62	2.4952	1.3791	1.5859	257.01

This article is copyrighted as indicated in the article. Reuse of AIP content is subject to the terms at: http://scitation.aip.org/termsconditions. Downloaded to IP: 131.111.164.128 On: Tue, 21 Oct 2014 07:26:40

TABLE . —Continued

T (K)	p (MPa)	$\hat{\rho}$ (kg m^{-3})	$\hat{h}$ (kJ kg^{-1})	$\hat{s}$ (kJ kg^{-1} K^{-1})	$\hat{c}_v$ (kJ kg^{-1} K^{-1})	$\hat{c}_p$ (kJ kg^{-1} K^{-1})	w (m s^{-1})
338.85	0.06	748.67	–36.479	–0.10551	2.3412	2.8001	1008.3
		1.0041	832.86	2.4601	1.4222	1.6379	259.25
345.70	0.08	742.14	–17.049	–0.04882	2.3921	2.8697	985.85
		1.3188	841.93	2.4359	1.4561	1.6801	260.75
351.24	0.10	736.74	–0.9772	–0.00278	2.4330	2.9277	967.52
		1.63	849.18	2.4177	1.4847	1.7163	261.84
351.57	0.101325	736.41	0.00	0.0000	2.4354	2.9313	966.41
		1.6505	849.61	2.4166	1.4865	1.7186	261.90
361.85	0.15	726.03	30.751	0.08602	2.5105	3.0435	931.68
		2.3978	862.81	2.3854	1.5424	1.7919	263.60
369.86	0.20	717.59	55.506	0.15349	2.5680	3.1350	903.86
		3.1565	872.80	2.3632	1.5887	1.8548	264.61
376.36	0.25	710.47	76.171	0.20869	2.6139	3.2124	880.65
		3.9101	880.70	2.3464	1.6280	1.9101	265.21
381.88	0.30	704.22	94.108	0.25581	2.6522	3.2802	860.46
		4.6606	887.24	2.3327	1.6627	1.9602	265.56
390.99	0.40	693.44	124.56	0.33424	2.7134	3.3965	826.04
		6.1578	897.65	2.3115	1.7227	2.0504	265.80
398.42	0.50	684.15	150.20	0.39883	2.7609	3.4949	796.87
		7.6549	905.74	2.2952	1.7743	2.1317	265.66
404.74	0.60	675.86	172.61	0.45429	2.7991	3.5806	771.21
		9.1561	912.32	2.2819	1.8201	2.2072	265.28
410.29	0.70	668.27	192.69	0.50319	2.8305	3.6564	748.11
		10.664	917.83	2.2706	1.8618	2.2788	264.74
415.24	0.80	661.23	210.98	0.54712	2.8567	3.7245	726.98
		12.18	922.52	2.2607	1.9002	2.3475	264.09
423.84	1.00	648.35	243.54	0.62401	2.8978	3.8422	689.22
		15.244	930.15	2.2440	1.9698	2.4796	262.55
440.65	1.50	620.63	309.87	0.77563	2.9632	4.0689	612.07
		23.134	942.73	2.2118	2.1170	2.7991	257.91
453.60	2.00	596.72	363.34	0.89338	3.0059	4.2556	549.73
		31.437	949.82	2.1863	2.2421	3.1308	252.60
464.30	2.50	574.94	409.16	0.99136	3.0429	4.4521	495.66
		40.262	953.41	2.1635	2.3551	3.5018	246.77
473.48	3.00	554.2	450.07	1.0767	3.0807	4.6982	446.06
		49.749	954.25	2.1415	2.4614	3.9446	240.43
481.58	3.50	533.57	487.81	1.1538	3.1220	5.0402	398.47
		60.103	952.60	2.1189	2.5649	4.5108	233.49
488.85	4.00	512.04	523.72	1.2258	3.1688	5.5592	351.18
		71.647	948.31	2.0944	2.6690	5.2976	225.83
495.45	4.50	488.16	559.11	1.2957	3.2238	6.4448	302.95
		84.948	940.78	2.0661	2.7781	6.5239	217.24
501.50	5.00	459.23	595.84	1.3673	3.2932	8.2790	253.10
		101.16	928.60	2.0308	2.8989	8.8139	207.44
507.09	5.50	418.71	637.89	1.4484	3.3907	13.531	203.55
		123.32	907.84	1.9807	3.0472	14.913	195.90
512.24	6.00	351.69	695.34	1.5585	3.5209	39.917	166.24
		168.36	857.83	1.8757	3.2964	71.713	180.43
514.71	6.268	273.19	758.74	1.6803			

11. References

[1]F. A. M. M. Gonçalves, A. R. Trindade, C. S. M. F. Costa, J. C. S. Bernardo, I. Johnson, I. M. A. Fonseca, and A. G. M. Ferreira, J. Chem. Thermodyn. **42**, 1039 (2010).

[2]A. R. Bazaev, I. M. Abdulagatov, E. A. Bazaev, and A. Abdurashidova, Int. J. Thermophys. **28**, 194 (2007).

[3]Y. Takiguchi and M. Uematsu, J. Chem. Thermodyn. **28**, 7 (1996).

[4]D. Bhattacharyya and G. Thodos, Can. J. Chem. Eng. **43**, 150 (1965).

[5]M. Gomez-Nieto and G. Thodos, Can. J. Chem. Eng. **54**, 438 (1976).

[6]I. Cibulka and I. Nagata, Fluid Phase Equilib. **35**, 19 (1987).

[7]B. Cho, J. Appl. Phys. **64**, 4236 (1988).

[8]M. J. Lee and K. C. Chao, AIChE J. **34**, 825 (1988).

[9]T. F. Sun, J. A. Schouten, P. J. Kortbeek, and S. N. Biswas, Phys. Chem. Liq. **21**, 231 (1990).

[10]M. Massucci and C. J. Wormald, J. Chem. Soc., Faraday Trans. **88**, 3547 (1992).

[11]P. Sauermann, K. Holzapfel, J. Oprzynski, F. Kohler, W. Poot, and T. W. de Loos, Fluid Phase Equilib. **112**, 249 (1995).

[12]K. Fotouh and K. Shukla, Chem. Eng. Commun. **159**, 209 (1997).

[13]H. E. Dillon and S. G. Penoncello, Int. J. Thermophys. **25**, 321 (2004).

This article is copyrighted as indicated in the article. Reuse of AIP content is subject to the terms at: http://scitation.aip.org/termsconditions. Downloaded to IP: 131.111.164.128 On: Tue, 21 Oct 2014 07:26:40

[14]S. B. Kiselev, J. F. Ely, I. M. Abdulagatov, and M. L. Huber, Ind. Eng. Chem. Res. **44**, 6916 (2005).
[15]N. G. Polikhronidi, I. M. Abdulagatov, G. V. Stepanov, and R. G. Batyrova, J. Supercrit. Fluids **43**, 1 (2007).
[16]M. Gude and A. S. Teja, J. Chem. Eng. Data **40**, 1025 (1995).
[17]E. Álvarez, D. Gómez-Díaz, M. D. La Rubia, J. M. Navaza, R. Pacheco, and S. Sánchez, J. Chem. Eng. Data **52**, 2059 (2007).
[18]T. M. Aminabhavi and V. B. Patil, J. Chem. Eng. Data **43**, 504 (1998).
[19]M. I. Aralaguppi, C. V. Jadar, and T. M. Aminabhavi, J. Chem. Eng. Data **44**, 216 (1999).
[20]M. I. Aralaguppi and J. G. Baragi, J. Chem. Thermodyn. **38**, 434 (2006).
[21]A. E. Arbusow, Z. Phys. Chem. **131**, 49 (1927).
[22]G. C. Benson and P. J. D'Arcy, J. Chem. Eng. Data **27**, 439 (1982).
[23]W. V. Bhagwat and M. V. Subnis, J. Indian Chem. Soc. **25**, 165 (1948).
[24]V. E. Bich, M. Ramsdorf, and G. Opel, Z. Phys. Chem., Leipzig **265**, 401 (1984).
[25]P. W. Bridgman, Proc. Natl. Acad. Sci. U.S.A. **49**, 1 (1913).
[26]M. Dzida and W. Marczak, J. Chem. Thermodyn. **37**, 826 (2005).
[27]A. J. Easteal and L. A. Woolf, J. Chem. Thermodyn. **16**, 391 (1984).
[28]G. García-Miaja, J. Trocoso, and L. Romaní, Fluid Phase Equilib. **274**, 59 (2008).
[29]A. Z. Golik, Y. I. Shimansky, and N. M. Kobiichuk, Ukr. Fiz. Zh. **3**, 536 (1958).
[30]I. F. Golubev, T. N. Vasil'kovskaya, and V. S. Zolin, Inzh. Fiz. Zh. **38**, 668 (1980).
[31]E. Gómez, B. González, N. Calvar, E. Tojo, and Á. Domínguez, J. Chem. Eng. Data **51**, 2096 (2006).
[32]B. González, N. Calvar, Á. Domínguez, and J. Tojo, J. Chem. Thermodyn. **39**, 322 (2007).
[33]A. C. Gupta and R. W. Hanks, Thermochim. Acta **21**, 143 (1977).
[34]T. Hilczer and R. Goc, Bull. Soc. Amis Sci. Lett. Poznan, Ser. B **16**, 201 (1961).
[35]J. Hu, K. Tamura, and S. Murakami, Fluid Phase Equilib. **131**, 197 (1997).
[36]M. Hugo, K. Schlüter, and A. Würflinger, Z. Phys. Chem. **175**, 235 (1992).
[37]U. B. Kadam, A. P. Hiray, A. B. Sawant, and M. Hasan, J. Chem. Thermodyn. **38**, 1675 (2006).
[38]D. D. Kalafati, D. S. Rasskazov, and E. K. Petrov, Teploenergetika **14**, 77 (1967).
[39]T. S. Khasanshin and A. A. Aleksandrov, Inzh. Fiz. Zh. **47**, 411 (1984).
[40]H. Kitajima, N. Kagawa, S. Tsuruno, and H. Endo, T. Jpn. Soc. Mech. Eng. **69**, 1921 (2003).
[41]H. Kubota, Y. Tanaka, and T. Makita, Int. J. Thermophys. **8**, 47 (1987).
[42]E. Langa, A. M. Mainar, J. I. Pardo, and J. S. Urieta, J. Chem. Eng. Data **50**, 1255 (2005).
[43]J. M. Lasarte, L. Martín, E. Langa, J. S. Urieta, and A. M. Mainar, J. Chem. Eng. Data **53**, 1393 (2008).
[44]T. D. Ling and M. Van Winkle, Ind. Eng. Chem., Chem. Eng. Data Ser. **3**, 88 (1958).
[45]H. Y. Lo and L. I. Stiel, Ind. Eng. Chem. Fundam. **8**, 713 (1969).
[46]D. Matkowska, A. Goldon, and T. Hofman, J. Chem. Eng. Data **55**, 685 (2010).
[47]V. Mutalik, L. S. Manjeshwar, M. Sairam, and T. M. Aminabhavi, J. Chem. Thermodyn. **38**, 1620 (2006).
[48]P. S. Nikam, L. N. Shirsat, and M. Hasan, J. Chem. Eng. Data **43**, 732 (1998).
[49]C. Ormanoudis, C. Dakos, and C. Panayiotou, J. Chem. Eng. Data **36**, 39 (1991).
[50]J. Ortega, J. Chem. Eng. Data **27**, 312 (1982).
[51]S. Ozawa, N. Ooyatsu, M. Yamabe, S. Honmo, and Y. Ogino, J. Chem. Thermodyn. **12**, 229 (1980).
[52]D. Papaioannou, D. Ziakas, and C. Panayiotou, J. Chem. Eng. Data **36**, 35 (1991).
[53]D. Papaioannou, M. Bridakis, and C. G. Panayiotou, J. Chem. Eng. Data **38**, 370 (1993).
[54]D. Pečar and V. Doleček, Fluid Phase Equilib. **230**, 36 (2005).
[55]J. Peleteiro, J. Troncoso, D. González-Salgado, J. L. Valencia, C. A. Cerdeiriña, and L. Romaní, Int. J. Thermophys. **25**, 787 (2004).
[56]J. Peleteiro, J. Troncoso, D. González-Salgado, J. L. Valencia, M. Souto-Caride, and L. Romani, J. Chem. Thermodyn. **37**, 935 (2005).
[57]V. K. Rattan, S. Singh, and B. P. S. Sethi, J. Chem. Eng. Data **49**, 1074 (2004).
[58]A. Rodríguez, J. Canosa, and J. Tojo, J. Chem. Eng. Data **46**, 1506 (2001).
[59]M. R. Schroeder, B. E. Poling, and D. B. Manley, J. Chem. Eng. Data **27**, 256 (1982).
[60]D. Sommer, R. Kleinrahm, R. Span, and W. Wagner, J. Chem. Thermodyn. **43**, 117 (2011).
[61]Y. Takiguchi and M. Uematsu, Int. J. Thermophys. **16**, 205 (1995).
[62]G. Tammann and A. Ruhenbeck, Ann. Phys. **405**, 63 (1932).
[63]Y. Tanaka, T. Yamamoto, Y. Satomi, H. Kubota, and T. Makita, Rev. Phys. Chem. Jpn. **47**, 12 (1977).
[64]C. Tu, H. Ku, W. Wang, and Y. Chou, J. Chem. Eng. Data **46**, 317 (2001).
[65]E. Vercher, A. V. Orchillés, P. J. Miguel, and A. Martínez-Andreu, J. Chem. Eng. Data **52**, 1468 (2007).
[66]J. M. Walsh and M. H. Rice, J. Chem. Phys. **26**, 815 (1957).
[67]N. N. Wankhede, D. S. Wankhede, M. K. Lande, and B. R. Arbad, Indian J. Chem. Technol. **13**, 149 (2006).
[68]G. Watson, C. K. Zéberg-Mikkelsen, A. Baylaucq, and C. Boned, J. Chem. Eng. Data **51**, 112 (2006).
[69]L. A. Watts and B. Louie, Int. J. Thermophys. **21**, 1139 (2000).
[70]K. S. Wilson, D. D. Lindley, W. B. Kay, and H. C. Hershey, J. Chem. Eng. Data **29**, 243 (1984).
[71]M. Yusa, G. P. Mathur, and R. A. Stager, J. Chem. Eng. Data **22**, 32 (1977).
[72]M. T. Zafarani-Moattar and N. Tohidifar, J. Chem. Eng. Data **53**, 785 (2008).
[73]C. K. Zéberg-Mikkelsen, L. Lugo, and J. Fernández, J. Chem. Thermodyn. **37**, 1294 (2005).
[74]K. Bennewitz and W. Rossner, Z. Phys. Chem. Abt. B **39**, 126 (1938).
[75]F. E. Blacet, P. A. Leighton, and E. P. Bartlett, J. Phys. Chem. **35**, 1935 (1931).
[76]E. Bose, Z. Phys. Chem. **58**, 585 (1907).
[77]J. F. Counsell, J. O. Fenwick, and E. B. Lees, J. Chem Thermodyn. **2**, 367 (1970).
[78]J. Q. Dong, R. S. Lin, and W. H. Yen, Can. J. Chem. **66**, 783 (1988).
[79]V. A. Eucken and E. U. Franck, Z. Electrochem., Angew. Phys. Chem. **52**, 195 (1948).
[80]E. F. Fiock, D. C. Ginnings, and W. B. Holton, J. Res. Nat. Bur. Stand. **6**, 881 (1931).
[81]J. L. Fortier and G. C. Benson, J. Chem. Thermodyn. **8**, 289 (1976).
[82]M. Fulem, K. Ruzicka, and V. Ruzicka, Thermochim. Acta **382**, 119 (2002).
[83]G. E. Gibson, G. S. Parks, and W. M. Latimer, J. Am. Chem. Soc. **42**, 1542 (1920).
[84]O. Haida, H. Suga, and S. Seki, J. Chem. Thermodyn. **9**, 1133 (1977).
[85]S. C. P. Hwa and W. T. Ziegler, J. Phys. Chem. **70**, 2572 (1966).
[86]K. K. Kelley, J. Am. Chem. Soc. **51**, 779 (1929).
[87]J. Mazur, Acta Phys. Pol. **8**, 6 (1940).
[88]S. Mitsukuri and K. Hara, Bull. Chem. Soc. Jpn. **4**, 77 (1929).
[89]G. S. Parks, J. Am. Chem. Soc. **47**, 338 (1925).
[90]M. J. Pedersen, W. B. Kay, and H. C. Hershey, J. Chem. Thermodyn. **7**, 1107 (1975).
[91]S. L. Rivkin and A. N. Vinnikova, Teploenergetika **6**, 59 (1964).
[92]G. C. Sinke and T. De Vries, J. Am. Chem. Soc. **75**, 1815 (1953).
[93]M. Stephens and J. D. Olson, Thermochim. Acta **76**, 79 (1984).
[94]E. Strömsöe, H. G. Rönne, and A. L. Lydersen, J. Chem. Eng. Data **15**, 286 (1970).
[95]F. Veselý, M. Zábranský, V. Svoboda, and J. Pick, Collect. Czech. Chem. Commun. **44**, 3529 (1979).
[96]J. W. Williams and F. Daniels, J. Am. Chem. Soc. **46**, 903 (1924).
[97]Q. Yu, W. Fang, H. Zong, and R. Lin, Thermochim. Acta **275**, 173 (1996).
[98]A. A. Alexandrov and A. I. Kochetkov, Trans. MEI **532**, 8 (1981).
[99]J. M. Brown, L. J. Slutsky, K. A. Nelson, and L.-T. Cheng, Science **241**, 65 (1988).
[100]E. H. Carnevale and T. A. Litovitz, J. Acoust. Soc. Am. **27**, 547 (1955).
[101]H. F. Eden and E. G. Richardson, Acustica **10**, 309 (1960).
[102]E. B. Freyer, J. C. Hubbard, and D. H. Andrews, J. Am. Chem. Soc. **51**, 759 (1929).
[103]S. Hawley, J. Allegra, and G. Holton, J. Acoust. Soc. Am. **47**, 137 (1970).
[104]G. Onori, J. Chem. Phys. **89**, 4325 (1988).
[105]M. Sakurai, K. Nakamura, and N. Takenaka, Bull. Chem. Soc. Jpn. **67**, 352 (1994).
[106]T. F. Sun, J. A. Schouten, and S. N. Biswas, Int. J. Thermophys. **12**, 381 (1991).
[107]T. F. Sun, C. A. Ten Seldam, P. J. Kortbeek, N. J. Trappeniers, and S. N. Biswas, Phys. Chem. Liq. **18**, 107 (1988).

This article is copyrighted as indicated in the article. Reuse of AIP content is subject to the terms at: http://scitation.aip.org/termsconditions. Downloaded to IP: 131.111.164.128 On: Tue, 21 Oct 2014 07:26:40

[108]W. Wilson and D. Bradley, J. Acoust. Soc. Am. **36**, 333 (1964).
[109]J. A. Abusleme and J. H. Vera, Fluid Phase Equilib. **45**, 287 (1989).
[110]A. Aucejo, S. Loras, R. Muñoz, and L. M. Ordoñez, Fluid Phase Equilib. **156**, 173 (1999).
[111]J. A. Barker, I. Brown, and F. Smith, Discuss. Faraday Soc. **15**, 142 (1953).
[112]G. M. Barrow, J. Chem. Phys. **20**, 1739 (1952).
[113]D. H. Knoebel and W. C. Edmister, J. Chem. Eng. Data **13**, 312 (1968).
[114]C. B. Kretschmer and R. Wiebe, J. Am. Chem. Soc. **76**, 2579 (1954).
[115]J. D. Lambert, Discuss. Faraday Soc. **15**, 226 (1953).
[116]M. Massucci, M. M. von Kralik, and C. J. Wormald, J. Chem. Soc. Faraday Trans. **88**, 985 (1992).
[117]R. Noppe, M. Ramsdorf, W. Lichtenstein, and G. Opel, Z. Phys. Chem. **262**, 1157 (1981).
[118]C. Tsonopoulos, J. H. Dymond, and A. M. Szafranski, Pure Appl. Chem. **61**, 1387 (1989).
[119]D. Ambrose and C. H. S. Sprake, J. Chem. Thermodyn. **2**, 631 (1970).
[120]D. Ambrose, C. H. S. Sprake, and R. Townsend, J. Chem. Thermodyn. **7**, 185 (1975).
[121]H. H. Amer, R. R. Paxton, and M. Van Winkle, Ind. Eng. Chem. **48**, 142 (1956).
[122]J. Timmermans, *Physico-Chemical Constants of Pure Organic Compounds*, Vols. I and II (Elsevier, Amsterdam, 1950).
[123]A. Deák, A. I. Victorov, and T. W. de Loos, Fluid Phase Equilib. **107**, 277 (1995).
[124]V. I. Devyatko and V. N. Stabnikov, Izv. Vysshikh. Uchebn. Zaved., Pishchevaya Tekhnol. **6**, 117 (1963).
[125]K. A. Dulitskaya, Zh. Obshch. Khim. **7**, 185 (1945).
[126]G. Figurski and S. K. Malanowski, Fluid Phase Equilib. **148**, 161 (1998).
[127]J. R. Khurma, O. Muthu, S. Munjal, and B. D. Smith, J. Chem. Eng. Data **28**, 100 (1983).
[128]C. B. Kretschmer and R. Wiebe, J. Am. Chem. Soc. **71**, 1793 (1949).
[129]M. J. Lee and C. H. Hu, Fluid Phase Equilib. **109**, 83 (1995).
[130]A. L. Lydersen and V. Tsochev, Chem. Eng. Tech. **13**, 125 (1990).
[131]R. W. Merriman, J. Chem. Soc. Trans. **103**, 628 (1913).
[132]K. P. Mishchenko and V. V. Subbotina, Zh. Prikl. Khim. **40**, 1156 (1967).
[133]A. H. N. Mousa, J. Chem. Eng. Jpn. **20**, 635 (1987).
[134]J. P. Pokki, K. Rehák, Y. Kim, J. Matous, and J. Aittamaa, J. Chem. Eng. Data **48**, 75 (2003).
[135]Y. Takiguchi, M. Kamiya, and M. Uematsu, Trans. Jpn. Soc. Mech. Eng. B **61**, 644 (1995).
[136]R. C. Wilhoit and B. J. Zwolinski, J. Phys. Chem. Ref. Data **2**(Suppl. 1), 55 (1973).
[137]H. Wolff and R. Götz, Z. Phys. Chem. **100**, 25 (1976).
[138]J. L. Hales and J. H. Ellender, J. Chem. Thermodyn. **8**, 1177 (1976).
[139]J. O. Halford and G. A. Miller, J. Phys. Chem. **61**, 1536 (1957).
[140]A. J. Barnes and H. E. Hallam, Trans. Faraday Soc. **66**, 1932 (1970).
[141]F. G. Brickwedde, M. Moskow, and J. G. Aston, J. Res. Nat. Bur. Stand. **37**, 263 (1946).
[142]J. R. Durig, W. E. Bucy, C. J. Wurrey, and L. A. Carreira, J. Phys. Chem. **79**, 988 (1975).
[143]J. H. S. Green, Trans. Faraday Soc. **57**, 2132 (1961).
[144]J. Chao, K. R. Hall, K. N. Marsh, and R. C. Wilhoit, J. Phys. Chem. Ref. Data **15**, 1369 (1986).
[145]R. K. Kakar and C. R. Quade, J. Chem. Phys. **72**, 4300 (1980).
[146]F. J. Lovas, J. Phys. Chem. Ref. Data **11**, 251 (1982).
[147]J. Chao and K. R. Hall, Int. J. Thermophys. **7**, 431 (1986).
[148]Thermodynamics Research Center, *Selected Values of Properties of Chemical Compounds* (Thermodynamics Research Center, Texas A&M University, College Station, Texas, 1997).
[149]W. Wagner, J. Ewers, and W. Pentermann, J. Chem. Thermodyn. **8**, 1049 (1976).
[150]E. W. Lemmon and A. R. H. Goodwin, J. Phys. Chem. Ref. Data **29**, 1 (2000).
[151]E. W. Lemmon and R. T. Jacobsen, J. Phys. Chem. Ref. Data **34**, 69 (2005).
[152]J. M. Prausnitz, R. N. Lichtenthaler, and E. G. de Azevedo, *Molecular Thermodynamics of Fluid-Phase Equilibria*, 3rd ed. (Prentice-Hall PTR, New Jersey, 1999).
[153]U. Setzmann and W. Wagner, J. Phys. Chem. Ref. Data **20**, 1061 (1991).
[154]E. W. Lemmon, M. O. McLinden, and W. Wagner, J. Chem. Eng. Data **54**, 3141 (2009).
[155]E. W. Lemmon, M. L. Huber, and M. O. McLinden, *NIST Standard Reference Database 23: Reference Fluid Thermodynamic and Transport Properties*— REFPROP, Version 9.0 (National Institute of Standards and Technology, Standard Reference Data Program, Gaithersburg, 2010).
[156]G. A. Iglesias-Silva and K. R. Hall, Ind. Eng. Chem. Res. **40**, 1968 (2001).
[157]J. Wang and M. A. Anisimov, Phys. Rev. E **75**, 051107 (2007).
[158]K. M. de Reuck and R. J. B. Craven, *International Thermodynamic Tables of the Fluid State-12 Methanol, International Union of Pure and Applied Chemistry* (Blackwell Scientific Publications, London, 1993).
[159]T. F. Sun, J. A. Schouteden, N. J. Trappeniers, and S. N. Biswas, Ber. Bunsenges. Phys. Chem. **92**, 652 (1988).

This article is copyrighted as indicated in the article. Reuse of AIP content is subject to the terms at: http://scitation.aip.org/termsconditions. Downloaded to IP: 131.111.164.128 On: Tue, 21 Oct 2014 07:26:40